



**Interpretation of Feed Zones to Map Sub-Surface
Permeability Structures and Natural State Simulation: A
Case Study of Olkaria Domes Geothermal System in
Kenya**

Urbanus Kioko Mbithi



**Faculty of Civil and Environmental
Engineering
University of Iceland
2016**

Interpretation of Feed Zones to Map Sub-Surface Permeability Structures and Natural State Simulation: A Case Study of Olkaria Domes Geothermal System in Kenya

Urbanus Kioko Mbithi

30 ECTS thesis submitted in partial fulfillment of a
Magister Scientiarum degree in Environmental Engineering

Advisors

Lárus Þorvaldsson
Valdís Guðmundsdóttir
Gudni Axelsson
Sigurður Magnús Garðarsson

External Examiner

Gunnar Gunnarsson

Faculty of Civil and Environmental Engineering
School of Engineering and Natural Sciences
University of Iceland
Reykjavik, June 2016

Interpretation of Feed Zones to Map Sub-Surface Permeability Structures and Natural State Simulation: A Case Study of Olkaria Domes Geothermal System in Kenya
30 ECTS thesis submitted in partial fulfillment of a *Magister Scientiarum* degree in Environmental Engineering

Copyright © 2016 Urbanus Kioko Mbithi
All rights reserved

Faculty of Civil and Environmental Engineering
School of Engineering and Natural Sciences
University of Iceland
Hjarðarhagi 6
107, Reykjavík
Iceland

Telephone: 525 4000

Bibliographic information:

Mbithi, U. K. (2016). *Interpretation of Feed Zones to Map Sub-Surface Permeability Structures and Natural State Simulation: A Case Study of Olkaria Domes Geothermal System in Kenya*, Master's thesis, Faculty of Civil and Environmental Engineering, University of Iceland, 66 pp.

Printing: Háskólaprent, Fálkagata 2
101 Reykjavík, Iceland, June 2016

Abstract

The Olkaria Geothermal Area is a high temperature geothermal field located to the west of Longonot volcano in the southern sector of the Kenya Rift system. Exploration of the geothermal resources in Olkaria started in the 1950's. The structural domains of the Greater Olkaria volcanic complex depict diverse structural trending patterns. Currently, Olkaria has a total installed capacity of 654 MW_e.

In this thesis, sub-surface permeability structures were mapped according to major feedzones at the depths of 1000 m -2000 m and 2000 m – 3000 m and their distribution across the Olkaria Domes geothermal field. It is clear that the structures in this field are mostly trending in NW-SE, N-S and ENE-WSW. They also confirmed the location of the existing structures as earlier mapped such as the ring structure and Gorge Farm fault. Analysis of temperature distribution across the Olkaria Domes field coupled with the knowledge of how permeability is controlled by sub-surface structures can be used to site both make up and re-injection wells. Re-injection wells are highly recommended for this field for pressure support and to enhance energy extraction efficiency. Analysis of isotope data from boreholes should be conducted in order to draw conclusions regarding the flow patterns within the Olkaria Domes geothermal system.

A numerical model for this field was developed to simulate the natural state of the system in its pre-exploitation state. The primary purpose of a natural state model is to verify the validity of conceptual models and quantify the natural flow within the system. The simulated results of some wells did not match the observed data. Most of these wells are located at the inferred colder regions of this geothermal field. This could partly be attributed to the permeability distribution of the reservoir rock domain and the intensity of the heat sources assigned in the numerical model. Mapping of sub-surface structures is recommended in this field to accurately assign permeability distribution which has a great impact on the output of the simulated results in this study.

Útdráttur

Jarðhitakerfið í Olkaria er háhitakerfi sem er staðsett vestan Longonot eldfjallsins í suðurhluta sigdalsins í Kenya. Jarðhitarannsóknir í Olkaria hófust á sjötta áratug síðustu aldar. Jarðfræðileg bygging Stór-Olkaria svæðisins er fjölbreytt og breytileg milli mismunandi hluta svæðisins. Í dag er uppsett afl í Olkaria alls um 654 MWe.

Í þessari ritgerð voru lekar jarðmyndanir í Domes-hluta Olkaria kerfisins kortlagðar á grundvelli stærri vatnsæða á dýptarbilunum 1000 – 2000 m og 2000 – 3000 m og dreifing þeirra skoðuð. Það er ljóst að lektin í þessum hluta stefnir aðallega NV-SA, N-S og ANA-SVS. Kortlagningin staðfestir einnig tengsl lektardreifingarinnar í Domes við staðsetningu jarðmyndana, sem hafa áður verið kortlagðar, eins og öskjubrot og Gorge Farm sprunguna. Greining á hitadreifingunni í Olkaria Domes ásamt þekkingunni á því hvernig lekt er stjórnað a jarðmyndunum neðanjarðar, má nota til að staðsetja uppbotarborholur og niðurdælingarholur. Mjög ákveðið er mælt með niðurdælingu á þessu svæði til að styðja við þrýsting í jarðhitakerfinu og til að aukna nýti orkuvinnslunnar úr því. Gögn um styrk samsæta í borholum ætti að skoða til þess að greina rennislísiðir vatns innan jarðhitakerfisins í Olkaria Domes.

Nákvæmt forðafraðilegt reiknilíkan hefur verið sett upp til að herma náttúrulegt ástand jarðhitakerfisins, áður en vinnsla úr því hófst. Aðaltilgangur líkans af náttúrulegu ástandi er að sannreyna hugmyndalíkan kerfisins og meta náttúrulegt flæði innan þess. Hermdar niðurstöður fyrir sumar holur herma tiltæk gögn ekki nægilega vel. Þar er um að ræða holur sem eru í kaldari hlutum jarðhitakerfisins. Þetta má að hluta rekja til til lektardreifingar líkansins og staðsetningar hitagjafa í botni þess. Mælt er með nákvæmari kortlagningu lekra jarðmyndana neðanjarðar á svæðinu svo hægt sé að skilgreina lektradreifingu líkansins betur, en hún hefur mikil áhrif á ástand og hegðun reiknilíkansins.

Dedication

This work is dedicated to my beloved wife, Carolyn Mutheu for her remarkable patience and enduring my long absence and my two lovely kids, Bridgit Ndanu and Oscar Mbithi.

Table of Contents

List of Figures	xiii
List of Tables.....	xv
Nomenclature	xvii
Acknowledgements	xix
1 INTRODUCTION	1
1.1 Motivation	1
1.2 Goals of the project	1
1.3 Organization of thesis.....	1
2 BACKGROUND	3
2.1 The Olkaria geothermal system.....	3
2.2 The Olkaria Domes geothermal system.....	6
2.2.1 Regional geology	6
2.2.2 Geophysical studies.....	8
2.2.3 Overview of Olkaria Domes geochemistry data	9
2.2.4 Well data	10
2.3 Literature review	10
2.3.1 Field development.....	10
2.3.2 Conceptual model	11
3 METHODS.....	17
3.1 Interpretation of feedzones	17
3.1.1 Correlation of feed zones with permeability.....	18
3.1.2 Subsurface permeability structures and numerical modelling	21
3.1.3 Olkaria Domes Conceptual Model.....	21
3.2 Numerical Modelling	23
3.2.1 Theoretical background of numerical modelling using TOUGH2	23
3.2.2 Forward modelling using TOUGH2	23
3.2.3 Space and time discretization in TOUGH2 numerical modelling	25
3.2.4 Inverse Modelling	27
3.2.5 Mesh design and boundary conditions.....	27
3.2.6 Initial conditions	30
4 RESULTS AND DISCUSSION	31
4.1 Natural state model.....	31
4.1.1 Comparison between simulated and observed data	33
4.2 Mapped new sub-surface structures	38

5 CONCLUSIONS AND RECOMMENDATIONS	39
References	41
Appendix A: Reservoir Formation (Steady State Temperature and Pressure) and Natural state model simulation	43

List of Figures

<i>Figure 1 Location map of geothermal prospects in the Kenya Rift valley (Modified from Ofwona et al, 2006).</i>	5
<i>Figure 2 A Map showing different sectors in the Greater Olkaria Geothermal Field (modified from Otieno and Kubai, 2013).</i>	6
<i>Figure 3 The volcano tectonic map of the greater Olkaria volcanic complex showing the structures in the area (Lagat, 2004).</i>	8
<i>Figure 4 Water types of the Domes geothermal area. (Kamunya et al., 2014).</i>	10
<i>Figure 5 An early conceptual model of the Olkaria East geothermal system (SWECO and Virkir, 1976).</i>	11
<i>Figure 6 A revised conceptual model of the Olkaria East geothermal system from 2002 (Ofwona, 2002).</i>	12
<i>Figure 7 Horizontal view of 2009 conceptual model of the Greater Olkaria geothermal system (West-JEC, 2009).</i>	14
<i>Figure 8 Revised conceptual model of the Greater Olkaria geothermal system (Mannvit Consortium, 2014).</i>	15
<i>Figure 9 Wells with feed zones at 1000 m – 2000 m</i>	19
<i>Figure 10 Wells with feed zones at 2000 m – 3000 m</i>	20
<i>Figure 11 Map showing well locations and cross-sections across Olkaria Domes geothermal field.</i>	22
<i>Figure 12 A map showing temperature model cross-section A - A'.</i>	22
<i>Figure 13 A map showing temperature model cross-section B - B'.</i>	23
<i>Figure 14 Space Discretization and geometry data (Pruess, 1999).</i>	25
<i>Figure 15 The numerical model grid of the Olkaria geotherma system with emphasis on the Domes production field.</i>	28
<i>Figure 16 Vertical view of the mesh with layers named in alphabetical order.</i>	29
<i>Figure 17 Location of the heat sources in the Olkaria Domes geothermal field on a temperature contour map (at sea level which is at approximately 2000 m depth).</i>	33

<i>Figure 18 Field observed temperature contour at layer H (550 m.a.s.l).....</i>	<i>34</i>
<i>Figure 19 Model calculated temperature contour at layer H (550 m.a.s.l).</i>	<i>34</i>
<i>Figure 20 Field observed temperature contour at layer J (150 m.a.s.l).</i>	<i>35</i>
<i>Figure 21 Model calculated temperature contour at layer J (150 m.a.s.l).</i>	<i>35</i>
<i>Figure 22 Field observed temperature contour at layer N (650 m.b.s.l).</i>	<i>36</i>
<i>Figure 23 Model calculated temperature contour at layer N (650 m.b.s.l).</i>	<i>36</i>
<i>Figure 24 Comparison between measured and simulated temperature and pressure profiles of wells OW-905A and OW-910A.....</i>	<i>37</i>
<i>Figure 25 New mapped structures according to major feedzones at both 1000 m – 2000 m and 2000 m – 3000 m depths on a temperature model at 500m.a.s.l (at approximately 1500 m depth).</i>	<i>38</i>

List of Tables

*Table 1 Estimated physical properties of the numerical model of the Olkaria Domes
geothermal system 30*

Table 2 Permeabilities of the rock types assigned to the reservoir domain. 30

*Table 3 Table showing the heat sources, their enthalpies and mass flow rates for the
natural state model. 32*

Table 4 Change of permeability parameter after inverse modelling..... 32

Nomenclature

A	Area [m^2]
D	Distance [m]
R	Residual
P	Pressure [Pa]
T	Temperature [$^{\circ}\text{C}$]
S	Saturation [m^3/m^3]
X	mass fraction
M	Mass per volume [kg/m^3]
V	Volume [m^3]
F	Mass or heat flux [$\text{kg}/\text{s}.\text{m}^2$]
n	Normal vector
q	Mass flow rate [kg/s]
t	Time [s]
h	Reservoir thickness [m] or enthalpy [J/kg]
C_R	Specific heat of the rock
k	Absolute permeability [m^2]
m	Metres
m.a.s.l	Metres above sea level
m.b.s.l	Metres below sea level
ρ	Density [kg/m^3]
ϕ	Rock porosity
β	Specific heat capacity [$\text{kJ}/\text{kg}.\text{k}$]
κ	Thermal conductivity [$\text{W}/\text{m}^{\circ}\text{C}$]
μ	Dynamic viscosity [$\text{kg}/\text{m}.\text{s}$]
Γ	Surface area [m^2]

Acknowledgements

My sincere acknowledgement to the Government of Iceland through the United Nations University (UNU-GTP) and Kenya Electricity Generating Company Ltd (KenGen) for funding this M.Sc. study.

I appreciate and thank the UNU-GTP staff Mr. Ludvik S. Georgsson, Director of UNU-GTP, Mr. Ingimar G. Haraldsson, Deputy Director, Ms. Thorhildur Isberg, School Manager, Mr. Markus A.G. Wilde, Service Manager and Ms. Malfridur Omarsdottir, Environmental Scientist for their great assistance during my study and stay in Iceland.

I would like to thank my supervisors Mr. L  rus Þorvaldsson, Ms. Vald  s Gu  mundsd  ttir, Prof. Sigur  ur Magn  s Gar  arsson and Dr. Gudni Axelsson for their guidance and support throughout the project. I also appreciate the valuable input and advice from Dr. Andri Arnaldsson on numerical modelling.

Finally to my family and friends for their love, support and encouragement.

1 INTRODUCTION

1.1 Motivation

Geothermal power, which is generated from natural steam from the earth, some as far as three kilometers underground, is, when properly managed, a renewable source of energy and unlike hydro, its output is not affected by vagaries of weather. Kenya's government has recently stepped up geothermal development in order to supply reliable, clean energy and lower the cost of electricity to consumers. The World Bank Group and other development partners are making a significant contribution in increasing electricity access to Kenyans, raising prospects for growth and shared prosperity. Increasing climate changes demand for a global reduction in greenhouse gases and one of the advantages of geothermal energy is that its use can reduce CO₂ emissions. The efficient use of this natural resource can be optimized by applying numerical heat-transport models (Rühaak, Renz, Schätzl, & Diersch, 2010). Several simulation codes for flow and heat transport are available, featuring different numerical methods.

There has been a lot of production drilling going on in the Greater Olkaria Geothermal Area and a 140 MW_e power plant has currently been installed in Olkaria Domes. An increased understanding of this geothermal system is therefore needed for sustainable resource management.

1.2 Goals of the project

The objectives of the work described in this thesis are;

- To identify sub-surface structures in Olkaria Domes geothermal system, which is a sub-system of the Greater Olkaria geothermal system, through interpretation of the location of feed zones in the system. The results can, consequently, be used to update the conceptual model of this part of the system.
- To develop a numerical simulation model of the Olkaria Domes geothermal system, which matches the natural state of the system.

1.3 Organization of thesis

The thesis is organized as follows:

Chapter 2: This chapter briefly describes the geographical location of the Greater Olkaria Volcanic Complex. It also gives an overview of the geology, geophysics and geochemistry

of this geothermal field. Brief history and development of Olkaria geothermal field, previous studies carried out in this field is also discussed.

Chapter 3: This chapter presents the data and the methodology used to map sub-surface structures using major feedzones and use of TOUGH2 code to carry out numerical modelling of the Olkaria Domes geothermal field.

Chapter 4: The results and discussions are summarized and their limitations presented.

Chapter 5: Conclusions are presented here where the goals of the project are described. Future work is also recommended.

2 BACKGROUND

2.1 The Olkaria geothermal system

The Olkaria Geothermal Area is located to the west of Longonot Volcano in the southern sector of the Kenya rift system (Figure 1). The Kenya rift is part of the East African rift system that runs from Afar triple junction at the Gulf of Eden in the north to Beira, Mozambique in the south (Abbate, Passerini, & Zan, 1995). The rift is part of a continental divergent zone where spreading occurs resulting to the thinning of the crust hence eruption of lavas and associated volcanic activities. Olkaria geothermal field is a high temperature geothermal field. Structures in the Greater Olkaria geothermal complex include; the ring structure, the Ol'njorowa gorge, the ENE-WSW Olkaria fault and N-S, NNE-SSW, NW-SE and WNW-ESE trending faults (Figure 3).

The faults are more prominent in the East, Northeast and West Olkaria fields but are scarce in the Olkaria Domes area possibly due to the thick pyroclastics cover. The NW-SE and WNW-ESE faults are thought to be the oldest and are associated with the development of the rift. This field is one of the most exploited fields in the world and has been subdivided into seven fields for ease of geothermal development purposes namely; Olkaria East, Olkaria Northeast, Olkaria Domes, Olkaria Central, Olkaria Northwest, Olkaria Southwest and Olkaria Southeast (Figure 2). The Olkaria West and Olkaria East fields are believed to be separated hydrologically by the Ololbutot fault, which runs N-S between the two fields. This structure delineates a well-defined lithologic offset, whereby the Olkaria East reservoirs draw from the plateau trachytes and the Olkaria West field largely draws from the relatively uplifted Mau Tuff units. (P. A. Omenda, 1994). The ENE Olkaria fault zone is a major structural component in Olkaria East and transects through the north eastern boundary of the Olkaria West field; this feature play a significant role in faulted upflow for Olkaria III. (Owens, Porras, Spielman, & Walsh, 2015).

The exploration of geothermal resources in Kenya started in 1950's with mainly geological investigations in the region between Olkaria and lake Bogoria in the north rift. In the 1970s exploration was carried out in Olkaria and by 1976, six deep geothermal wells had been drilled. After the evaluation of these initial wells, development was found to be feasible. By 1981 the first 15 MW_e generating unit located in Olkaria East was commissioned. More wells were drilled and connected to the steam gathering system. Units 2 and 3, each 15 MW_e, were commissioned in 1982 and 1985, respectively. Olkaria II, located in Olkaria Northeast, was commissioned in 2003. The plant has been generating 70 MW_e since and an additional 35 MW_e turbine was commissioned in May 2010, increasing the generation capacity to 105 MW_e. An additional 150 MW_e were commissioned in Olkaria Domes and further 150 MW_e in Olkaria I Units 4 and 5 in October, 2014. Olkaria III which is operated by an Independent Power Producer, Orpower4 Inc, currently generates 140 MW_e. After the

latest commissioning, the total power generated from the Olkaria geothermal field is 590 MW_e. In addition, several wellhead power plants are being put up to allow early generation as the company sources for more funds to construct a big power plant. The total power currently generated directly from wellheads is approximately 64 MW_e. (KenGen internal report).

Crucial to the successful utilisation of a geothermal system is the knowledge of the permeability structure, and specifically feed zones which are the sources of geothermal fluid entry into the wellbore. Understanding the nature and distribution of feed zones is particularly relevant for well targeting and useful in providing the constraints to reservoir models. Feed zone locations in the wellbore are initially located during completion tests with a temperature – pressure – spinner (PTS) probe.

Important to note is that during exploration and initial stages of exploitation, the main focus is on geological studies, geophysical exploration, geochemical studies and reservoir engineering well studies once some wells have been drilled. The main quantitative resource assessment method used during the early exploration stages is the volumetric assessment method. This method involves estimating the energy content within the system volume and how much of that can be extracted within a given time period and ultimately used to generate electricity.

A natural state model is a description of the physical state of a geothermal system in its pre-exploitation state. The primary purpose of a numerical natural state model is to verify the validity of conceptual models and quantify the natural flow of fluids within the system. It consists running a model for a long time in a simulation of the development of the geothermal field over a geological time until a steady state has been reached. (O’Sullivan et al., 2001). At steady state, the heat and mass entering into the model are equal to heat and mass released through the boundaries and thus no change is observed in the thermodynamic variables

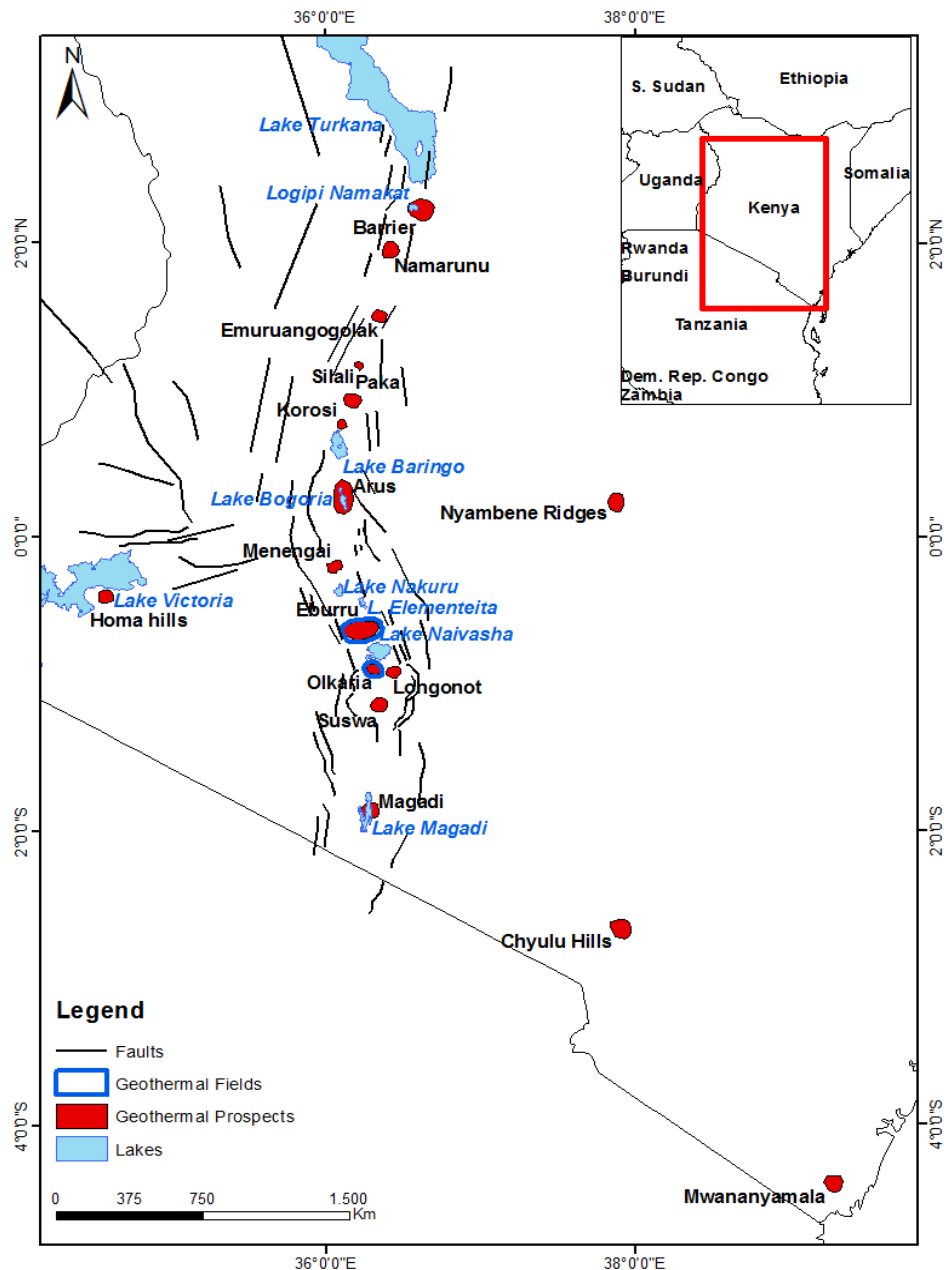


Figure 1 Location map of geothermal prospects in the Kenya Rift valley (Modified from Ofwona et al, 2006).

Numerical modelling has been applied in Olkaria geothermal resource development. The latest revision of the conceptual and numerical models was performed in 2012 when Mannvit/ISOR/Vatnaskil/Verkis consortium (Axelsson et al., 2013a and 2013b unpublished report) undertook a comprehensive study of the field. In the current study a smaller natural state model covering the Olkaria Domes field is developed. The model is then calibrated using well test temperature and pressure logs. The results of this calibration are presented in the form of a natural state model describing the pre-exploitation state of Olkaria Domes geothermal system.

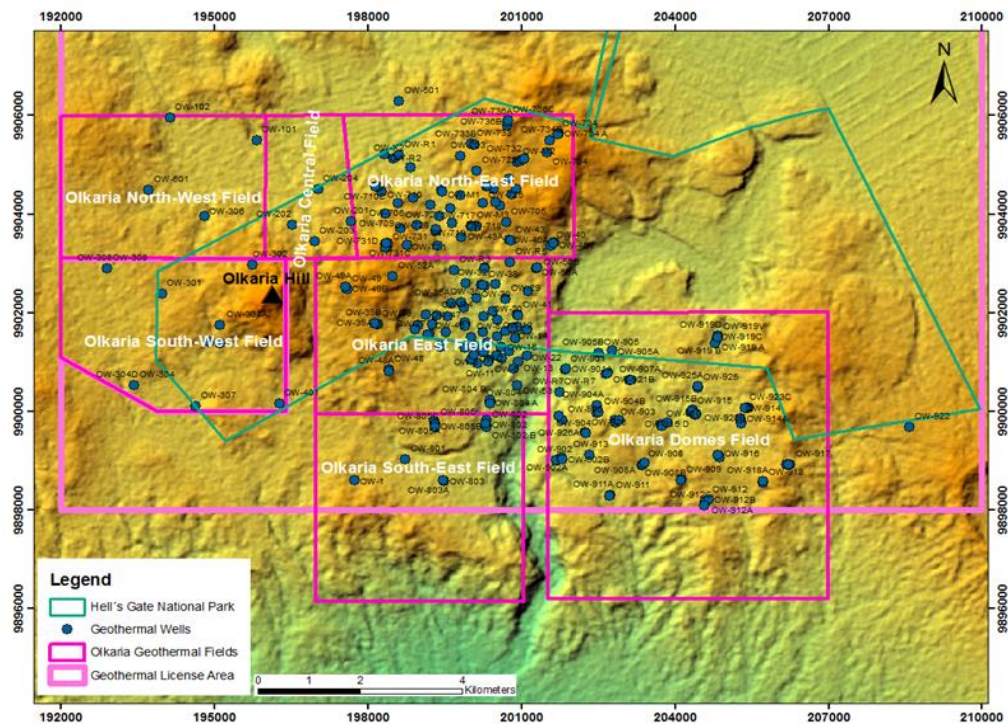


Figure 2 A Map showing different sectors in the Greater Olkaria Geothermal Field (modified from Otieno and Kubai, 2013).

2.2 The Olkaria Domes geothermal system

2.2.1 Regional geology

The Olkaria volcanic system is located south of Lake Naivasha on the southern segment of the Kenya rift. It is characterised by numerous volcanic centres of Quaternary age and is the only area within the Kenya rift with occurrences of comendite on surface (Lagat, 2004). The other Quaternary volcanic centres adjacent to Olkaria include Longonot volcano to the southeast, Suswa caldera to the south, and the Eburru volcanic complex to the north. (Figure 1).

Whereas the other volcanoes are associated with calderas of varying sizes, the Olkaria volcanic complex does not have a clear caldera association. The presence of a ring of volcanic domes in the east and south, and south west has been used to invoke the presence of a buried caldera (Lagat, 2004). Seismic wave attenuation studies for the whole of the Olkaria area also indicate an anomaly in an area coinciding with the proposed caldera. (Simiyu et al, 1998)

The Olkaria basalt underlies the Upper Olkaria volcanics in the area to the east of Olkaria Hill while the formation is absent to the west. The formation consists of basalt flows and minor pyroclastics and trachytes. The formation varies in thickness from 100m to 500m and is considered to act as cap-rock for the Olkaria geothermal system (C. B. Haukwa, 1984). The Upper Olkaria formation consists of comendite lavas and their pyroclastic

equivalents, ashes from Suswa and Longonot volcanoes and minor trachytes and basalts. (Peter A. Omenda, 1998). These rocks occur from the surface down to about 500m depth. Comendite is the dominant rock in this formation. The youngest of the lavas is the Ololbutot comendite, which, has been dated at 180 ± 50 years (Clarke et al, 1990) The vents for these young lavas and pyroclastics were structurally controlled with most of the centres occurring along N-S faults/ fractures and a ring structure (Figure 3).

The faults are more prominent in the East, Northeast and West Olkaria fields but are scarce in the Olkaria Domes area, possibly due to the thick pyroclastics cover. The NW-SE and WNW-ESE faults are thought to be the oldest and are associated with the development of the rift. The most prominent of these faults is the Gorge Farm fault, which bounds the geothermal fields in the Northeastern part and extends to the Domes area. The most recent structures are the N-S and the NNE-SSW faults (Lagat, 2004). Four fault systems characterize the field and are associated with fluid movement. These include ENE-WSW, NW-SE, N-S, E-W structures and they are all defined as normal faults through the correlation of lithology and alteration mineralogy zones. These include, but are not limited to the Ololbutot fault, Olkaria fault, Olkaria fracture, Gorge Farm fault, the ring structure and Ol'Njorowa Gorge.

Olkaria Domes, which is the field of focus in this study is the area approximately bound by the Hell's Gate – Ol'Njorowa gorge to the west and a ring of domes to the east and south of the area. (Figure 3). Hydroclastic craters located on the northern edge of the Olkaria Domes area mark magmatic explosions, which occurred in a submerged country (Mungania, 1999). These craters form a row along where the extrapolated caldera rim trace passes. Dyke swarms exposed in the Ol'Njorowa gorge trend in a NNE direction further attesting to the recent reactivation of faults with that trend.

Drilling of Olkaria Domes field began in 1998 with the first three exploration wells, namely OW-901, OW-902 and OW-903. The wells encountered a high temperature system and they discharged on testing. Appraisal drilling began in 2007 with six deviated wells being drilled to a depth of about 2800m. Trachytes are dominant rock in most wells in the Olkaria Domes. They occur in these wells from 554m to bottom depth (Ronoh, 2015) forming stratigraphic sequences with rhyolite, basalt and tuff. The units vary depending on color, texture and intensity of alteration. The interaction of geothermal fluids with rocks under favourable conditions leads to changes in the compositions of both fluids and the rocks. The mineralogy, colour and texture are then altered as a result of either heating or cooling. The main hydrothermal minerals in Olkaria Domes field are zeolites, fine to coarse grained clays, albite, actinolite, calcite, chlorite, chalcedony and quartz. (Ronoh, 2015).

The geology of the Greater Olkaria field and more specifically Domes production field is relevant to this masters thesis. The caprock of this field is mainly of basalt rock type and its occurrence depth was used to estimate vertical permeability in the numerical model. The fault system explained forms the conduits for fluid movement which enter the wellbore through the feedzones. In this study, Feedzones were used to interpret the subsurface structures.

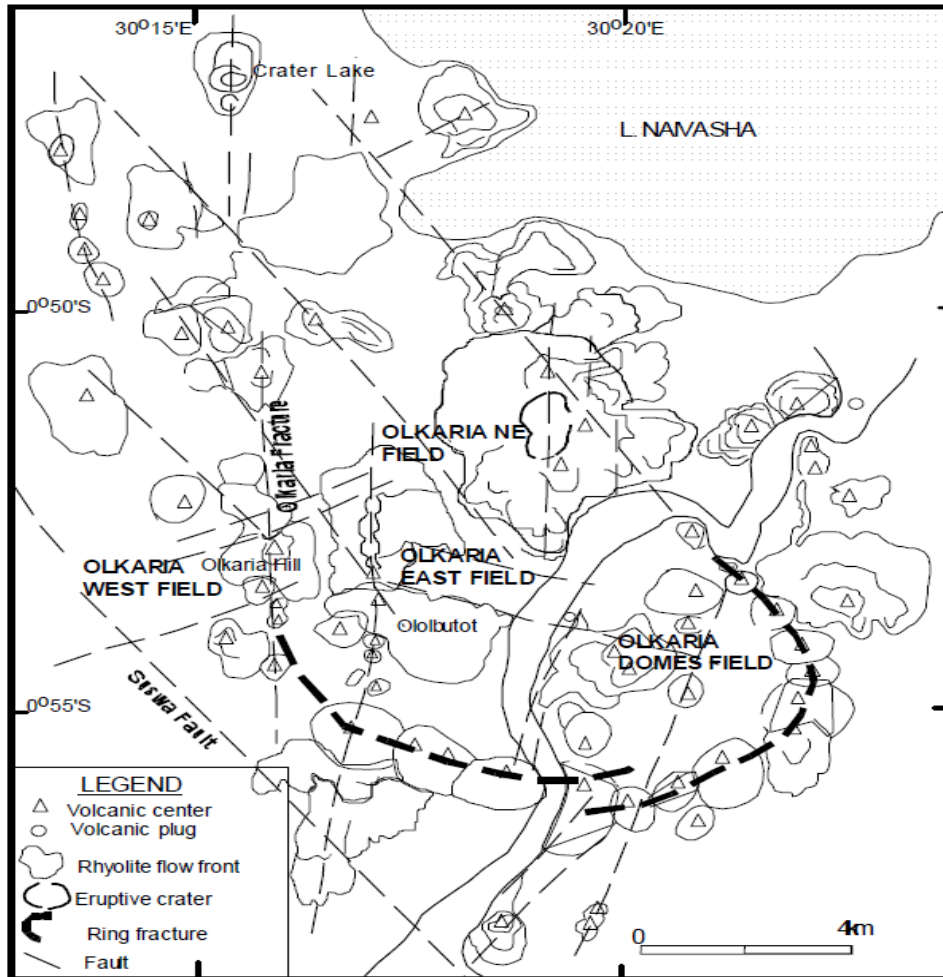


Figure 3 The volcano tectonic map of the greater Olkaria volcanic complex showing the structures in the area (Lagat, 2004).

2.2.2 Geophysical studies

Geophysical studies carried out in Olkaria geothermal area included resistivity, gravity, seismology and magnetics. The study was based on transient electromagnetic (TEM), DC schlumberger and Magnetotelluric (MT) soundings. In magnetotellurics (MT), fluctuations in the natural magnetic field of the earth and the induced electric field are measured. Their ratio is used to determine the apparent resistivity. The transient electromagnetic (TEM) method is where a magnetic field is built up by transmitting a constant current into a loop or grounded dipole; the current is turned off and the transient decay of the magnetic field is used. (Mwakirani M., 2011) Measuring the electrical resistivity of the subsurface is a

powerful prospecting method in surface geothermal exploration. The results from these measurements indicate that the low resistivity anomalies are controlled by structural trends and that the geothermal resource is defined by a low resistivity of 15 Ω m at 1000 m.a.s.l (Onacha, 1993).

Seismic monitoring of micro earthquakes indicates that the Greater Olkaria geothermal area is characterized by a relatively high level of micro-earthquake activity (Simiyu & Keller, 2000). The analysis of focal depth, event location and classification shows that the high frequency events and deep low frequency events occur at the intersection of structures in the area. These shallow events are associated with fluid movements along the structures. Residual aeromagnetic data acquired within the Rift Valley shows that the Olkaria area has a positive anomaly that has a NW-SE trend. The negative anomalies correspond to normally magnetized rocks whereas the positive anomaly occurs in a demagnetized zone corresponding to the heat source that is of silicic origin. This provides some evidence for heat source at a temperature above the Curie point of magnetite (above 575°C) close to the surface (Onacha, 1990).

2.2.3 Overview of Olkaria Domes geochemistry data

Geothermal reservoir fluids in the Olkaria Domes are bicarbonate in nature and correspond to peripheral waters (Malimo, 2009). Solute and gas geothermometry indicate high temperatures in the range of 250°C – 350°C (Malimo, 2009). Fluids extracted from Olkaria Domes wells contain low calcium concentrations and high pH. Calcite scaling can be expected to be minimal in these wells but the fluid has to be separated above 100°C to prevent silica scaling (Karingithi, 2000). Studies done by (Kamunya et al; 2015), show that wells in the Olkaria Domes field discharge a mixture of chloride and bicarbonate end-member, as shown (Figure 4). The chemical content of fluids from the Domes sector supported the possibility of a hot up-flow in the southeast part of Domes as well as supporting the contention that the resources there extend further to the east and southeast. The existence of these up-flow zones was supported by Cl^- concentration and Na/ K temperature estimates as well as resistivity data (Mannvit/ISOR/Vatnaskil/Verkis Consortium, 2011).

Bicarbonate waters are found in areas to the northeast and southwest of the Olkaria Domes field. This could be due to the contribution of recharge fluids through the NE-SW faulting and the interpreted buried caldera that forms a concentric series of rhyolitic ash domes in the east, frequently referred to as the ring structure (Kamunya et al; 2015). Well OW-901 fluids exhibited relatively lower molecular gas ratios of $\text{CO}_2/\text{H}_2\text{S}$, CO_2/H_2 compared to wells OW-902 and OW-903. The lowest gas ratios of $\text{CO}_2/\text{H}_2\text{S}$ and CO_2/H_2 and the highest ratios of H_2/CH_4 often indicate fluids that are close to the upflow or have the most direct route to the surface. These ratios are also indicative of proximity to an underlying hot water source.(Opondo, 2008). Well OW-901 is on the north western part of the Olkaria Domes field as illustrated in Figure 11. The geochemistry of the Olkaria Domes geothermal system together with the analysis of the temperature contours was used in this study to estimate the location of heat and mass sources in the numerical modelling. More analysis of the geochemistry fluids is recommended to understand the fluid movement within the system. This will in future help to accurately map the subsurface structures.

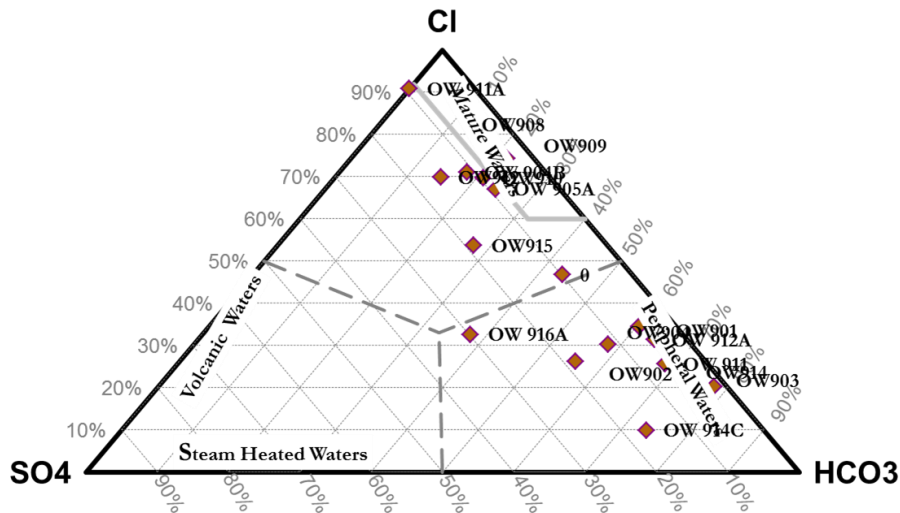


Figure 4 Water types of the Domes geothermal area. (Kamunya et al., 2014).

2.2.4 Well data

The borehole temperature and pressure data for the wells used in this study was obtained by use of kuster mechanical tools. It was adopted from the 2011/2012 optimization study of the Greater Olkaria geothermal field by the Mannvit/ISOR/Vatnaskil/Verkis consortium (Axelsson et al., 2013a and 2013b unpublished report). The optimization study was conducted by Mannvit Consortium to advise Kenya Electricity Generating Company Limited (KenGen) on how to manage the geothermal resources within the Greater Olkaria Geothermal Area (GOGA). There is ongoing production drilling in this field and it is prudent for KenGen to optimize the resource in a sustainable manner.

2.3 Literature review

2.3.1 Field development

Olkaria Domes field is located at the southeast of the Greater Olkaria geothermal area. It is a high-temperature field with most of the wells producing two-phase fluid. Surface exploration in Olkaria Domes field was completed in 1993 and drilling of the first three exploration wells was carried out in 1998 -1999. Drilling of six appraisal wells started in 2007 and the results from the drilled wells updated the conceptual model which led to the siting and drilling of the production wells.

Currently, Olkaria IV power plant located in Olkaria Domes was commissioned in October, 2014 and a two single flash condensing turbines are used to generate 150 MW_e. Drilling and well discharge testing is still ongoing in Olkaria geothermal field to provide steam for new power plants.

2.3.2 Conceptual model

The conceptual model of a geothermal system gives an understanding of the nature and characteristics of the system in question. It is created using analysis of the geological and geophysical information, temperature and pressure data, as well as information on the chemical content of the reservoir fluids. Conceptual models should explain the heat source for the reservoir in question and the location of recharge zones, location of the main flow channels, the general flow patterns within the reservoir as well as reservoir temperature and pressure conditions. A comprehensive conceptual model should furthermore, provide an estimate of the size of the reservoir involved.

The conceptual model of the Olkaria geothermal system has, ofcourse evolved through time as more information has been accumulated through surface exploration, drilling, utilization and reservoir engineering work. The first published version of the conceptual model was done by SWECO and Virkir (1976). This was a very simple model due to the limited drilling done at that time and included a boiling geothermal reservoir overlain by steam zone, capped by tuffaceous caprock. (Figure 5). Meteoric water was seen as percolating down to 1600 mbsl where it was heated to about 320 °C, in this first conceptual model. The hot water was then assumed to rise and eventually boil with the steam condensing below the caprock to sink again in a kind of convective cycle.

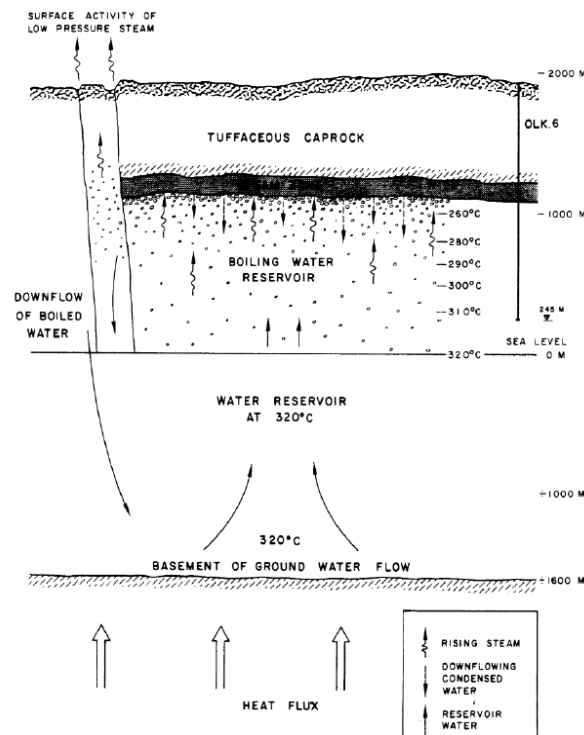


Figure 5 An early conceptual model of the Olkaria East geothermal system (SWECO and Virkir, 1976).

Later revisions saw the model expanding to cover more of the Olkaria area and include several zones of hot up-flow, first in the Northeast and West sectors and later in the East

sector as well (Ofwona, 2002). These versions of the model also assumed fluid recharge to come from more or less all sides of the Olkaria area, as well as a cold down-flow zone in the centre of the field associated with Ololbutot fault. In 2002 Ofwona (Ofwona, 2002) presented an updated version of the conceptual model, visualized as shown in Figure 6. According to this revised model, the hydrothermal systems of western and eastern Olkaria are clearly separated by the low pressure and low temperature zone of central Olkaria. Ofwona postulates two possible up-flow zones in Olkaria Northeast and Olkaria East. Extensive boiling also occurs in the up-flow zones to form steam caps below the caprock, according to this revision. Cold recharge into the Olkaria geothermal system is assumed to occur from all directions in the 2002 conceptual model.

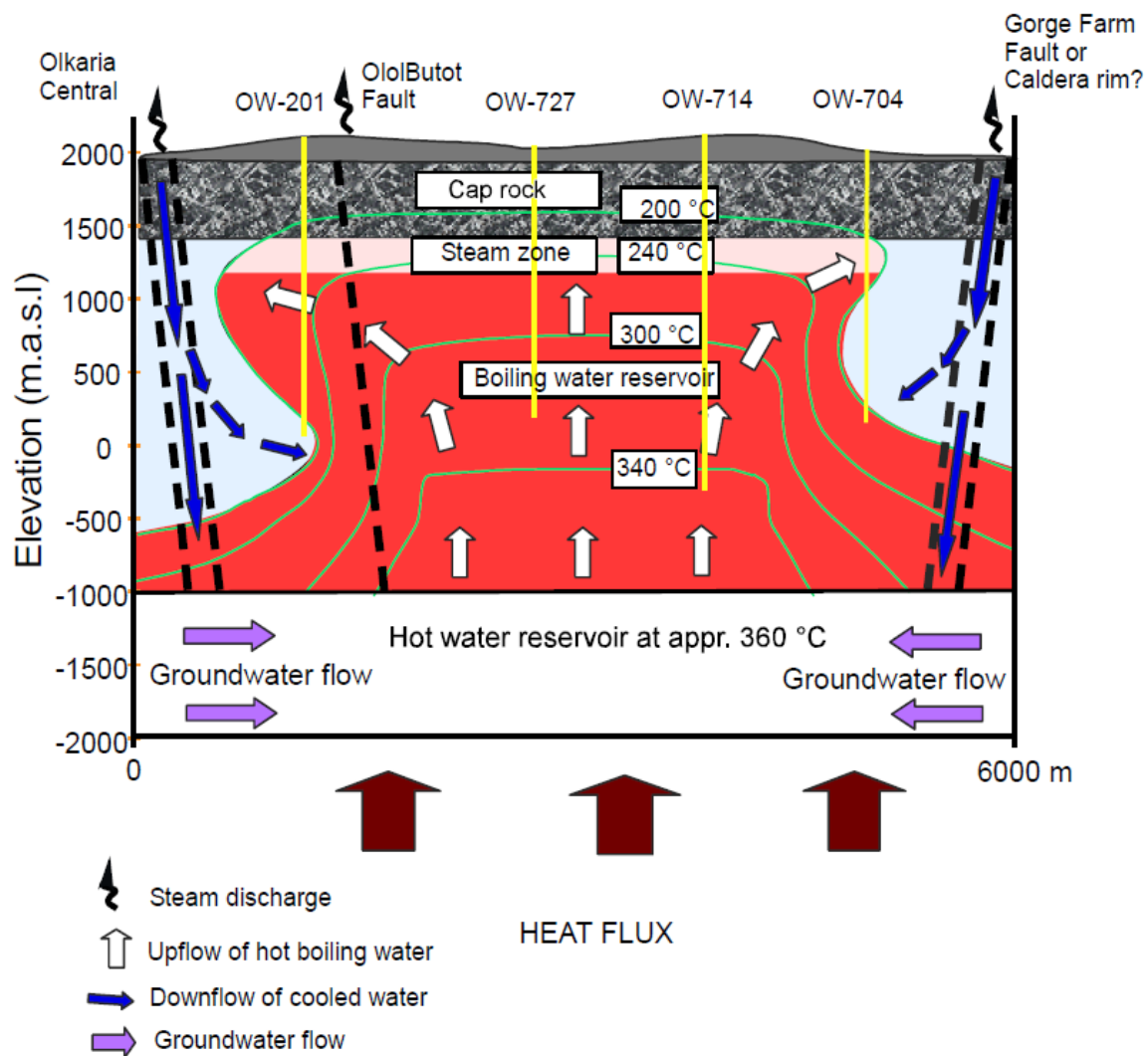


Figure 6 A revised conceptual model of the Olkaria East geothermal system from 2002 (Ofwona, 2002).

According to West-JEC 2009 conceptual model, the heat source of the Olkaria geothermal system is considered to be a magma chamber, which has fed the most recent volcanic events in the area. There is furthermore believed to be a possibility that the magma chamber peaks in several locations each creating convective heat transfer and providing hot recharge to different parts of the geothermal system. In addition to up-flows in the Northeast and East sectors such up-flow, another upflow is proposed in the Domes sector, in connection with what West-JEC refers to as R6 fault (Figure 7). From analysis of temperature data, production characteristics of tested wells and interpretation of geophysical data, possible locations of up-flow zones are proposed by West-JEC in the central part of the East production field, south eastern part of the Domes sector, as that sector was defined at the time, below wells OW-903A and OW-908. The West-JEC chemical model for the for the eastern half of the Olkaria geothermal system suggests that the fluids of the three sectors have a common origin at depth, as ~325- 340 °C water with Cl⁻ concentration at ~ 450 mg/l. A common NW-SE trending structure (Figure 7) and its extension northwards may connect all three upflow zones at great depth. (West-JEC Inc, 2009).

The Olkaria geothermal field is inside a major volcanic complex that has been cut by N-S trending normal rifting faults. It is characterized by numerous volcanic rhyolitic domes, some of which form a ring structure, which has been interpreted as indicating the presence of a buried volcanic caldera.

Olkaria Domes is one of the main sectors of the Greater Olkaria Geothermal Area (GOGA) that has been subdivided as shown in the Figure 2 above. The conceptual model of the GOGA area has been constantly updated and developed in past years (Mannvit/ISOR/Vatnaskil/Verkis Consortium, 2011 unpublished). This sector of the field encompasses one of the heavily explored parts where the existence of an exploitable resource has been confirmed by extensive drilling and long-term utilisation and where comprehensive information is available on the nature and production capacity of the geothermal system.

Micro-seismic monitoring in the Olkaria area from 1996 to 1998 has provided highly valuable data for the conceptual model of the Olkaria Geothermal System. This includes both the location of seismic events as well as information on S-wave attenuation derived from the data, which has been interpreted as reflecting volumes of partially molten material.

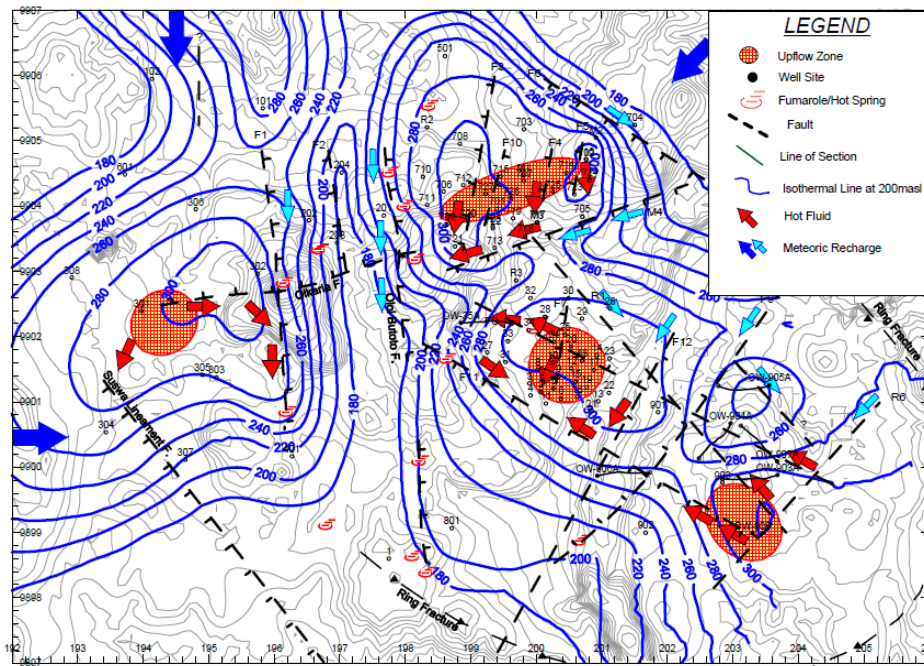


Figure 7 Horizontal view of 2009 conceptual model of the Greater Olkaria geothermal system (West-JEC, 2009).

Flow-paths are controlled by predominantly N-S, NW-SE and NE-SW trending faults. In addition to the main faults of the system, the ring structures encircling the Domes field (Figure 3) represent a possible inner and outer rim of the proposed Olkaria Caldera. Both the inner and the outer rim connect to the Gorge Farm fault, located north and east of the main production area and possibly extending to Lake Naivasha. Cold water is believed to flow into the system along the Ololbutot fault, which is also associated with plentiful geothermal surface manifestations.

The revision of the Greater Olkaria geothermal system conceptual model was again carried out towards the end of 2014. The new resistivity data from recent soundings, chemistry data and steam produced as well as production monitoring data since 2012 was incorporated. The heat sources that feed the system are believed to be magmatic bodies centred below the West Production Field (WPF), East Production Field (EPF) and Southeast Domes area as presented in Figure 8.

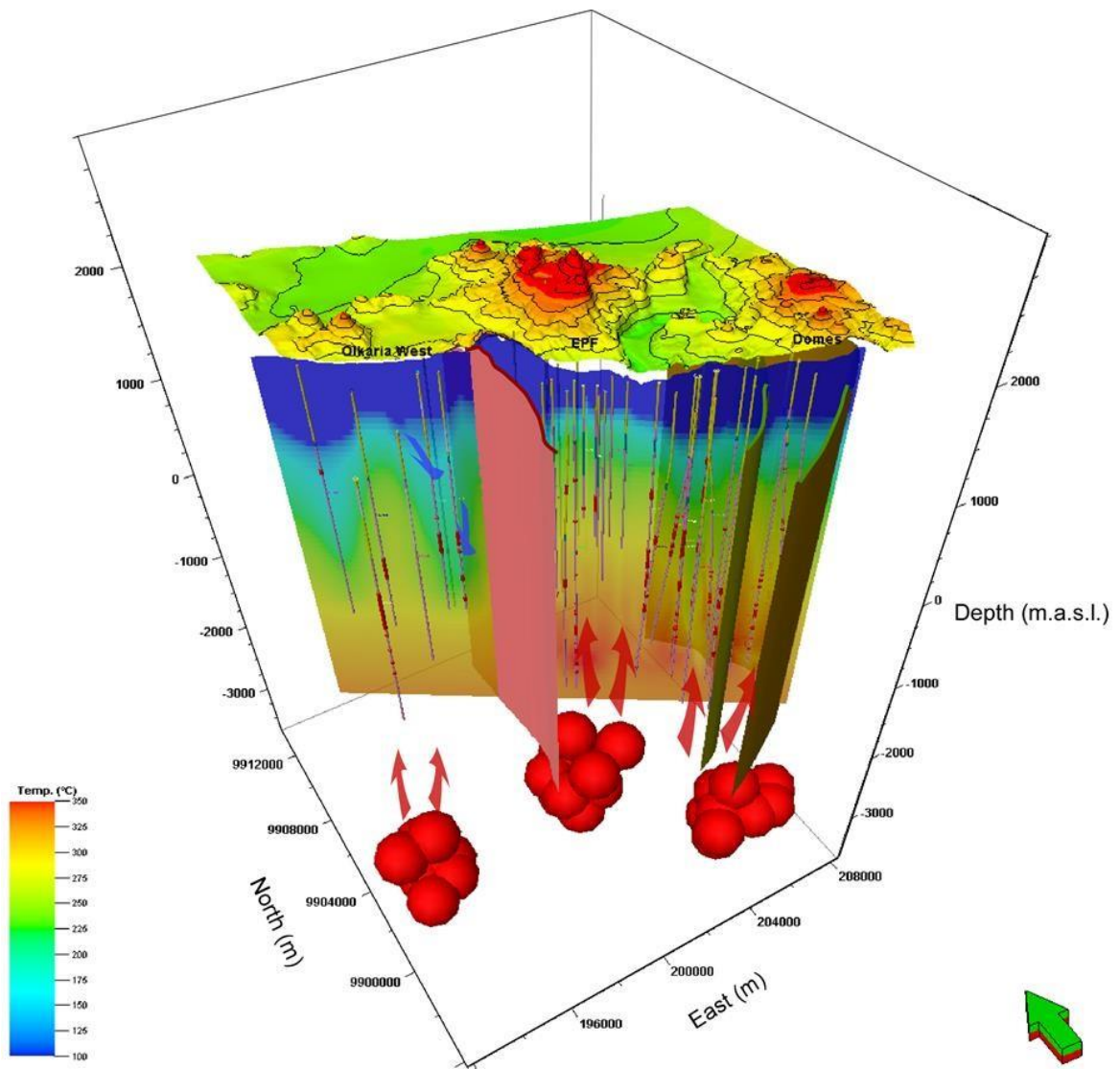


Figure 8 Revised conceptual model of the Greater Olkaria geothermal system (Mannvit Consortium, 2014).

3 METHODS

3.1 Interpretation of feedzones

Permeability is the ability of a rock to transmit fluids and hence controls fluid movements in the field. It is an important parameter in the understanding and development of a geothermal system and one of the main inputs in the development of field conceptual models and reliable numerical models for accurate field predictions. There are two types of permeability in geothermal systems; intrinsic and secondary permeability. Intrinsic permeability is formed from the nature of lithology deposition for example pore space interconnectivity and bedding structures while secondary permeability on the other hand is formed after deposition by the process of weathering, brittle deformation and hydrothermal alteration.

Crucial to the successful utilization of a geothermal system is the knowledge of the permeability structure and specifically feed zones which are the sources of geothermal fluid entry into the wellbore. Understanding the nature and distribution of feedzones is particularly relevant for well targeting and useful in providing the constraints to reservoir models. It should be noted that although feedzones are an indication of permeable zones in a well, not all permeable zones will be detected as feedzones during a PTS measurement. The distinction between a permeable zone and a feedzone is that a feedzone requires interconnected permeability and a pressure difference with respect to the fluid column in the wellbore at that depth. If the fluid pressure in the feedzone is greater than the fluid column at this depth, then the fluid will enter the well. Similarly, if the fluid pressure in the feedzone is under-pressured, then fluid will escape the well into the formation. This is a dynamic process and flow regimes at the permeable zones can make the feedzones ‘appear’ and ‘disappear’ as conditions change.

Understanding of feedzones is achieved by different methods. Feedzone locations in the wellbore are initially located during a well completion test with a temperature-pressure-spinner (PTS) probe. Well completion tests are performed on most wells immediately after the well has been drilled and the slotted liner landed, while the rig pumps are still on-site. The main purpose of a completion test is to identify and characterize the feedzones in a well. Some of the ways feedzones can be identified is by fluid loss or gain and temperature changes in the wellbore. Permeable zones at Olkaria are distributed in the formations from as shallow as a few metres to depths in excess of three kilometres.

Completion tests are conducted in Olkaria immediately after a well has been completed. It involves first conducting a temperature and pressure survey to determine the overall well recovery after drilling and identify the major feedzone depth at which the survey tools shall be stationed during the pumping test. Secondly, step pumping is done while varying the

injection rate from 1000 lpm to 1900 lpm in steps of 300 lpm. This pumping test is used to obtain bulk well permeability. The pressure increases as a result of increased water injection rate, therefore the less the pressure increase in relative terms, the greater the bulk permeability in the well. After this a pressure and temperature measurement is conducted while pumping to obtain the water loss zones in the well. A fall off test is conducted involving monitoring the pressure decay in the well after stopping injection followed by a temperature survey to monitor how it is heating up and the well behaviour after injection. After a well completion test the temperature and pressure in the well is monitored at intervals of seven days to see how the well heats up after drilling and testing. The water loss zones are then identified by plotting the depth against temperature measured while pumping. The feedzones are indicated in the curve by changes in the gradient with the most change showing the location of the biggest feedzones.

3.1.1 Correlation of feed zones with permeability

Targeting structurally controlled permeability in drilling geothermal wells in a high temperature geothermal system remains a challenge because of the difficulties in locating and characterising faults and fractures and their behaviour within the reservoir. Several techniques have been developed to map out these structures. These include visual surface observations for geological faults and fractures, alteration mineralogy, use of water loss zones during pumping tests and drilling, temperature and pressure recovery logs and conducting acoustic televiewer logs of the wellbore. Acoustic televiewer logs provide the most accurate data on faults and fractures; their orientations and the lithology of the boreholes. They can be used to refine the depth of the feedzones and provide new geological information on loss zones in a well.

Permeability structures also control the productivity of geothermal wells as they form the paths for fluid movement in the system either as upflow zones or recharge zones. This report presents the results of the analysis of the major feedzones encountered by wells drilled in Olkaria Domes geothermal field; their role in mapping out subsurface structures and their distribution across the field.

In this thesis, feedzones ranging from 1000 m – 2000 m for ten wells and 2000 m – 3000 m for 26 wells were analysed. The injection profiles for these wells were plotted as shown in figures 8 and 9. From the injection profiles it can be observed that some wells have feedzones at the well bottom. Such wells should have been deepened so as to utilize possible deeper feed zones and maximize well productivity. The current average depth for most of the wells in Olkaria Domes field is 3000m.

The feedzones were also mapped on a temperature model at sea level (approximately 2000 m depth) as shown in figures 8 and 9. These feedzones are aligned in the NW-SE, N-S and ENE-WSW directions confirming the geological structures in these directions. The feedzones also show regional distribution of permeability across the Domes field. It can be deduced that permeability in the Olkaria Domes field is good at the major up-flow zones and poor in the periphery of these upflow zones.

Wells with major feedzones at a depth of 1000 -2000

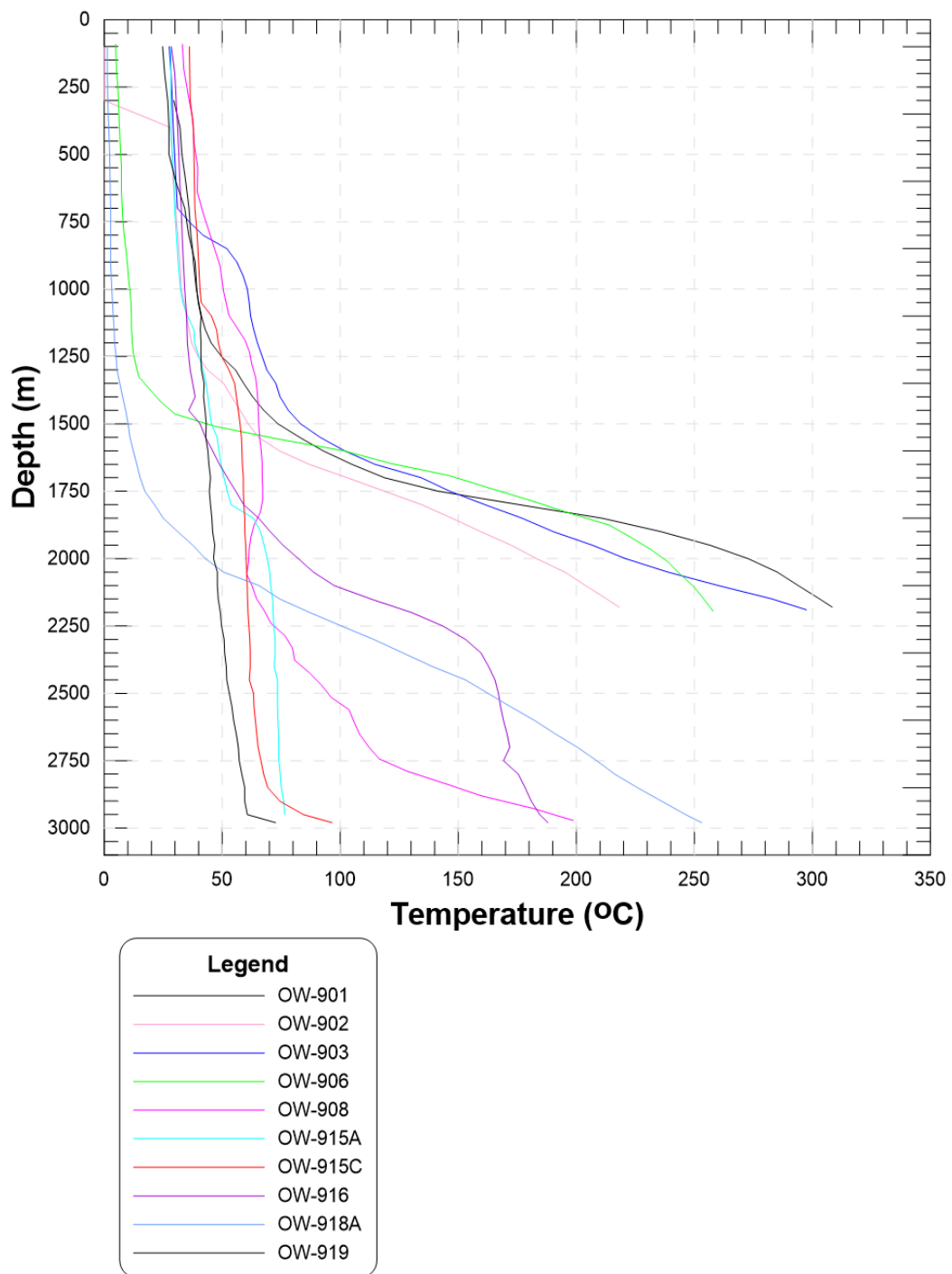


Figure 9 Wells with feed zones at 1000 m – 2000 m

Wells with Feedzones at a depth of 2000m - 3000m

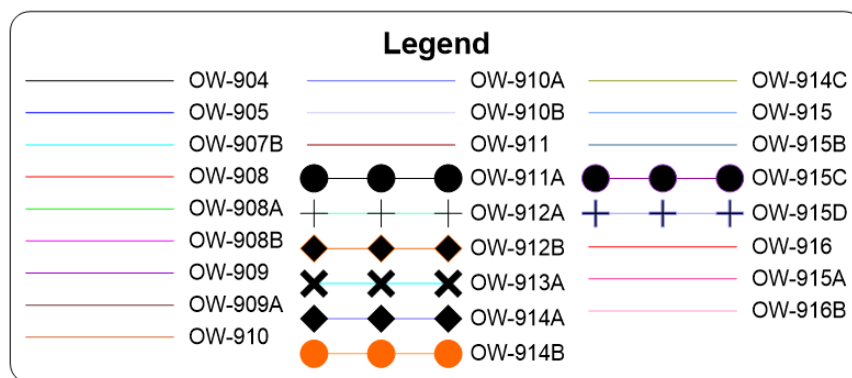
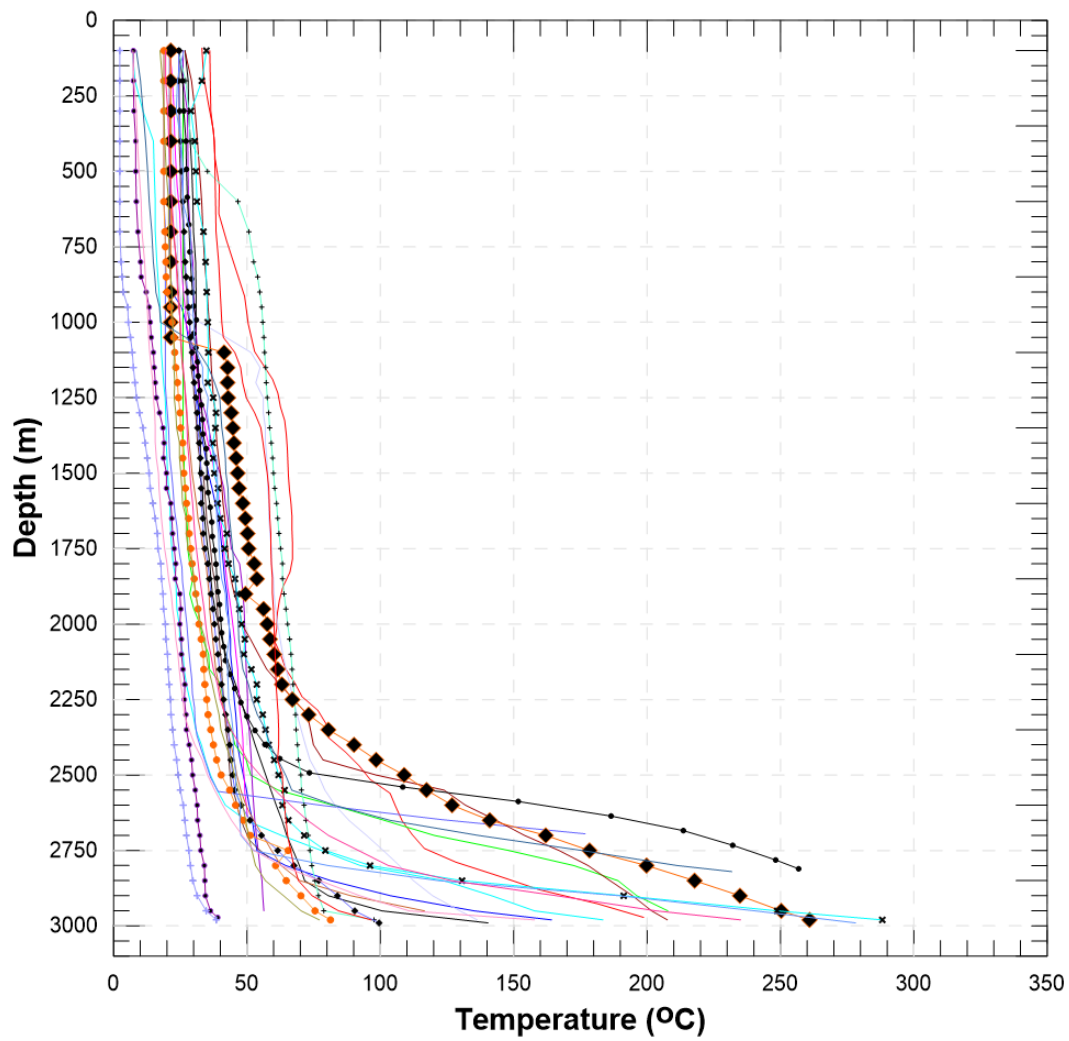


Figure 10 Wells with feed zones at 2000 m – 3000 m

3.1.2 Subsurface permeability structures and numerical modelling

Subsurface permeability structures provide fluid flow, within, into and out of a geothermal system. The information about permeability is an important parameter in conceptual models of geothermal systems. The conceptual models are an important tool throughout exploration, development and utilization of geothermal systems, whereby they are used in both field development planning and well siting. In this project, the understanding of subsurface permeability controls in Olkaria Domes geothermal system was emphasized when creating a numerical model of the system notably when assigning the permeability of the reservoir rocks.

3.1.3 Olkaria Domes Conceptual Model

Conceptual model development requires a multi-disciplinary approach where parameters from different geosciences involved in the exploration and development are put together. The model requires the understanding of the heat source, the fluid recharge to the system and the up-flow zones, the main permeable regions of the system, the initial temperature and pressure conditions of the system and the nature of the boundary conditions. In this study, the formation temperature isotherms were used to create the Olkaria Domes temperature model shown in figures 12 and 13

Figure 11 illustrates the well locations and cross-sections A – A' and B – B' across the Olkaria Domes geothermal field (figures 12 and 13). The two cross-sections were made for analysis of the vertical temperature models. Cross-section A – A' runs from wells OW-906A to OW-917. There is an updoming of isotherms at around wells OW-915 and OW-903, an indication of up-flow zone at this particular location. The temperature decreases slightly towards well OW-917 which is drilled close to the inferred ring structure at Olkaria Domes field.

The temperature cross-section B – B' also confirms a similar temperature decreasing trend towards wells OW-918 and OW-918A to the East of Olkaria Domes geothermal field. These wells may be drilled close to the downflow of this field. Cooler water may enter from the ring structure where it may be at a higher pressure due to the greater density of the cooler water column. It can still be inferred that wells OW-903 and OW-908B are close to an upflow zone. These temperature cross-sections were used in the initial estimation of the location of the heat sources in the numerical model in this study.

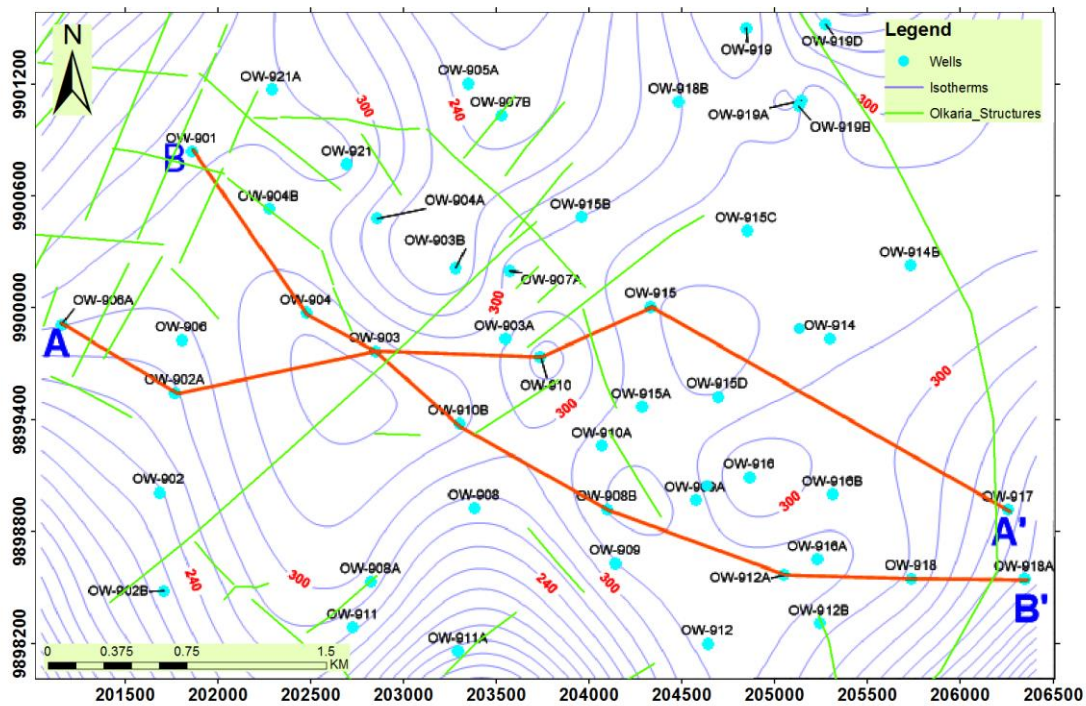


Figure 11 Map showing well locations and cross-sections across Olkaria Domes geothermal field.

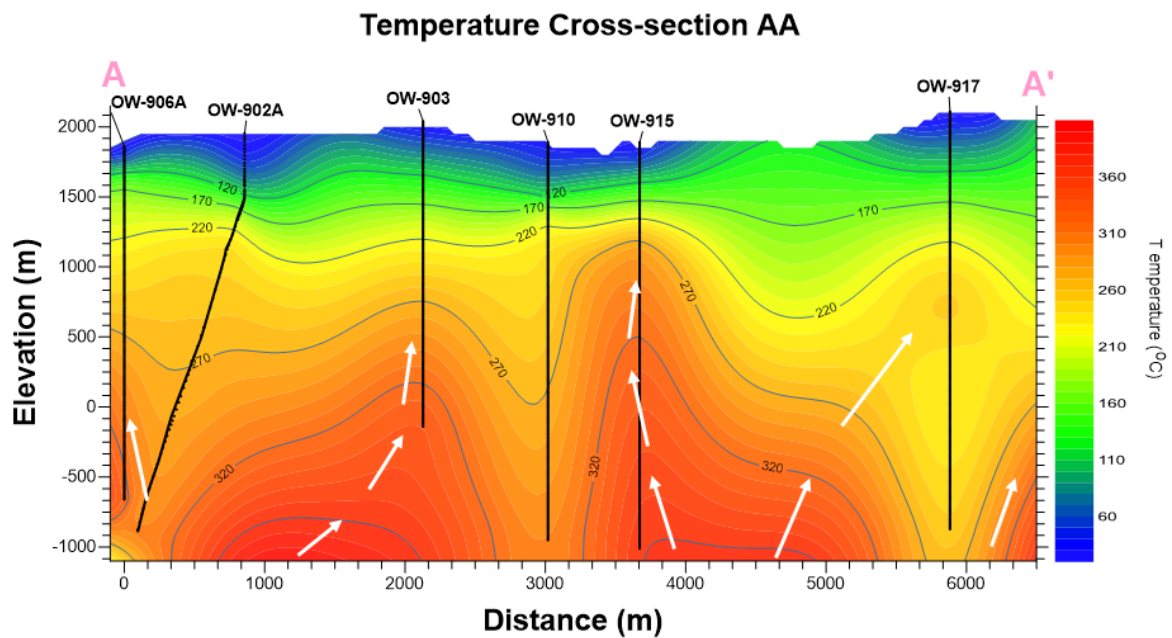


Figure 12 A map showing temperature model cross-section A - A'.

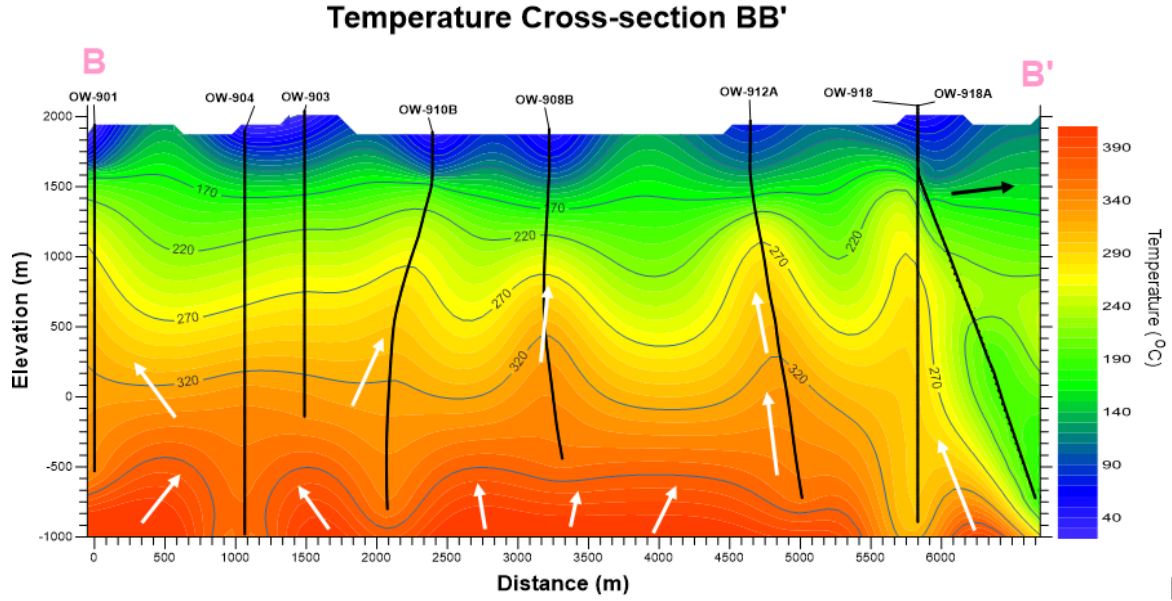


Figure 13 A map showing temperature model cross-section B - B'.

3.2 Numerical Modelling

3.2.1 Theoretical background of numerical modelling using TOUGH2

TOUGH2 is a numerical simulator for nonisothermal flows of multicomponent, multiphase fluids in one, two and three-dimensional porous and fractured media (Pruess et al; 2012). The code solves heat (energy) transfer and mass conservation equations into and out of every element of a mesh. It can be applied in geothermal reservoir engineering, nuclear waste disposal, environmental assessment and remediation and unsaturated zone hydrology.

3.2.2 Forward modelling using TOUGH2

The geothermal reservoir simulator used in this study is TOUGH2 (Pruess et al., 2012) which solves transient discretized mass and energy conservation equations. The basic mass and energy balance equations solved by TOUGH2 code can be written in the general form;

$$\frac{d}{dt} \int_{V_n} M^k dV_n = \int_{\Gamma_n} F^k \cdot n d\Gamma_n + \int_{V_n} q^k dV_n \quad (3.1)$$

F denotes the mass flux, q denotes sinks and sources while n is a normal vector on the surface element $d\Gamma_n$, pointing inwards into V_n and the quantity M appearing in the accumulation term represents mass or energy per volume, with $k=1, \dots, NK$ for mass components (like water, air or solutes-tracer) present in the flow system being modelled

and $k=NK+1$ for heat components being transported. Equation (3.1) expresses the fact that the rate of change of fluid mass in V_n is equal to the net inflow across the surface of V_n plus net gain from the fluid sources.

The general form of the mass accumulation term is;

$$M^k = \phi \sum_{\beta} S_{\beta} \rho_{\beta} X_{\beta}^k \quad (3.2)$$

In the above equation, the total mass of the component k is obtained by summing over the fluid phases β (that is liquid and gases). ϕ is the porosity, S_{β} is the saturation of the phase β , ρ_{β} is the density of phase β and X_{β}^k is the mass fraction of the component k present in phase β . Similarly the heat accumulation in the multiphase system is

$$M^{Nk+1} = (1 - \phi) \rho_R C_R T + \phi \sum_{\beta} S_{\beta} \rho_{\beta} u_{\beta} \quad (3.3)$$

Where ρ_R and C_R are grain density and specific heat of the rock respectively, T is temperature and u_{β} is specific internal energy in phase β .

Advective mass flux is the sum over phases.

$$F_{adv}^k = \sum_{\beta} X_{\beta}^k F_{\beta} \quad (3.4)$$

And individual phase flux is given by a multiple version of the Darcy's law:

$$F_{\beta} = \rho_{\beta} u_{\beta} = -k \frac{k_{r\beta} \rho_{\beta}}{\mu_{\beta}} (\nabla P_{\beta} - \rho_{\beta} g) \quad (3.5)$$

u_{β} is the Darcy velocity (volume flux) in phase β , k is absolute permeability, $k_{r\beta}$ is the relative permeability to phase β , μ_{β} is the viscosity while P_{β} is the fluid pressure in phase β normally obtained by summing the pressure of a reference gas phase and the capillary pressure of that phase. g is the vector of gravitational acceleration.

Heat flux includes conductive and convective components

$$F^{Nk+1} = -\lambda \nabla + \sum_{\beta} h_{\beta} F_{\beta} \quad (3.6)$$

where λ is thermal conductivity and h_{β} is the specific enthalpy in phase β

3.2.3 Space and time discretization in TOUGH2 numerical modelling

For numerical simulations, the continuous space and time must be discretized. The mass and energy balance in equation (3.1) is discretized in space using the integral finite difference method (C. Haukwa, 1998) by introducing appropriate volume and area averages. The discretization approach used in the integral finite difference method and the definition of the geometric parameters are illustrated in Figure 14.

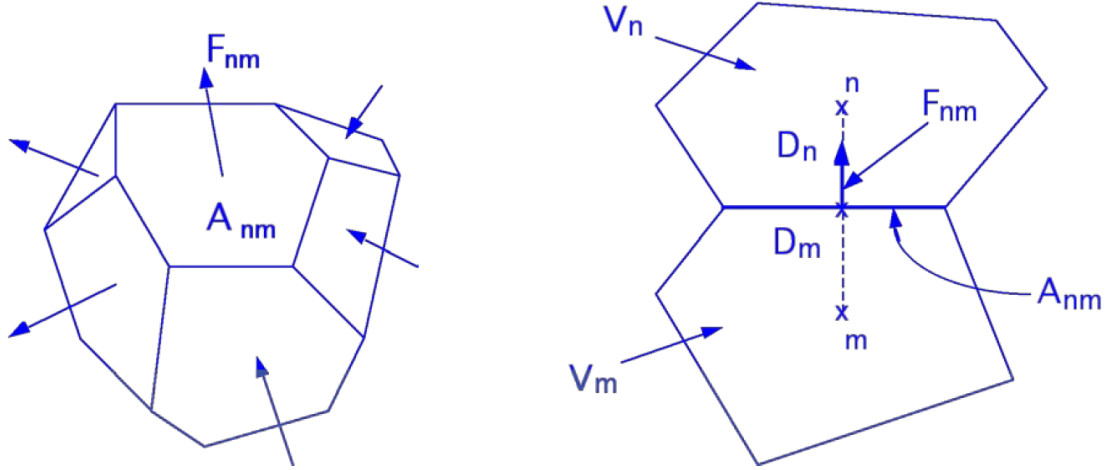


Figure 14 Space Discretization and geometry data (Pruess, 1999).

The mass and heat accumulation term becomes

$$\int_{V_n} M dV = V_n M_n \quad (3.7)$$

while the source and sink terms become

$$\int_{V_n} q^k dV_n = q_n V_n \quad (3.8)$$

where M_n and q_n are the average value of the two mass and energy balance terms over V_n . The total flux crossing over the two interfaces of the volume elements V_n and V_m as shown in Figure 14 can be approximated by discrete summation as

$$\int_{\Gamma_n} F^k \cdot n d\Gamma = \sum_m \int_{A_{nm}} F^k \cdot n d\Gamma = \sum_m A_{nm} F_{nm} \quad (3.9)$$

F_{nm} is the average over surface segment A_{nm} between the volume element V_n and V_m . The discretized flux corresponding to the basic Darcy flux term Equation (3.5) is expressed in terms of averages over parameters for volume elements V_n and V_m as follows

$$F_{\beta,nm} = -K_{nm} \left[\frac{K_{r\beta} \rho_{\beta}}{\mu_{\beta}} \right]_{nm} \left[\frac{P_{\beta,n} - P_{\beta,m}}{D_{nm}} - \rho_{\beta,nm} g_{nm} \right] \quad (3.10)$$

nm denotes a suitable averaging at the interface between the grid blocks n and m . $D_{nm} = D_m + D_n$ which is the distance between the nodal points in n and m while g_{nm} is the component of gravitational acceleration in the direction of m to n . The basic geometric parameters used in space discretization are illustrated in Figure 9.

Substituting equations (3.7), (3.8) and (3.9) into equation (3.1) results to a set of first-order ordinary differential equations in time.

$$\frac{dM_n^k}{dt} = \frac{1}{V_n} \sum_m A_{nm} F_{nm}^k + q_n^k \quad (3.11)$$

Time is discretized as a first order finite difference. The flux, sink and source terms on the right hand side of the equation (3.11) are evaluated at the new level $t^{k+1} = t^k + \Delta t$, to obtain the numerical stability needed for efficient calculation of multiphase flow. The time discretization results to equation (3.12) below with $R_n^{k,k+1}$ introduced as residuals

$$R_n^{k,k+1} = M_n^{k,k+1} - M_n^{k,k} - \frac{\Delta t}{V_n} \{ \sum_m A_{nm} F_{nm}^{k,k+1} + V_n q_n^{k,k+1} \} \cong 0 \quad (3.12)$$

Equation (3.12) is solved by Newton-Raphson iteration by introducing an iteration index p and expand the residual at iteration step $p + 1$ in a Taylor series in terms of those at index p

$$R_n^{k,k+1}(x_{i,p+1}) = R_n^{k,k+1}(x_{i,p}) + \sum_i \left. \frac{\partial R_n^{k,k+1}}{\partial x_i} \right|_p (x_{i,p+1} - x_{i,p}) = 0 \quad (3.13)$$

Retaining only terms up to first order results in;

$$-\sum_i \left. \frac{\partial R_n^{k,k+1}}{\partial x_i} \right|_p (x_{i,p+1} - x_{i,p}) = R_n^{k,k+1}(x_{i,p}) \quad (3.14)$$

All terms $\partial R_n / \partial x_i$ in the Jacobian matrix are evaluated by numerical differentiation to achieve maximum flexibility in the manner in which various terms in the governing equations may depend on the primary thermodynamic variable. Iterations are done until all the residuals are reduced below a preset convergence tolerance typically chosen as $\varepsilon = 10^{-5}$.

$$\left| \frac{R_n^{k,k+1}}{M_n^{k,k+1}} \right| \leq \varepsilon \quad \left| \frac{R_n^{k,k+1}}{M_n^{k,k+1}} \right| \leq \varepsilon \quad (3.15)$$

3.2.4 Inverse Modelling

iTOUGH2 which provides inverse modelling capabilities for the TOUGH2 code contributes to conceptual and numerical model development only in the sense that alternative model designs can be tested against one another in their ability to explain observed data. A failure to match certain data may point towards aspects of the model that need to be refined. Parameters can be estimated by automatically calibrating the multiphase flow model against measured data of the system response (Finsterle, 2007). Inferring model-related parameters from observations by means of a process model is termed as inverse modelling.

The parameters to be estimated are selected coefficients in the governing flow equations. They may include hydrogeologic and thermophysical properties, initial and boundary conditions and parameterized aspects of the conceptual model. The interpretation of these parameters depends on the model structure and the overall purpose of the specific model. Inverse modelling involves several interacting steps. Starting from a conceptual model of the system, the results of parameter estimation may indicate that the underlying model structure has to be modified. This process of iteratively updating the conceptual model and its parameters is sometimes referred to as model identification. iTOUGH2 focuses more on narrow aspect of inverse modelling, namely parameter estimation by automatic model calibration. This method has been used in this study to calibrate the model and automatically assign the permeability values of the different rock types in the model mesh.

3.2.5 Mesh design and boundary conditions

The mesh of the Olkaria geothermal field was generated using Steinar software package version 7.7. This software uses Amesh program. Amesh can generate 1D, 2D or 3D numerical grids for a given set of locations and the formulation is based on integral finite difference method (C. Haukwa, 1998). In this method, a mesh of elements is created within model domain where the interfaces between the neighbor elements are perpendicular bisectors of the line connecting the line centres. The interface distances are the meridians of the line connecting the centres. From the list of element locations (centre points), the program determines element volumes and the connection information, i.e areas, connection distances and the angle (C. Haukwa, 1998). The input file for TOUGH2 simulator is compatible with the output files generated by the RockEditor software package.

The mesh that was generated in this study for the Olkaria Domes field covers 500 km² and is about 3300 m thick, ranging between 1900 m.a.s.l to -1250 m.b.s.l. The mesh consists of 12241 elements and 47748 connections. The outermost elements of the grid are slightly larger and have same rock type with very low permeability to keep stable pressure and temperature at the boundary with the top and bottom layers set inactive and relatively impermeable. The mesh grid boundary was set far from Olkaria Domes geothermal system

in order to minimize the influence from the surrounding environment. The elements at the centre of the geothermal system were dense where the thermodynamic gradients are expected to be greater in space and time.

The model consists of 16 layers of varying thickness while the horizontal mesh remains the same for every layer. (Figure 16) shows the vertical view of the mesh with the layers named in alphabetical order. Layers A and P represent the top and bottom layers respectively and both layers are inactive. Layers B to E represent the caprock as is exhibited by the conductive temperature gradient in the measured data plots. Layers F to O constitute the high temperature reservoir. Most of the wells in Olkaria Domes geothermal field have been drilled as deep as layer O (at approximately 2850 m depth).

Different rock types were assigned to different regions in the model (see Figure 15). An assumption was made that all the elements have the same physical properties such as density, porosity, thermal conductivity and specific heat capacity but with different permeability.

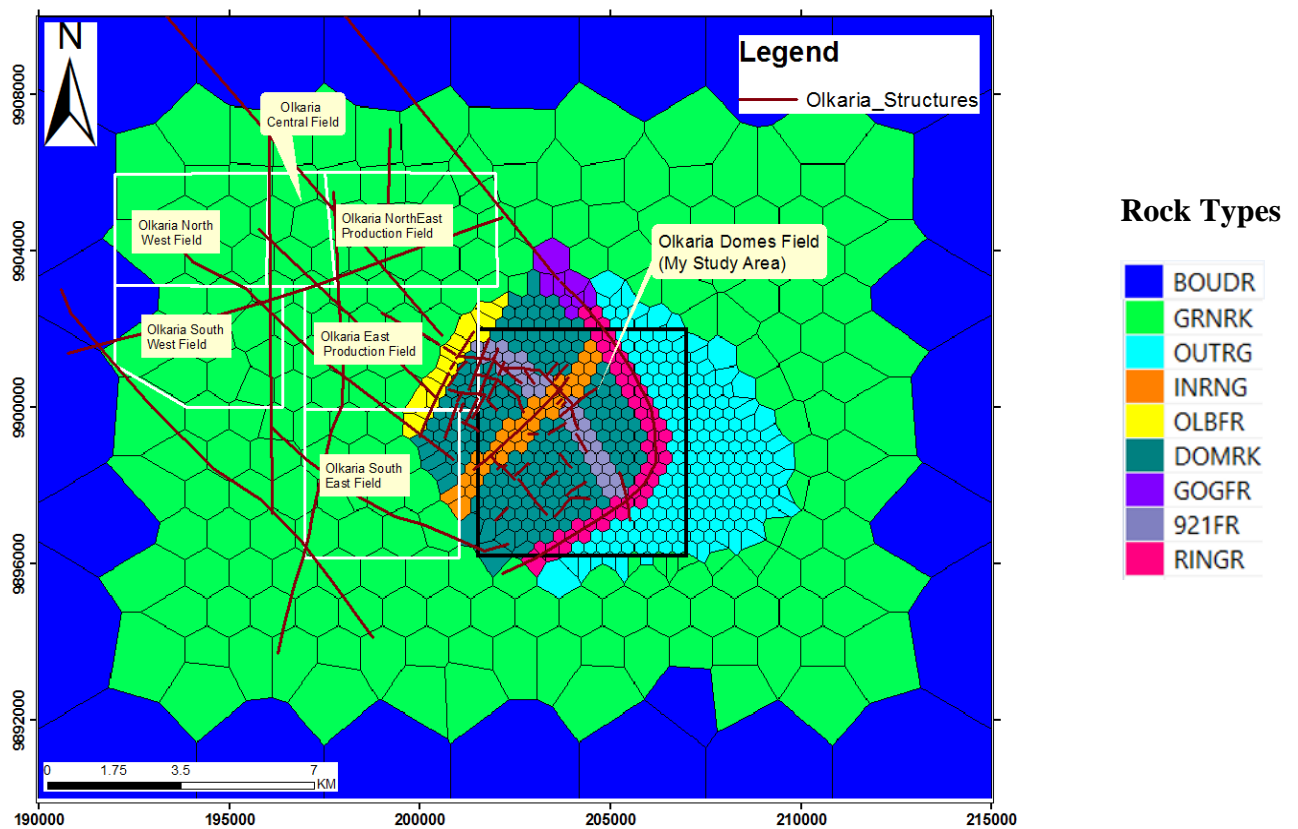


Figure 15 The numerical model grid of the Olkaria geotherma system with emphasis on the Domes production field.

The caprock was assigned the same permeability distribution while the permeability distribution in the reservoir rocks was such that high permeability rocks were assigned to the upflow zones and lower permeability further out. These initial guesses were made

before calibration process began. The rocks at the ring structure were assigned a different rock type as well as two NW-SE and NE-SW trending structures in Olkaria Domes field.

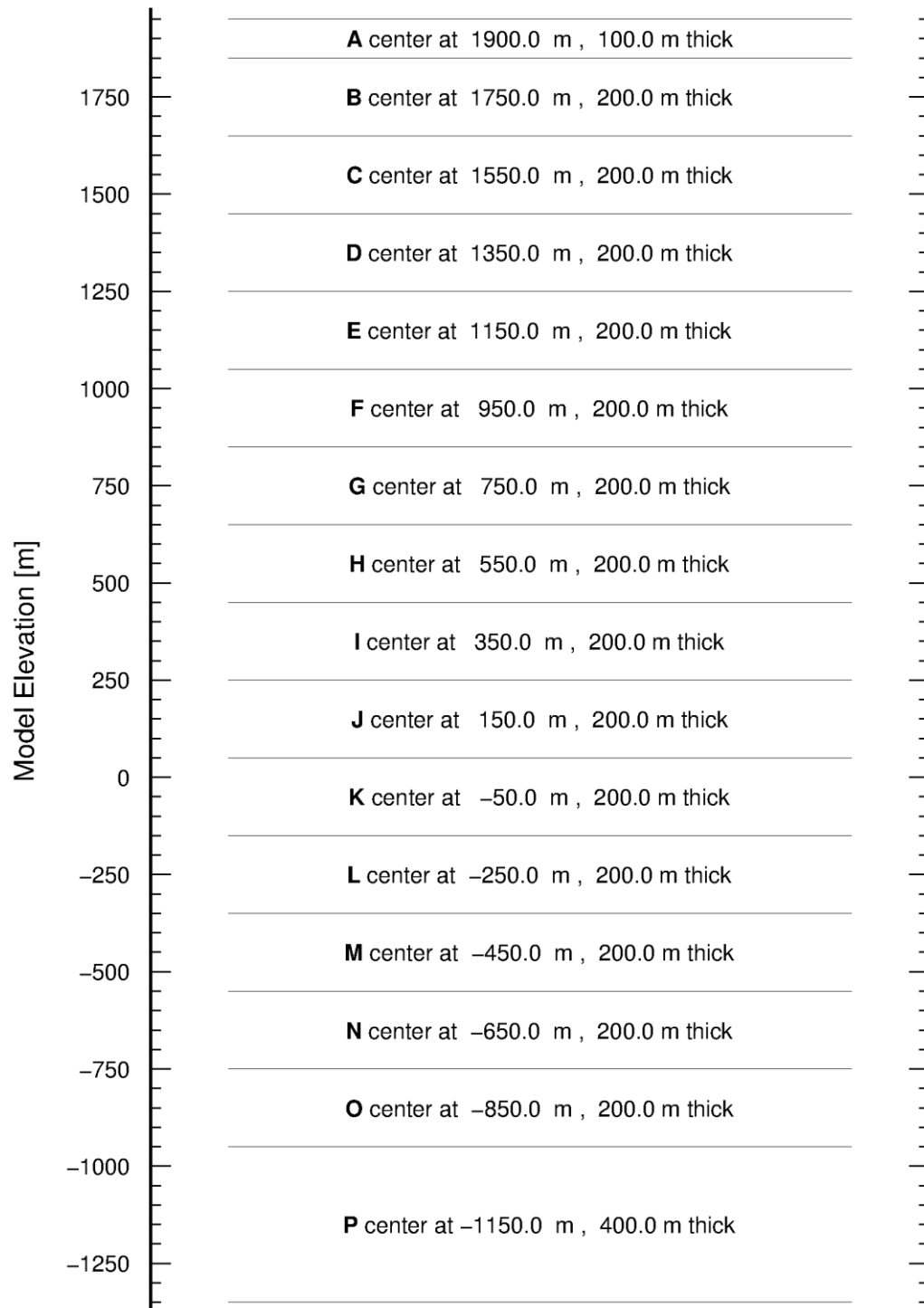











Figure 16 Vertical view of the mesh with layers named in alphabetical order

Table 1 Estimated physical properties of the numerical model of the Olkaria Domes geothermal system

Rock physical properties	
Density	2650 kg/m ³
Porosity	10%
Specific heat capacity	850 kJ/(kg.K)
Thermal conductivity	2.1 W/(m°K)

The permeability in each of the rocks subdivisions was progressively adjusted until a good match between simulated and observed data was achieved.

Table 2 Permeabilities of the rock types assigned to the reservoir domain.

Rock Type	Horizontal Permeability [mD]	Vertical Permeability [mD]
 BOUDR	1.0E-8	1.0E-8
 GRNRK	0.042	0.063
 OUTRG	0.409	0.014
 INRNG	0.703	0.058
 OLBFR	1.270	0.806
 DOMRK	1.870	0.920
 GOGFR	2.430	0.322
 921FR	7.050	1.570
 RINGR	11.70	2.450

3.2.6 Initial conditions

The fluid in the numerical model was assumed to be pure water. All water properties into the TOUGH2 model simulations were thus obtained from equation-of-state model 1 (EOS1) which contains steam table equations as given by the International Formulation Committee (1967). The flow systems in the model were initialised by assigning a complete set of primary variables to all grid blocks into which the flow domain was discretized. (Pruess et al., 2012).

4 RESULTS AND DISCUSSION

Natural state modelling simulates the physical state of a geothermal system in its pre-exploitation state. The primary purpose of a natural state model is to verify the validity of conceptual models and quantify the natural flow within the system.(Bodvarsson & Witherspoon, 1989). It consists of running a model for a long time to simulate the development of the geothermal field on a geological time scale until steady state has been reached. (O’Sullivan, Pruess, & Lippmann, 2001). When the steady state is reached, the heat and mass entering into the model are equal to heat and mass released through the boundaries and thus no change is observed in thermodynamic variables.

Feedzones were used in this study to map subsurface structures. This was an important input to describing the conceptual model for Olkaria Domes geothermal field and assigning the initial guess of permeability values of the reservoir rocks during numerical modelling. The values were then automatically improved with iTOUGH2 during iterations to attain a good fit between observed and simulated temperature and pressure data.

4.1 Natural state model









The model is constructed with an input of mass and heat at the bottom. Guided by the conceptual model, mass sources are set at layer O (approximately 2850 m depth), the bottom most active layer where the up flow is assumed to be located in the reservoir. The mass sources supply fluid of constant enthalpy of around 1650 kJ/kg with constant mass flow rate of 41 kg/s (Table 3). The permeability, strength of the heat and mass flow were manually adjusted until an acceptable natural state was achieved. It took a considerable amount of time but the good practice proposed by Malcolm & Bixley, 2011 was followed, which suggests starting with low permeability and then increasing it gradually until a good match is achieved. Automatic calibration was later attempted with iTOUGH2 which further improved the match between observed and model calculated data.

Table 3 Table showing the heat sources, their enthalpies and mass flow rates for the natural state model.

Name of Heat Source	Enthalpy [kJ/kg]	Mass [kg/s]
OB682DOM10	1650	5.194
OB777DOM11	1776	7.005
OB935DOM12	1693	6.086
OB771DOM13	1503	6.186
OB876DOM14	1753	7.086
OB816DOM15	1503	4.186
OB627DOM16	1651	5.012

The permeability distribution, the rate of mass and heat flow into the system are adjusted automatically by the iTOUGH2 until the residual difference between calculated and observed pressure and temperature is minimized. The numerical code used (TOUGH2) outputs information on the calculated heat and mass transfer between adjoining gridblock surfaces for each time step. In this study, an initial guess of the permeability of the reservoir rocks domain was given as shown in Table 4 which was automatically improved through inverse modelling until a good fit was achieved between the observed and simulated data. The relative change both in horizontal and vertical permeability is shown in the same table.

Table 4 Change of permeability parameter after inverse modelling.

ROCK TYPE	INITIAL PERMEABILITY [mD]		FINAL PERMEABILITY [mD]		RELATIVE CHANGE [%]	
	Horizontal	Vertical	Horizontal	Vertical	Horizontal	Vertical
 GRNRK	4.200	0.630	0.042	0.063	99.00	90.00
 OUTRG	0.409	0.014	0.409	0.014	0.000	0.000
 INRNG	70.30	58.20	0.703	0.058	99.00	99.00
 OLBFR	0.127	0.806	1.270	0.806	900.0	0.000
 DOMRK	1.3E5	0.806	1.870	0.920	14.7E3	14.00
 GOGFR	24.30	0.032	2.430	0.322	90.00	900.0
 921FR	70.50	1.570	7.050	1.570	90.00	0.000
 RINGR	1.170	2.450	11.70	2.450	900.0	0.000

4.1.1 Comparison between simulated and observed data

The natural state model corresponds to the physical state of a geothermal system prior to production. The natural state model of the Olkaria Domes geothermal field is developed and calibrated from the current conceptual model and thermophysical properties of the reservoir inferred using the TOUGH2 simulator. In this study, the simulated results of the natural state model were compared with measured temperature and pressure profiles of 46 wells as presented in appendix A. In order to simulate the natural state of the field key parameters were tweaked to obtain a minimal difference between simulated and measured data. This matching procedure was mainly conducted by automatically adjusting permeability of rock types and mass flow rates assigned at the bottom of the grid (Layer O) through inverse modelling using iTOUGH2.

The simulated data of some wells did not match the observed data. Most of these wells are located at the inferred colder regions of the Olkaria Domes geothermal field. This could partly be attributed to permeability distribution of the reservoir rock domain and the intensity of the heat sources assigned in the numerical model. The initial guess of the location of the heat and mass flow zones was guided by analysis of the temperature distribution at sea level (approximately 2000 m depth as shown in Figure 17).

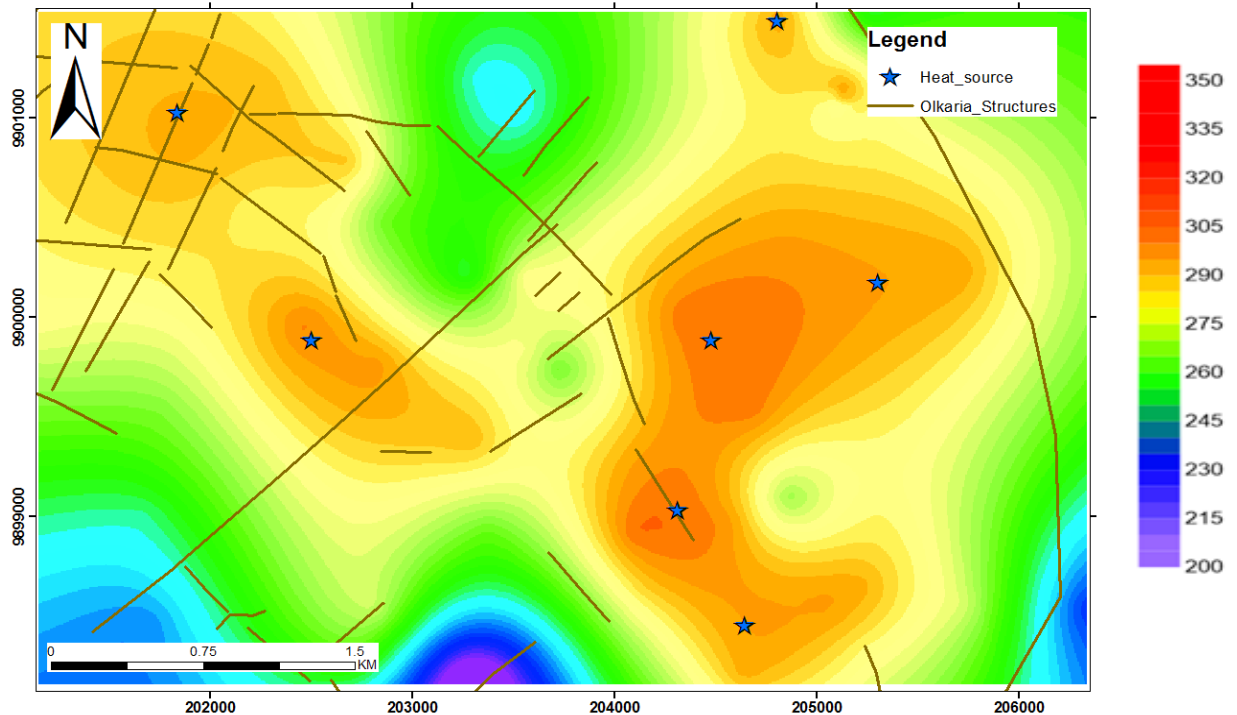


Figure 17 Location of the heat sources in the Olkaria Domes geothermal field on a temperature contour map (at sea level which is at approximately 2000 m depth).

Nine rock types were used as shown in Table 2 in order to assign different permeability values based on hydrogeological characteristics of the Olkaria Domes geothermal field. A relatively high permeability was initially assigned to the z direction for the upflow zone. The caprock and bedrock of this geothermal system were assigned the lowest permeability values of the the model. The elements at the top and bottom layers were also assigned a negative volume to make them inactive. The results of the field observed and model calculated temperature contours at 550 m.a.s.l (1450 m depth), 150 m.a.s.l (1850 m depth) and 650 m.b.s.l (2650 m depth) are as shown in figures 18, 19, 20, 21, 22 and 23 respectively. These figures are presented as pairs i.e. field observed and model calculated temperature contours at those particular depths. The observed contours of the temperature distribution of the field was interpolated from the measured data at the respective depths.

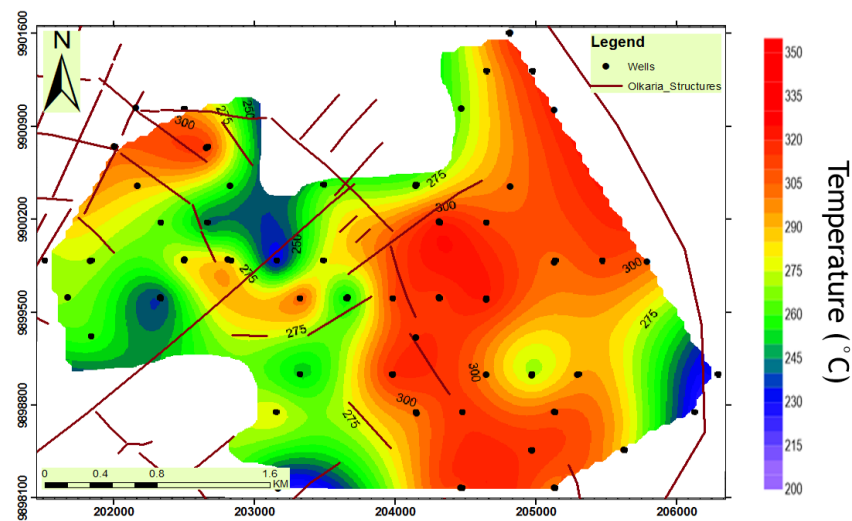


Figure 18 Field observed temperature contour at layer H (550 m.a.s.l).

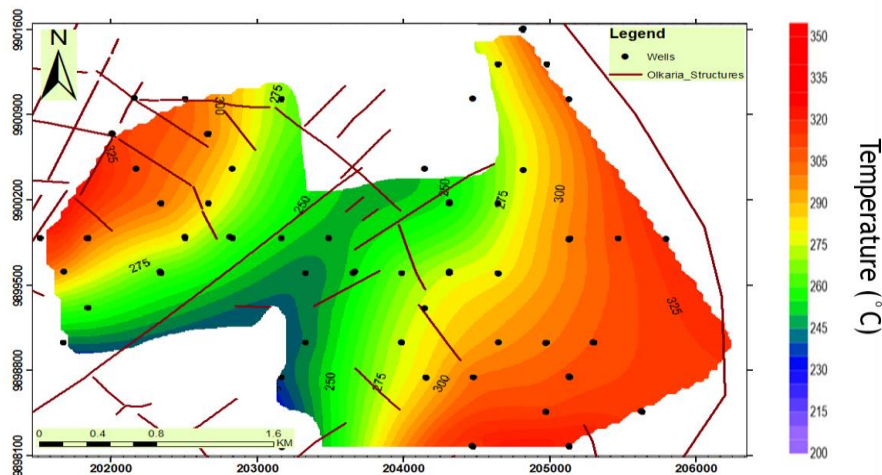


Figure 19 Model calculated temperature contour at layer H (550 m.a.s.l).

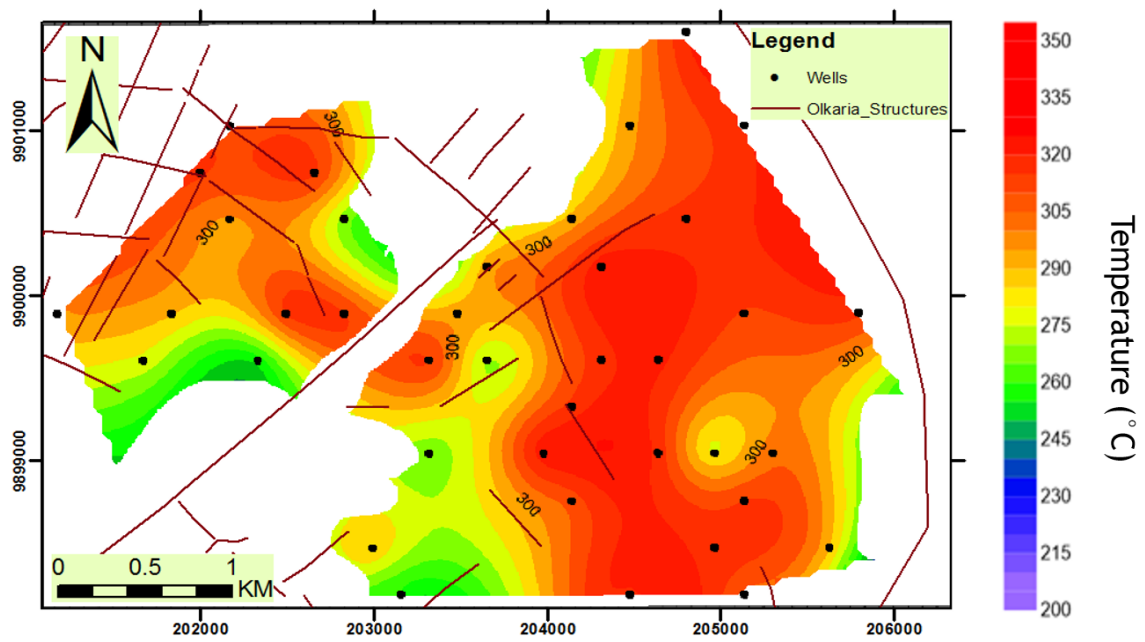


Figure 20 Field observed temperature contour at layer J (150 m.a.s.l).

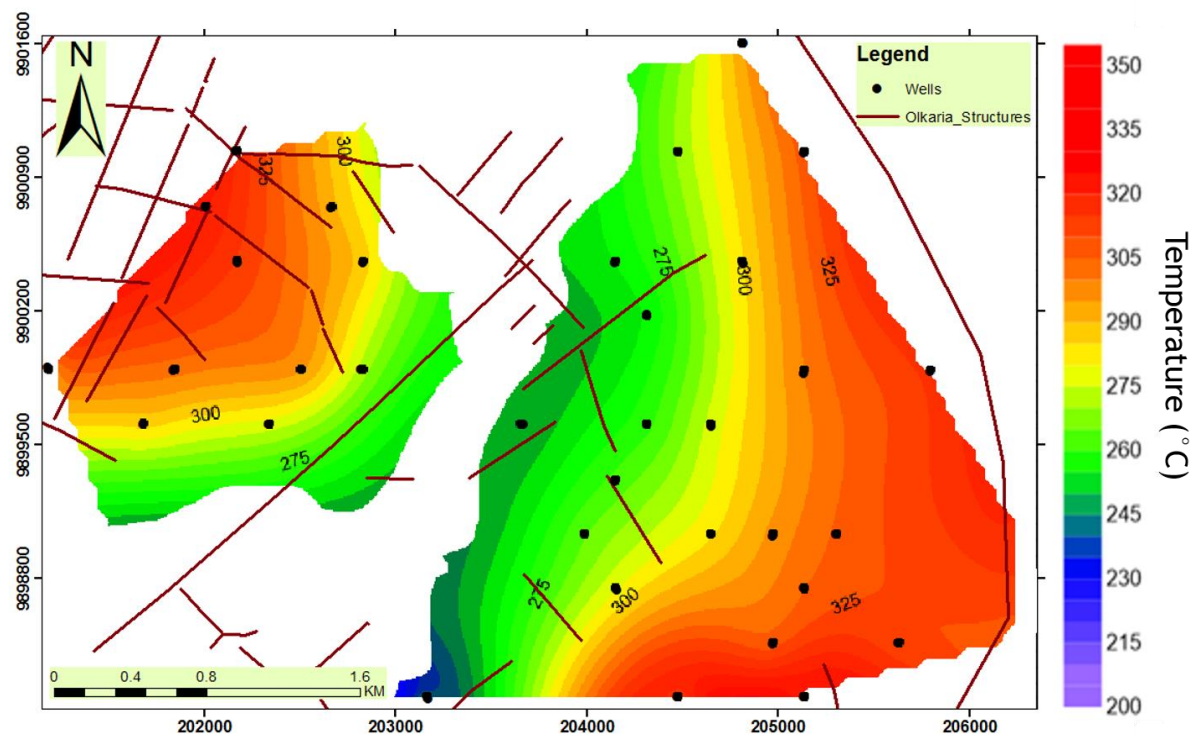


Figure 21 Model calculated temperature contour at layer J (150 m.a.s.l).

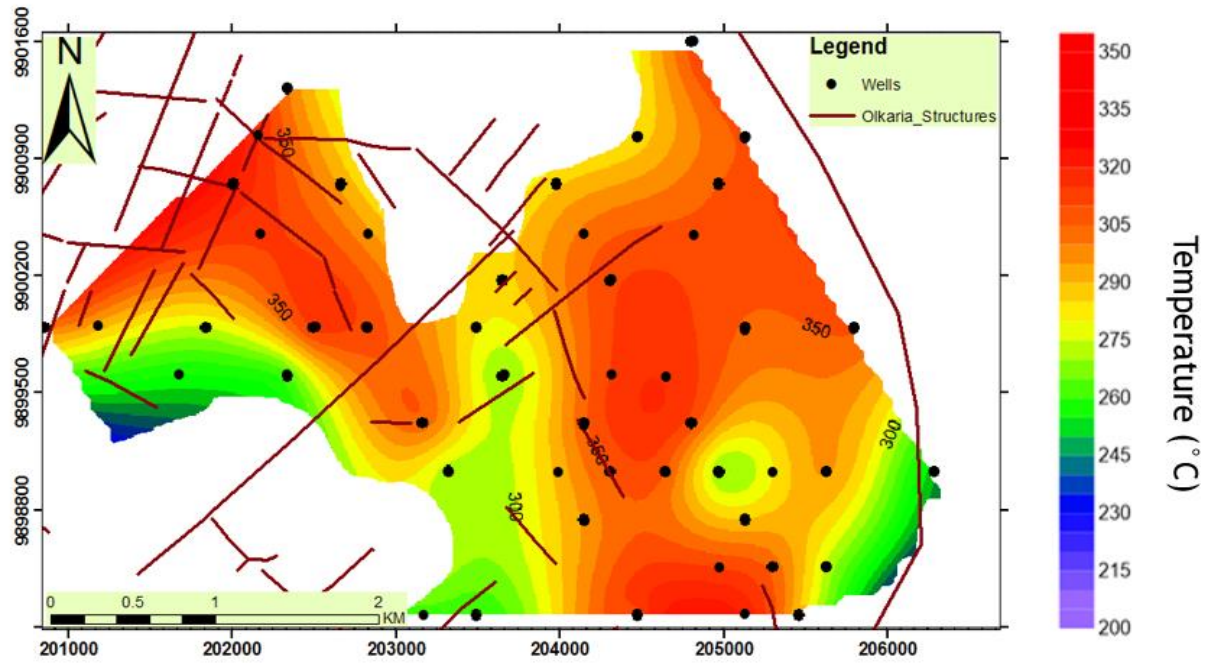


Figure 22 Field observed temperature contour at layer N (650 m.b.s.l).

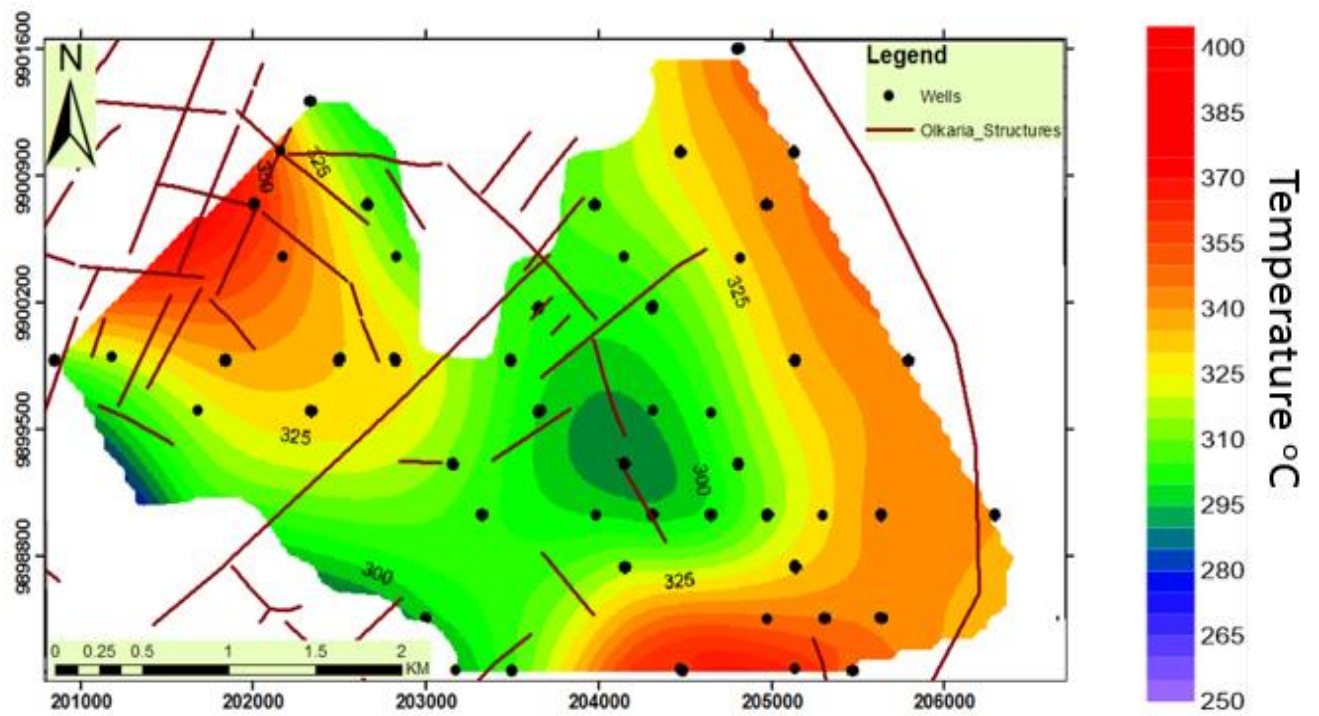


Figure 23 Model calculated temperature contour at layer N (650 m.b.s.l).

The temperature and pressure profiles of two wells were also compared between the field observed and simulated results (see Figure 24). From the results, well OW-910A matches the model simulated data quite well. This well is located in an inferred upflow zone. Well OW-905A which is located in a colder region in Olkaria Domes geothermal field did not match the model calculated data.

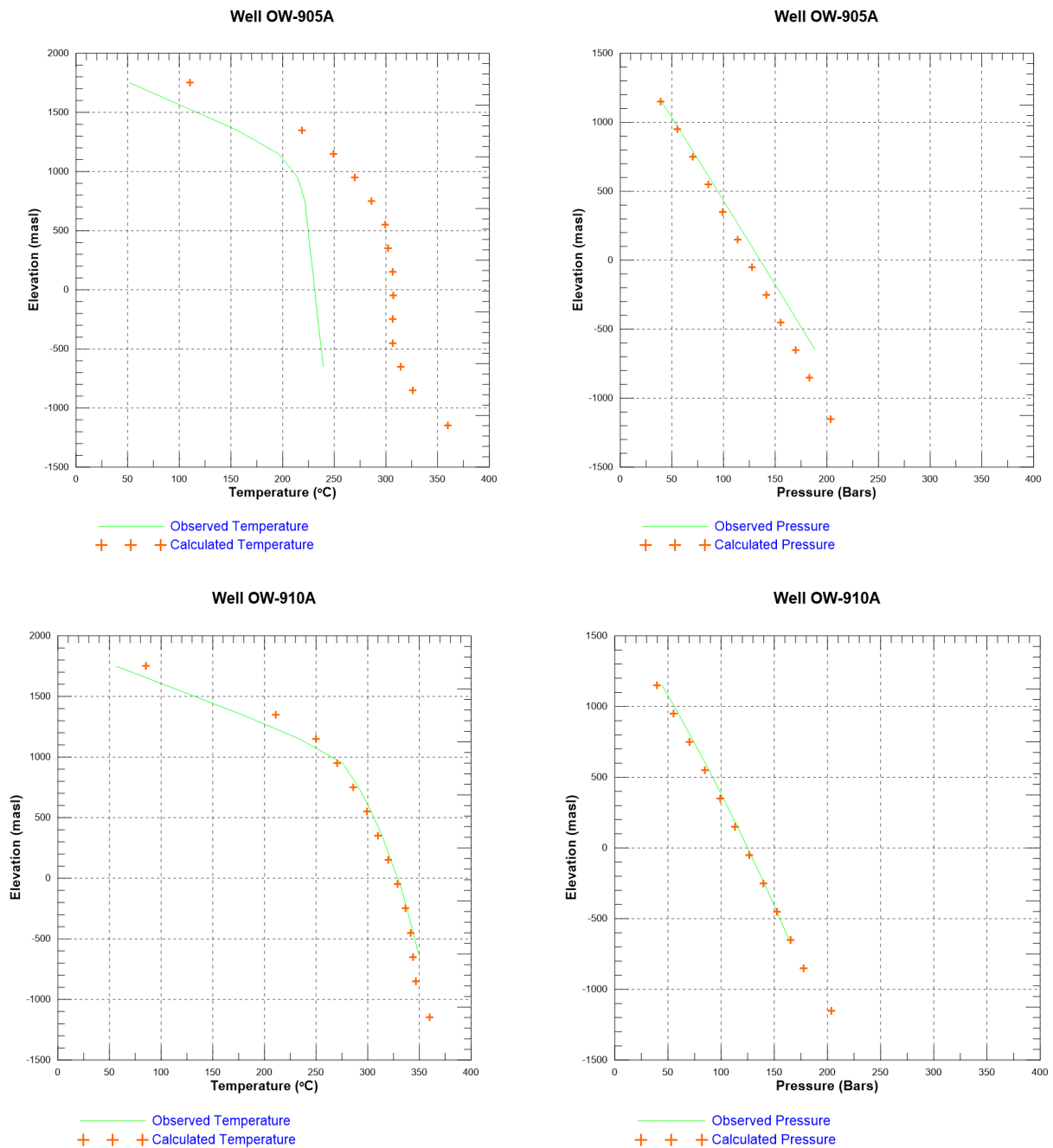


Figure 24 Comparison between measured and simulated temperature and pressure profiles of wells OW-905A and OW-910A.

4.2 Mapped new sub-surface structures

Subsurface permeability structures control the productivity of geothermal wells as they form the flow paths for fluid movement in the system either as upflow or recharge zones. Crucial to successful utilization of a geothermal system is the knowledge of the permeability structures and specifically feed zones, the sources of geothermal fluid entry into the wellbore. Understanding the nature and distribution of these feedzones is particularly relevant for well targeting and providing the constraints to reservoir models.

In this study, the analysis of major feed zones at the depths of 1000 m – 2000 m and 2000 m – 3000 m was used to map sub-surface permeability features in Olkaria Domes geothermal system. The results are presented in Figure 25. New fractures were mapped according to the major feedzones and overlaid on a temperature contour map at 500 m.a.s.l (at approximately 1500 m depth) interpolated from measured data. The orientation of these newly identified sub-surface fractures appears to follow the directions of the existing fractures in Olkaria Domes geothermal field.

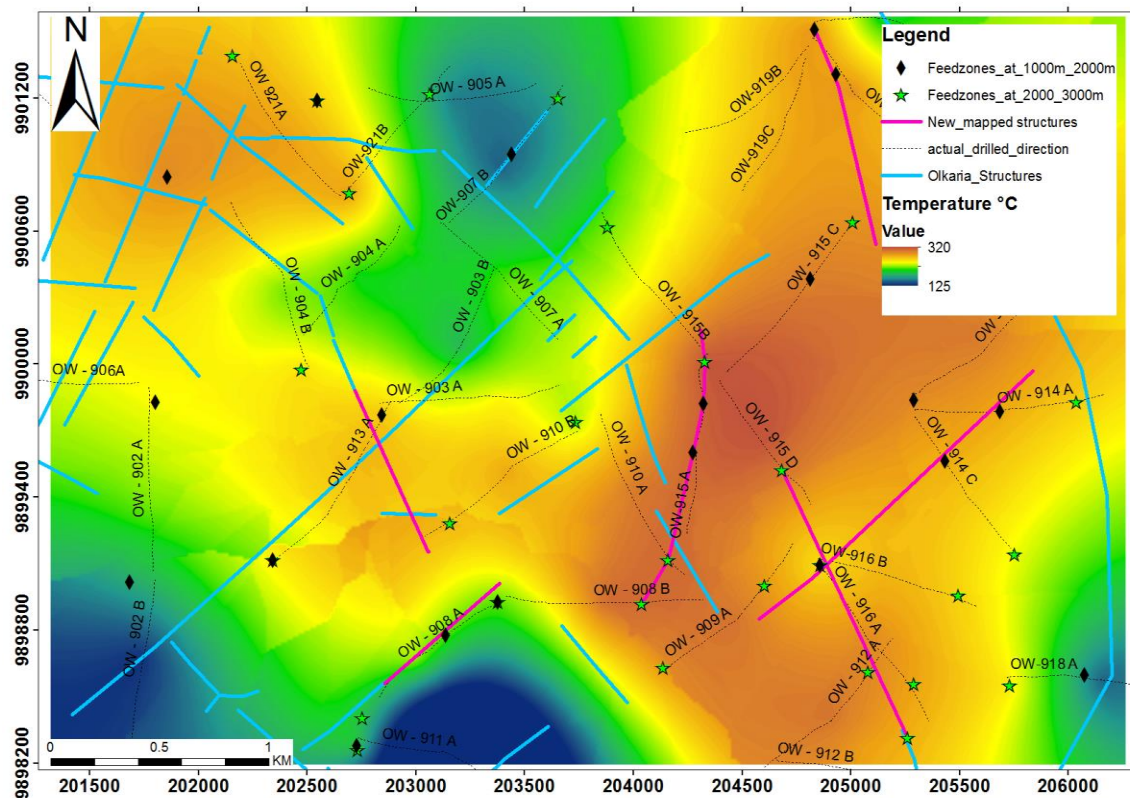


Figure 25 New mapped structures according to major feedzones at both 1000 m – 2000 m and 2000 m – 3000 m depths on a temperature model at 500m.a.s.l (at approximately 1500 m depth).

5 CONCLUSIONS AND RECOMMENDATIONS

A numerical reservoir model has been developed for the Olkaria Domes geothermal system. It covers an area of about 500 km² and has 16 layers. The natural state model matched well the available observed temperature and pressure data except some few wells like OW-905A, OW-918A, OW-917 and OW-907B as shown in appendix A. These wells are located at inferred colder regions of the Olkaria Domes field. The reason could partly be attributed to permeability distribution of the reservoir rocks and intensity of the heat sources assigned to the numerical model. The model developed was not used to match and predict production history because there has been a very short production period in this particular field. The first power plant was commissioned in October, 2014 and the production history is not long enough.

The use of feedzones to map subsurface permeability controls was an important input to describing the conceptual model for Olkaria Domes field and this played an important role in assigning the permeability to different rock types in the reservoir for the numerical modelling. It was used to guide in the initial guess of the permeability values of the rock types assigned to the model. This was set to a certain range in which iTOUGH2 automatically improved them during iterations to obtain a good fit between measured and simulated temperature and pressure which was then given as initial conditions for a subsequent simulations. Nine rock types were used to assign different permeability values based on the hydrogeological characteristics of the Olkaria Domes geothermal system. The temperature data from wells with very little heat up data was not used for numerical modelling in this study.

From analysis of feed zones and their distribution, it is clear that the structures in Olkaria Domes field are mostly trending in NW-SE, N-S and ENE-WSW. They also confirmed the location of the existing structures as earlier mapped across the field from their distribution pattern. Well OW-916 which produces 17 MW_e is located at an intersection of NE – SW and NW –SE trending faults. This well is among the biggest producers in Olkaria geothermal field. In this study, temperature distribution across the Olkaria Domes field coupled with the knowledge of permeability dominated by subsurface structures can be used to site both make up and re-injection wells. Re-injection wells are highly recommended for this field for pressure support and to enhance energy extraction efficiency.

The location of heat and mass sources of the model in this study was guided by the distribution of initial temperature at sea level (at approximately 2000 m depth). The mapping of subsurface structures is recommended in this field to accurately assign the permeability distribution which had a great impact on the output of the simulated results. A lateral recharge with relatively low temperature is recommended for inferred colder regions in order to match the temperatures and also place an impermeable boundary to constrain

the fluid flow within those regions. An interference test is recommended for this geothermal field because it will help to map the exact location of these impermeable boundaries within the reservoir.

In the future, it is recommended that;

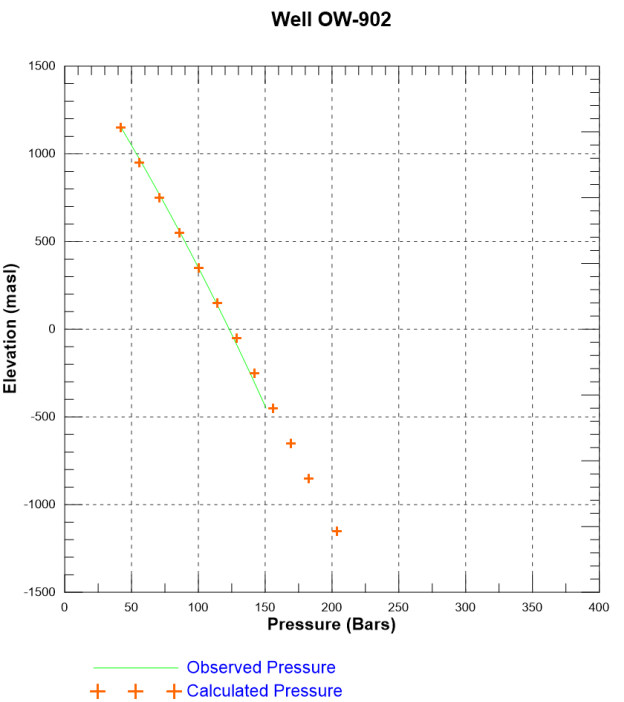
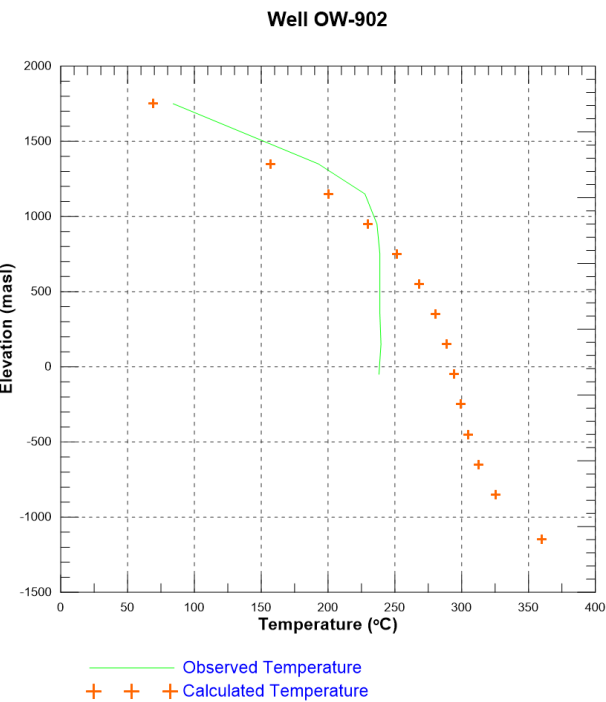
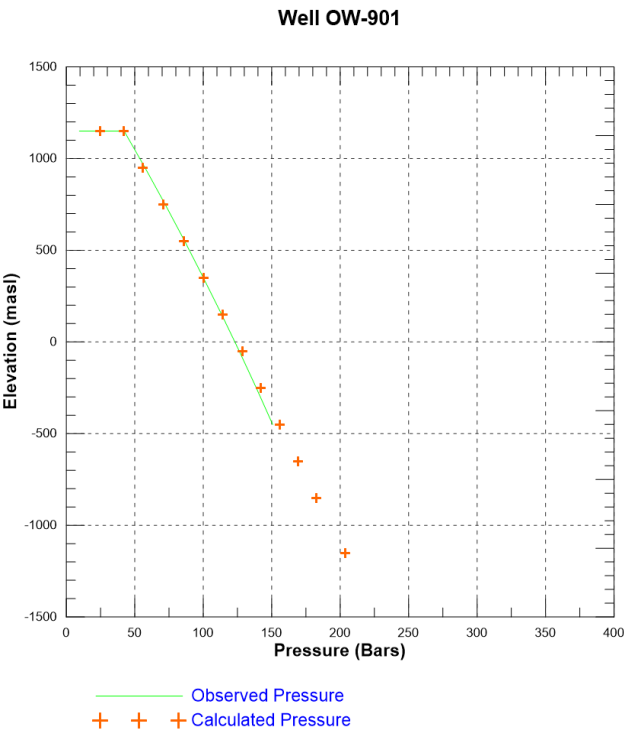
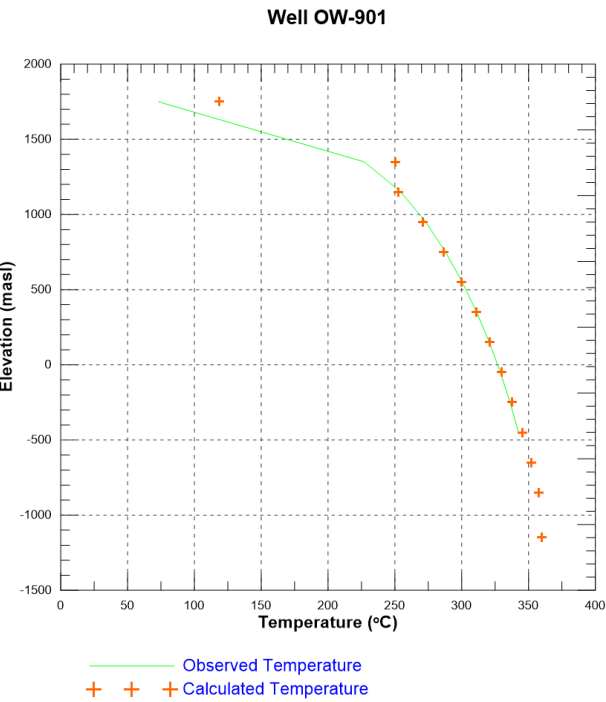
- The numerical model be refined, recalibrated and upgraded and a time dependent simulation be performed
- This would be important especially when more production data from production wells become available. The numerical model developed will then be used to predict the future behavior of the Olkaria Domes geothermal field, the effects of re-injection and the overall depletion of the geothermal reservoir. This would improve reservoir management as well as sustain stable operation of the power plants.
- Isotope data from boreholes should be analysed in order to draw conclusions regarding flow patterns or recharge of this field. This will also help in accurately mapping the sub-surface permeability structures.
- Geological mapping of the boreholes to find geological relationship of the aquifers encountered. The knowledge of this affects the construction of the reservoir model and perhaps more importantly, if the structure is known it can be extended out from the well and help on siting new wells.
- Tracer tests be carried out in Olkaria Domes geothermal system to characterize the flow channels. This will help us understand the connectivity of the subsurface fractures and therefore improve on the numerical model in assigning the rock types and permeability.

References

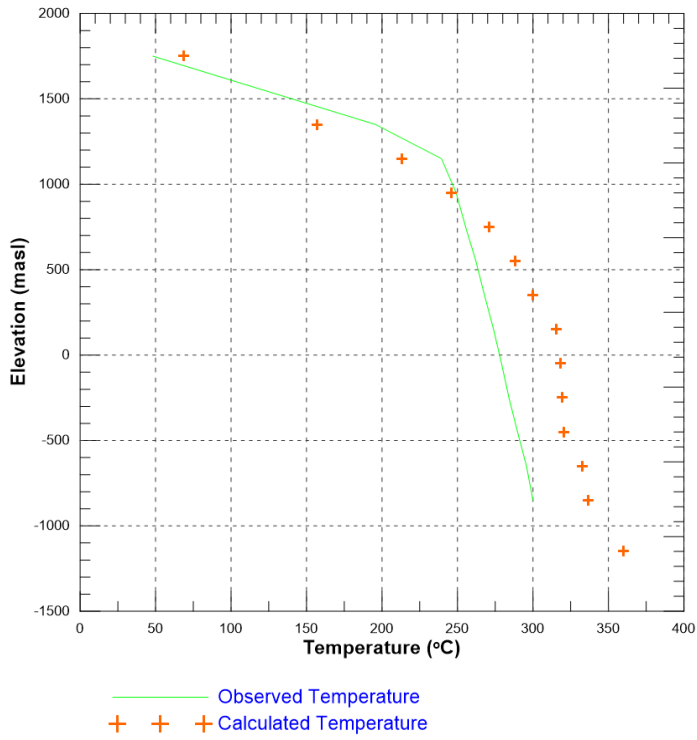
- Abbate, E., Passerini, P., & Zan, L. (1995). Strike-slip faults in a rift area: a transect in the Afar Triangle, East Africa. *Tectonophysics*, 241(1), 67–97.
- Bodvarsson, G. S., & Witherspoon, P. A. (1989). *Geothermal reservoir engineering* (Part 1). Geothermal Science and Technology.
- Clarke, M. C., Woodhall, D. ., Allen, D., & Darling, G. (1990). *Geological, Volcanological and Hydrogeological Controls on the Occurrence of Geothermal Activity in the Area Surrounding Lake Naivasha, Kenya: With Coloured 1: 250 000 Geological Maps*. Ministry of Energy, Nairobi, Kenya.
- Finsterle, S. (2007). iTOUGH2 User's guide. Earth Sciences Division, Lawrence Berkeley National Laboratory, University of California, USA (No. 137 pp).
- Haukwa, C. (1998). AMESH A mesh creating program for the integral finite difference method: A User's Manual. Lawrence Berkeley National Laboratory, USA (No. 54 pp).
- Haukwa, C. B. (1984). Recent measurements within Olkaria East and West fields. *Kenya Power Company Internal Report*, 13 pp.
- Kamunya, M. ., Wafula, E., & Wamalwa, R. (2015). *Update of the Olkaria geochemical Conceptual model*. Naivasha, Kenya: KenGen Internal report.
- Karingithi, C. W. (2000). *Geochemical characteristics of the Greater Olkaria geothermal field, Kenya* (No. 9) (pp. 165–188). Reykjavik: United Nations University Geothermal Training Program, UNUGTP.
- Koech, V. K. (2014). *Numerical Geothermal Reservoir Modelling and Infield Reinjection Design, Constrained by Tracer Test Data: Case Study for the Olkaria Geothermal Field in Kenya*. University of Iceland, Reykjavik. Retrieved from <http://skemman.is/en/item/view/1946/19847>
- Lagat, J. K. (2004). *Geology, hydrothermal alteration and fluid inclusion studies of Olkaria Domes geothermal field, Kenya*. University of Iceland.
- Malcolm, G., & Bixley, P. (2011). *Geothermal Reservoir Engineering, 2nd Edition / Malcolm Grant, Paul Bixley* (2nd Edition). Academic Press , NY, USA.
- Malimo, S. . (2009). *Interpretation of geochemical well test data for wells OW-903B, OW-904B and OW-909, Olkaria Domes Kenya* (Report 17, 319-344). UNU-GTP.
- Mannvit/ISOR/Vatnaskil/Verkis Consortium. (2011). *Revision of the conceptual model of the Greater Olkaria geothermal system -phase I* (unpublished internal No. 95 pp). KenGen.
- Mungania, J. (1999). *Summary of Updates of the Geology of the Olkaria Domes Geothermal Field*. Naivasha, Kenya: KenGen Internal report.
- Mwakirani M., R. (2011). *Resistivity Structure of Paka geothermal prospect in Kenya* (No. 26). United Nations Geothermal Training Program, UNUGTP, Iceland. Retrieved from <http://www.os.is/gogn/unu-gtp-report/UNU-GTP-2011-26-1.pdf>
- Ofwona, C. O. (2002). *Reservoir Study of Olkaria East Geothermal System*. University of Iceland, Reykjavik.

- Omenda, P. A. (1994). The geological structure of the Olkaria west geothermal field, Kenya. In *Proceedings of the Nineteenth Workshop on Geothermal Reservoir Engineering, Stanford University, California* (pp. 125–130).
- Omenda, P. A. (1998). The geology and structural controls of the Olkaria geothermal system, Kenya. *Elsevier Science Ltd*, 27(1), 55–74.
- Onacha, S. A. (1990). *Olkaria West Field information report*. Kenya Power Company internal report.
- Onacha, S. A. (1993). *Resistivity studies of the Olkaria-Domes geothermal project*. Kenya Power Company internal report.
- Opondo, K. . (2008). The Fluid characteristics of three exploration wells drilled at Olkaria Domes field, Kenya. In *Thirty-Third Workshop on Geothermal Reservoir Engineering Stanford University, Stanford, California, January 28-30, 2008* (p. 6 pp).
- O’Sullivan, M. J., Pruess, K., & Lippmann, M. J. (2001). State of the art of geothermal reservoir simulation. *Geothermics*, 30(4), 395–429.
- Owens, L., Porras, E., Spielman, P., & Walsh, P. (2015). Updated Geologic and Geochemical Assessment of the Olkaria III Field Following Recent Expansion to 110MW. In *Fourtieth Workshop on Geothermal Reservoir Engineering Stanford University, Stanford, California, January 26-28, 2015*.
- Pruess, K., Oldenburg, C. M., & Moridis, G. J. (2012). TOUGH2 user’s guide version 2. Lawrence Berkeley National Laboratory, USA (No. 195 pp).
- Ronoh, I. (2015). Appraising a Geothermal Field Using Hydrothermal Alteration Mineralogy: a Case Study of the East of Olkaria Domes Geothermal Field; Olkaria, Kenya. In *World Geothermal Congress 2015 Melbourne, Australia, 19-25 April 2015* (p. 12 pp).
- Rühaak, W., Renz, A., Schätzl, P., & Diersch, H.-J. . (2010). Numerical Modeling of Geothermal Applications - 3202.pdf. In *Proceedings World Geothermal Congress 2010* (p. 5). Bali, Indonesia, 25-29 April 2010.
- Simiyu, S. M., & Keller, G. R. (2000). Microseismic monitoring within the Olkaria geothermal area, Kenya. *Journal of Volcanology and Geothermal Research*, 95, 197–208.
- West-JEC Inc. (2009). *The Olkaria Optimization Study (Phase II)*. KenGen Internal report.

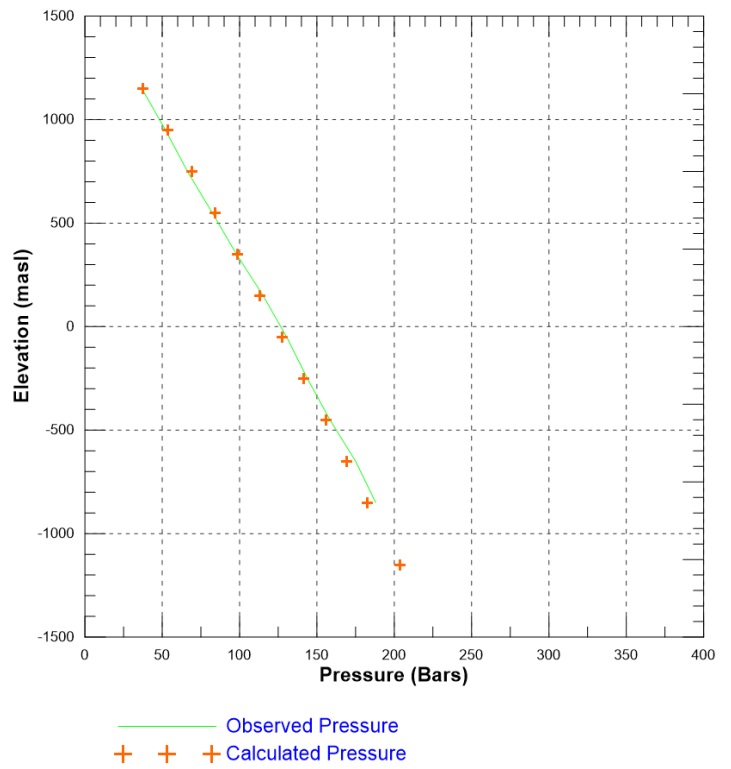
Appendix A: Reservoir Formation (Steady State Temperature and Pressure) and Natural state model simulation



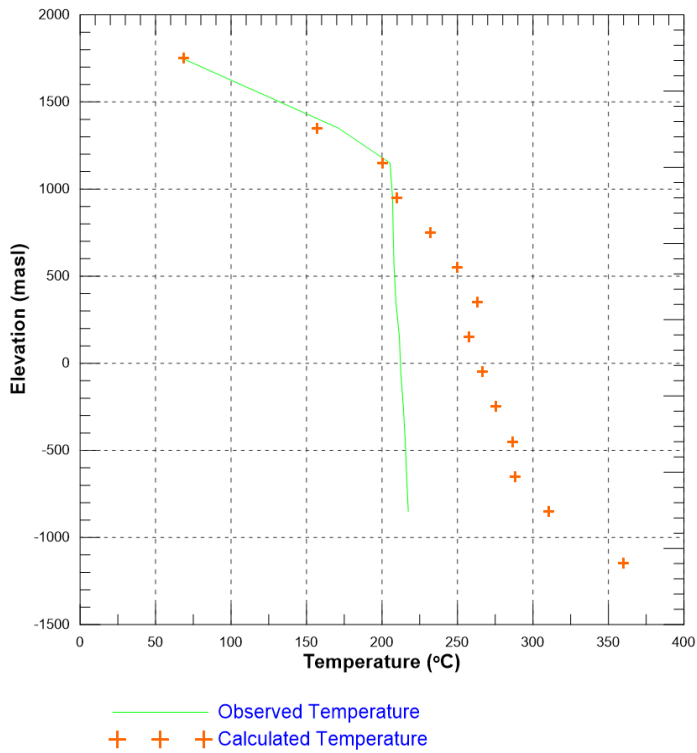
Well OW-902A



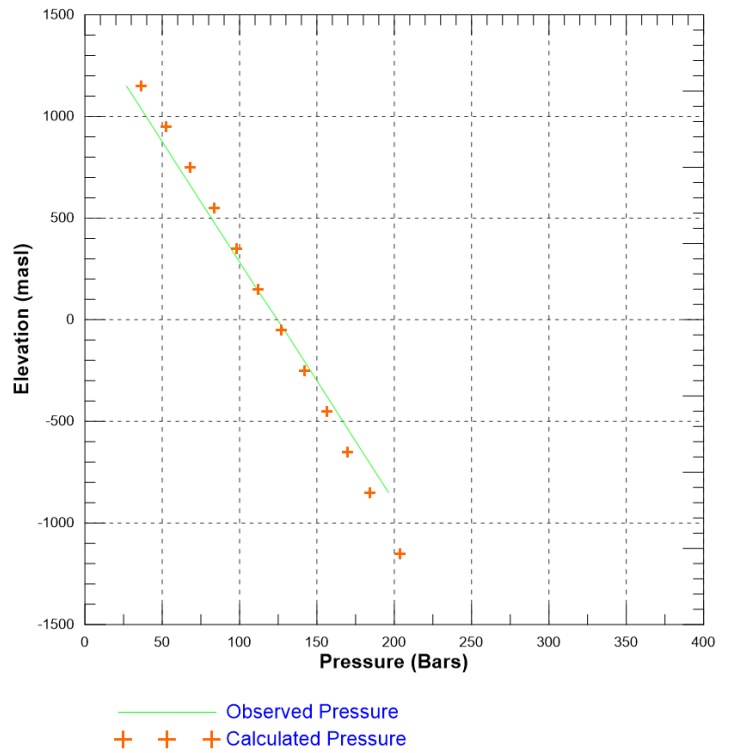
Well OW-902A



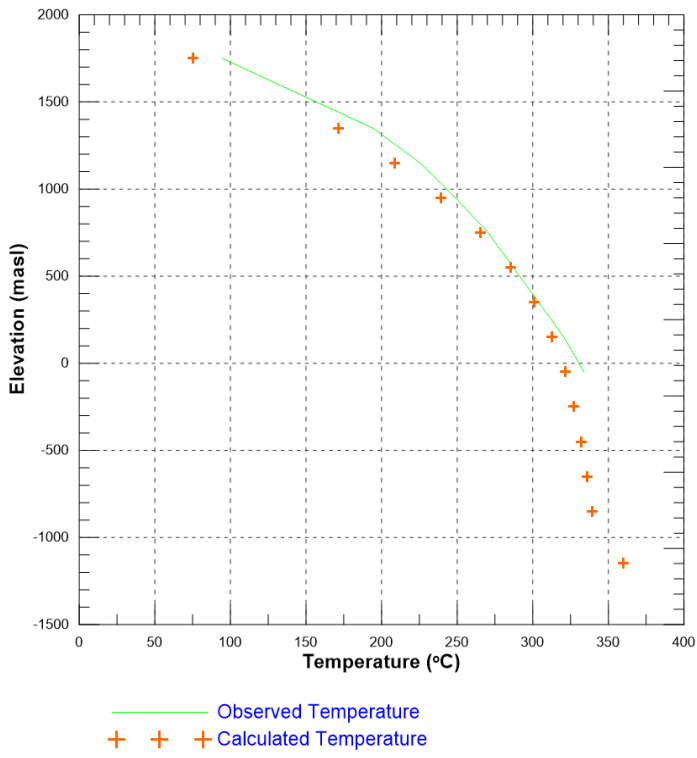
Well OW-902B



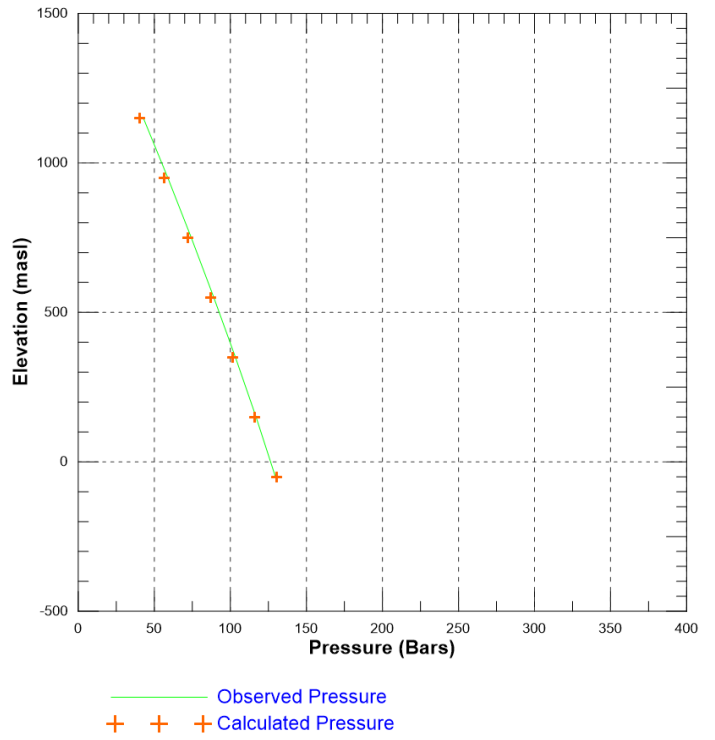
Well OW-902B



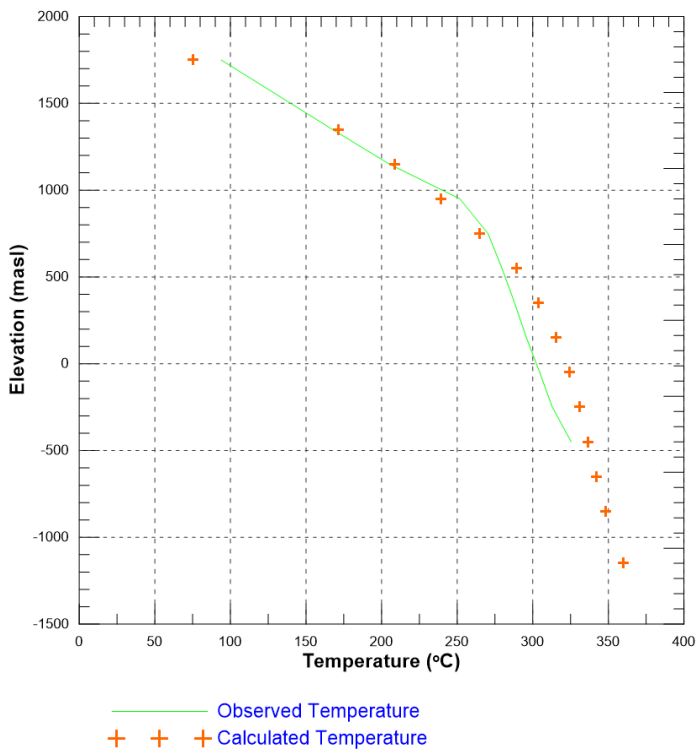
Well OW-903



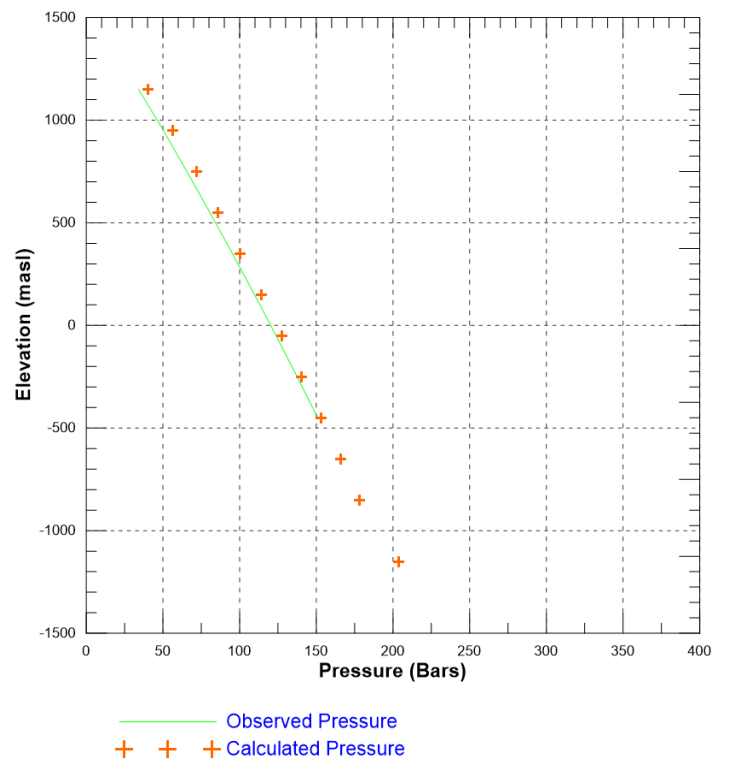
Well OW-903



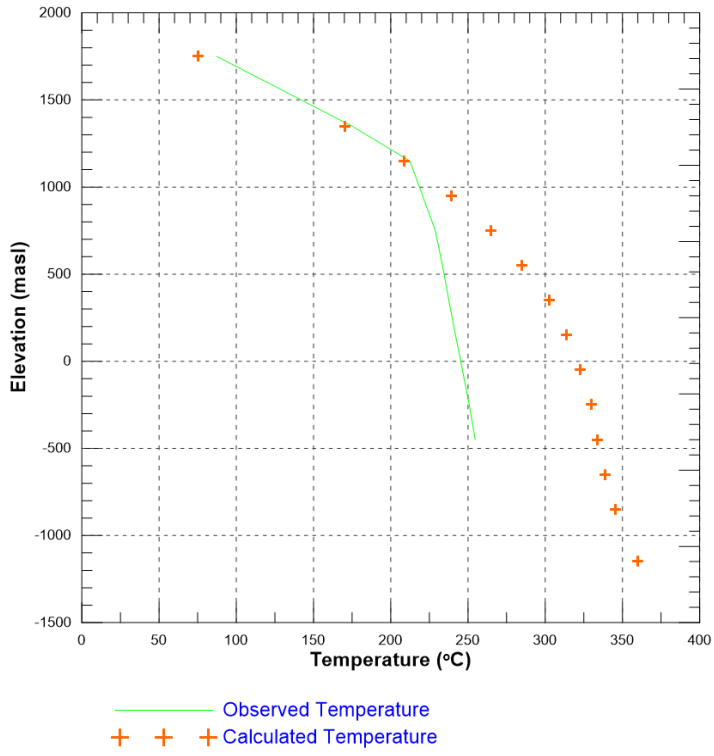
Well OW-903A



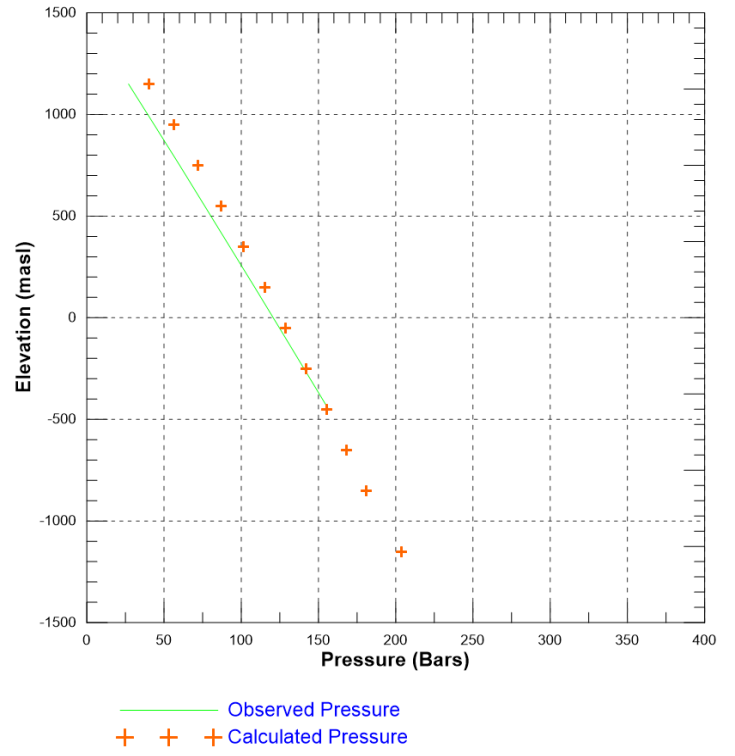
Well OW-903A



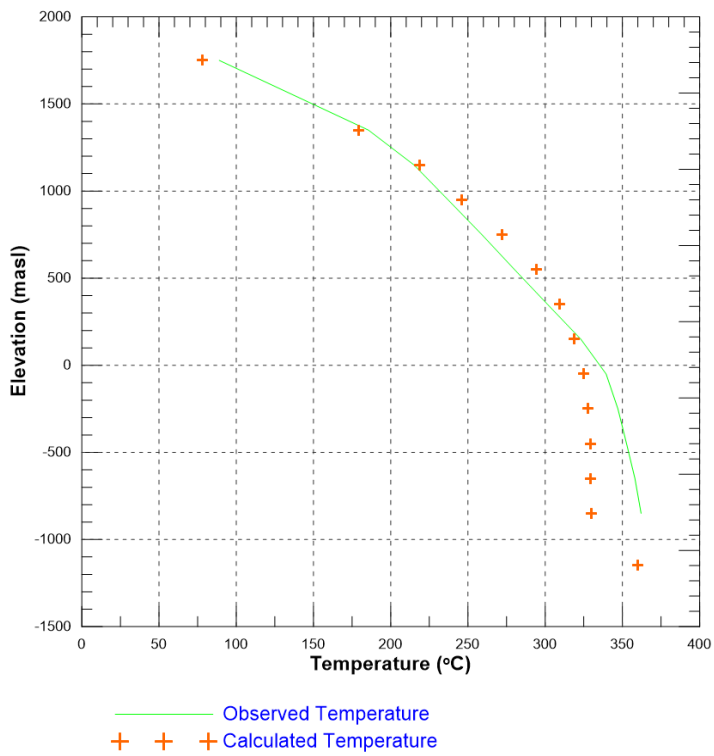
Well OW-903B



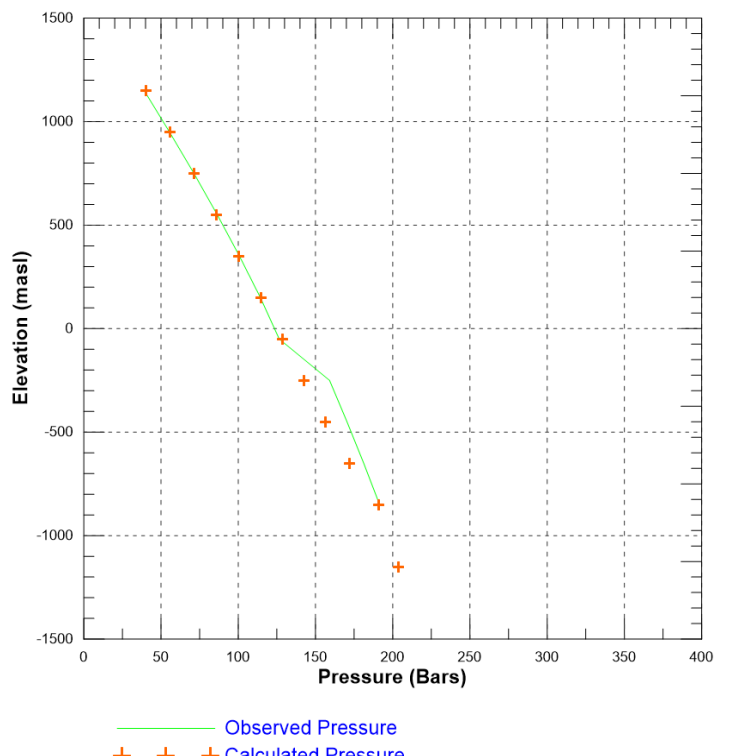
Well OW-903B



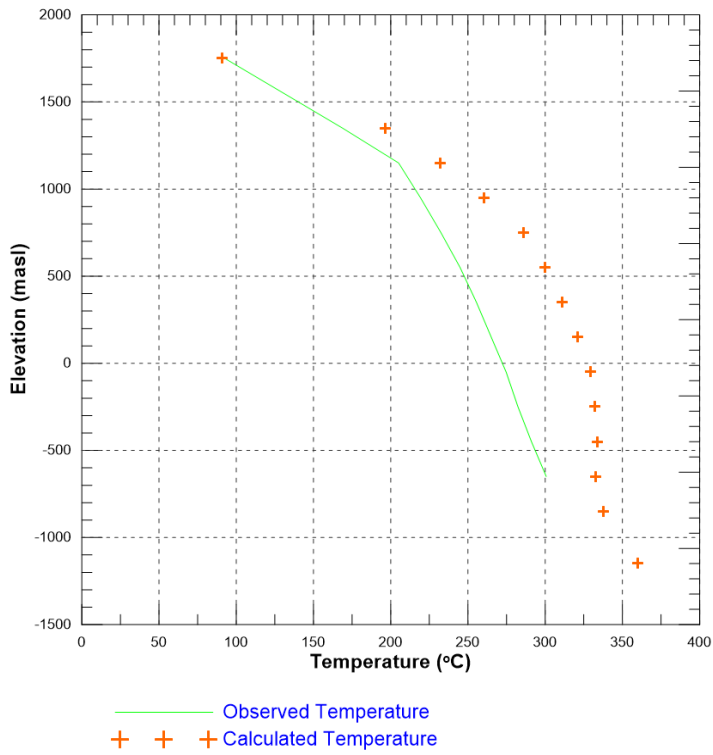
Well OW-904



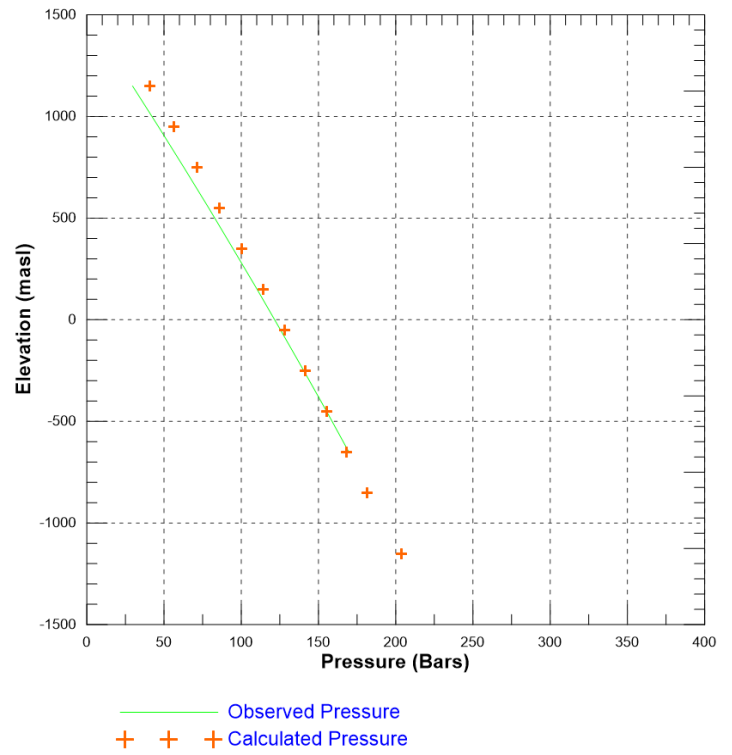
Well OW-904



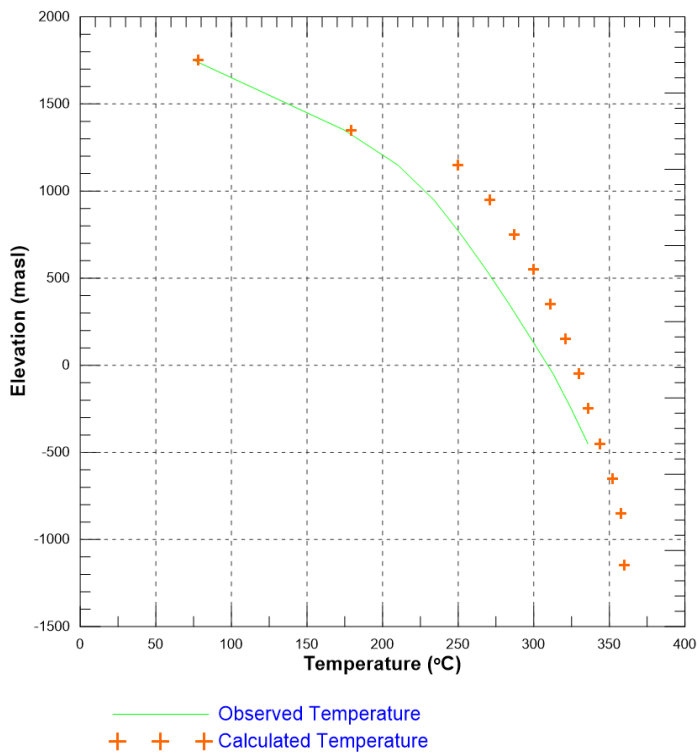
Well OW-904A



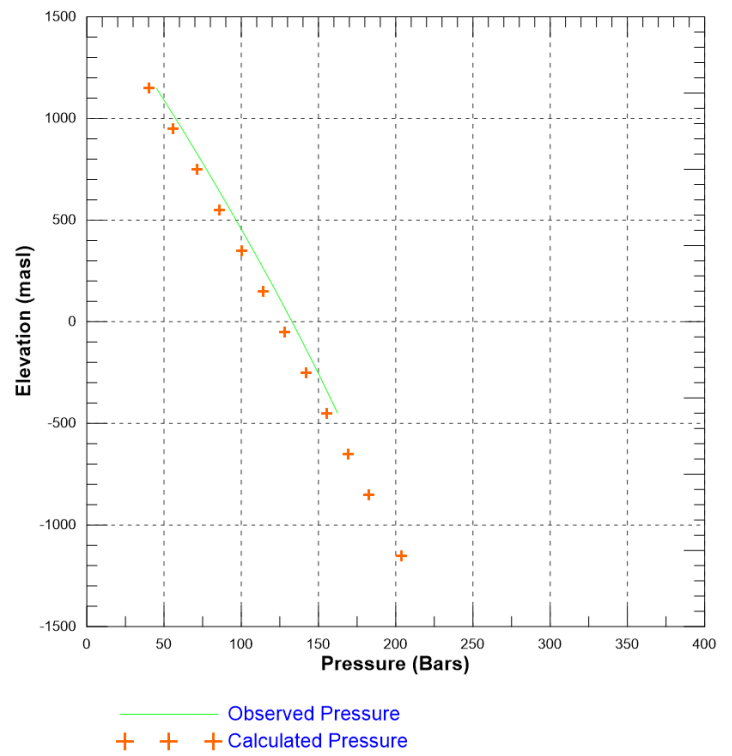
Well OW-904A



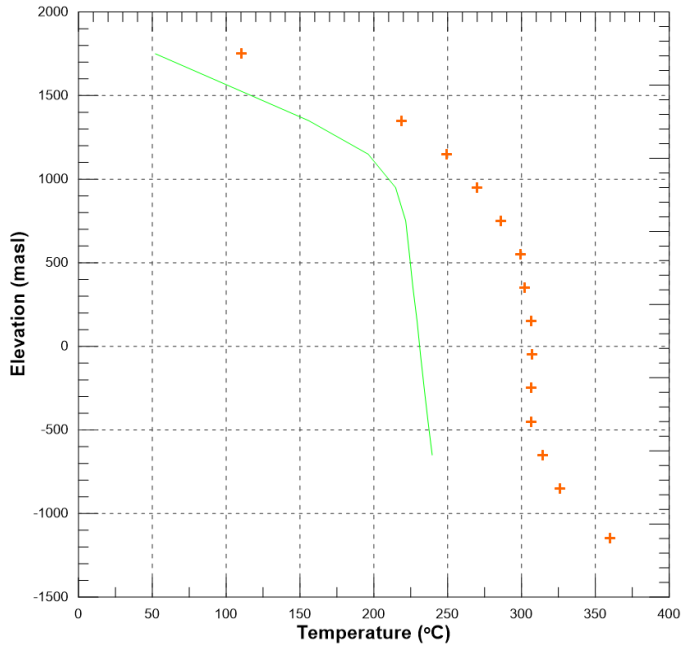
Well OW-904B



Well OW-904B

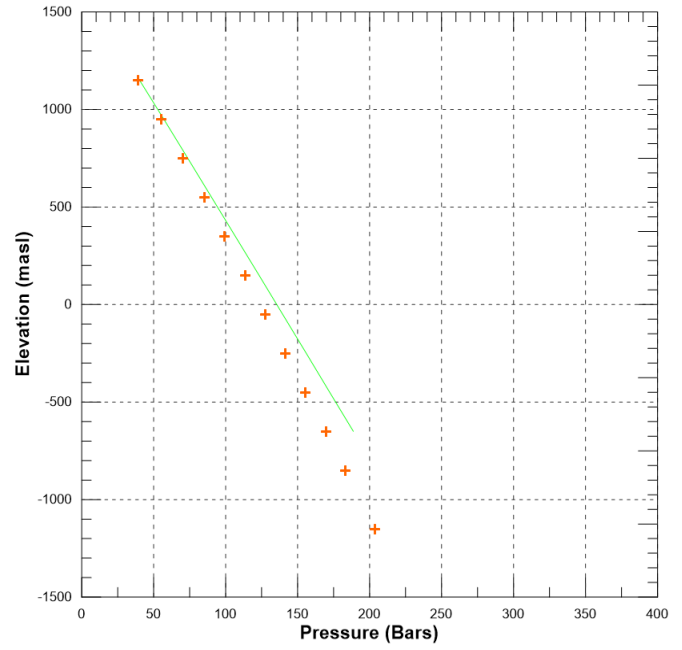


Well OW-905A



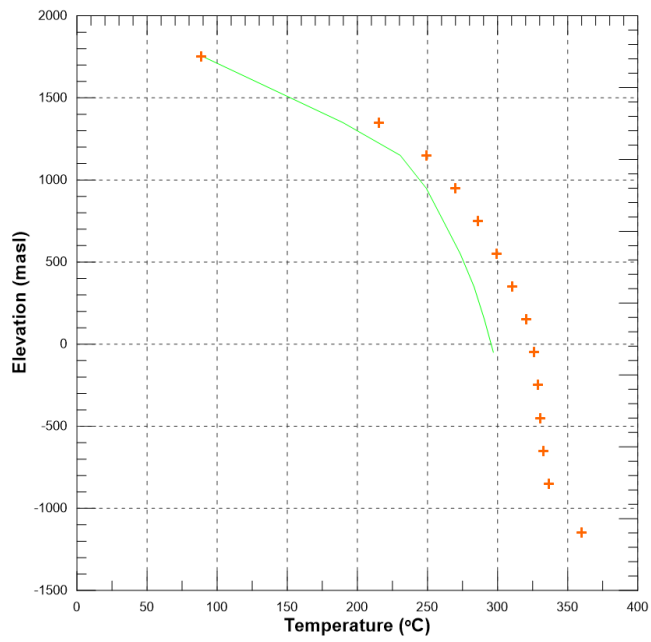
— Observed Temperature
+ + + Calculated Temperature

Well OW-905A



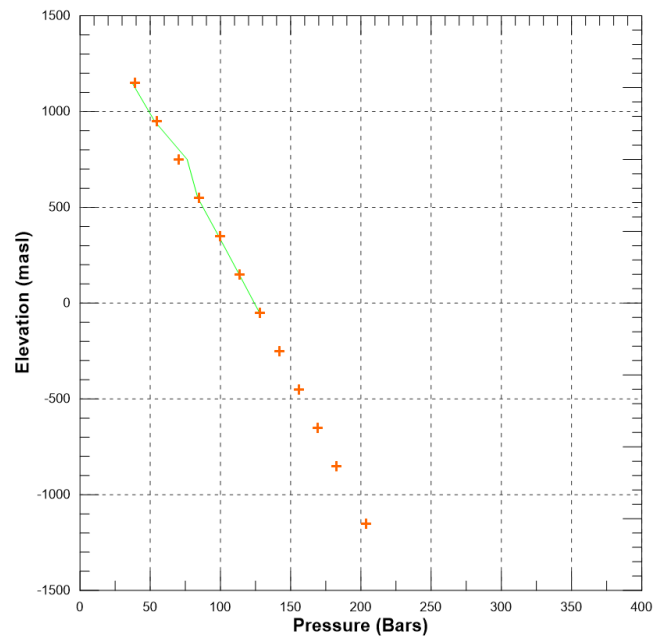
— Observed Pressure
+ + + Calculated Pressure

Well OW-906



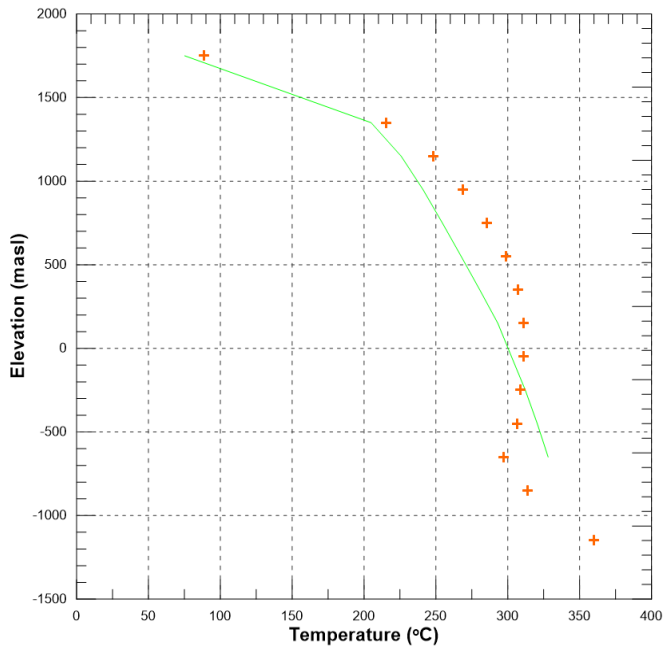
— Observed Temperature
+ + + Calculated Temperature

Well OW-906

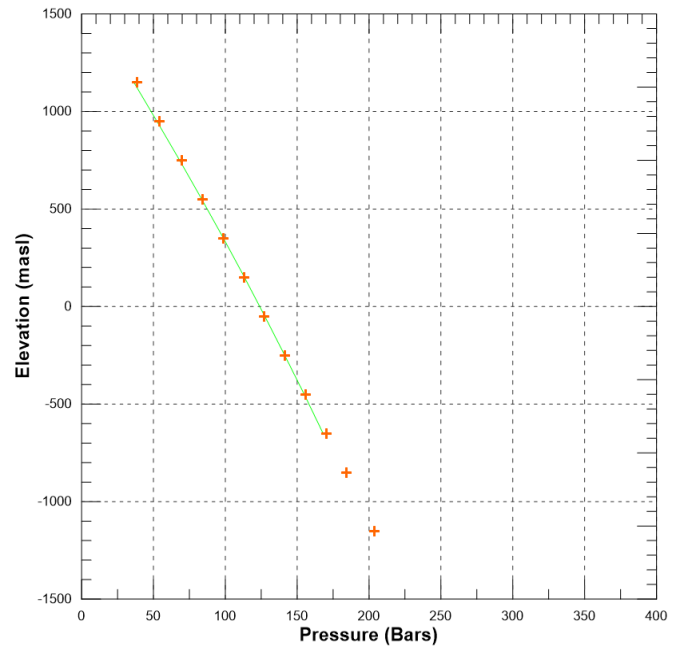


— Observed Pressure
+ + + Calculated Pressure

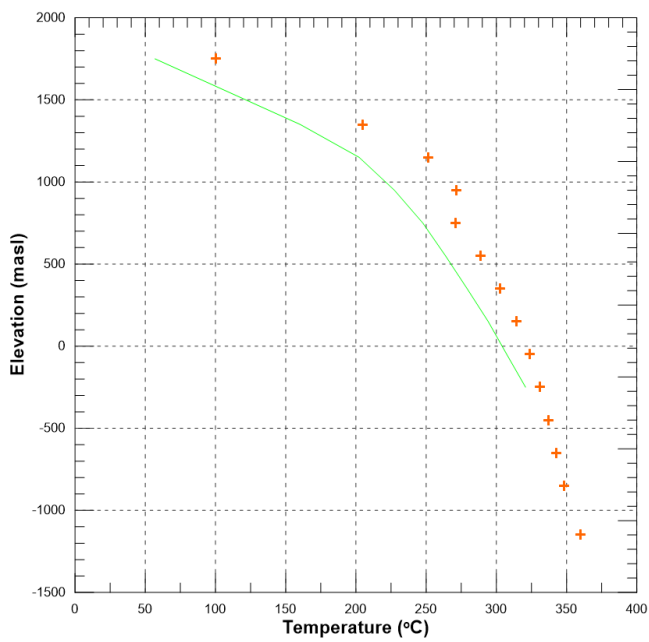
Well OW-906A



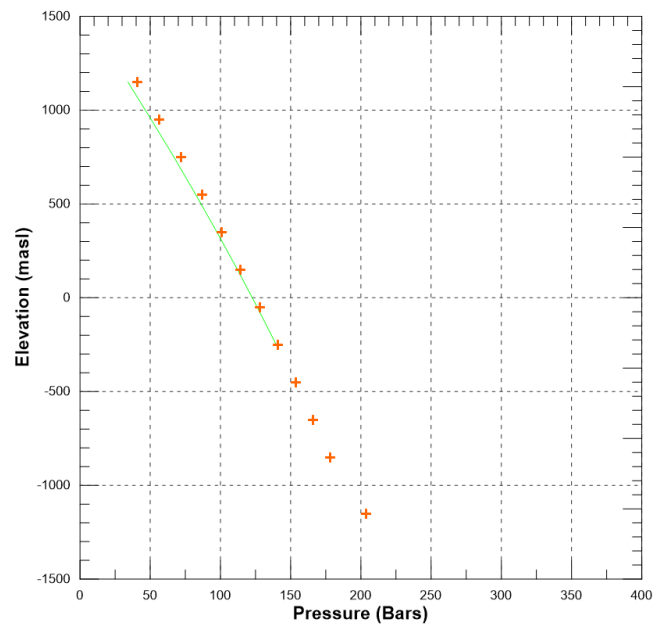
Well OW-906A



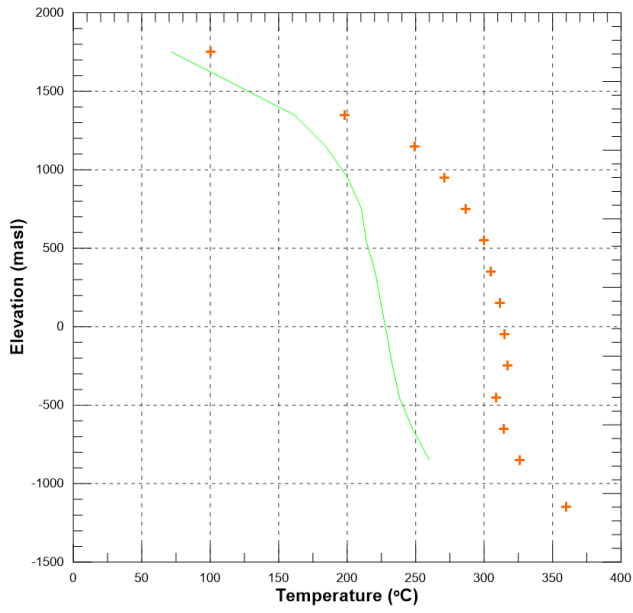
Well OW-907A



Well OW-907A

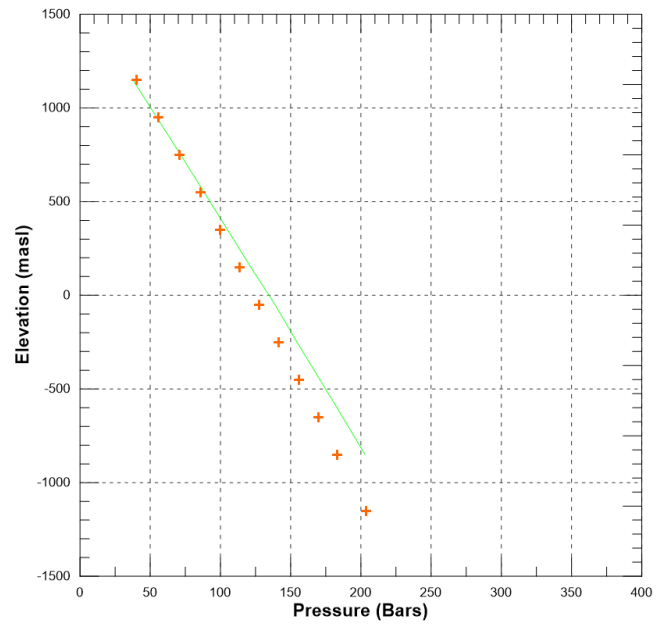


Well OW-907B



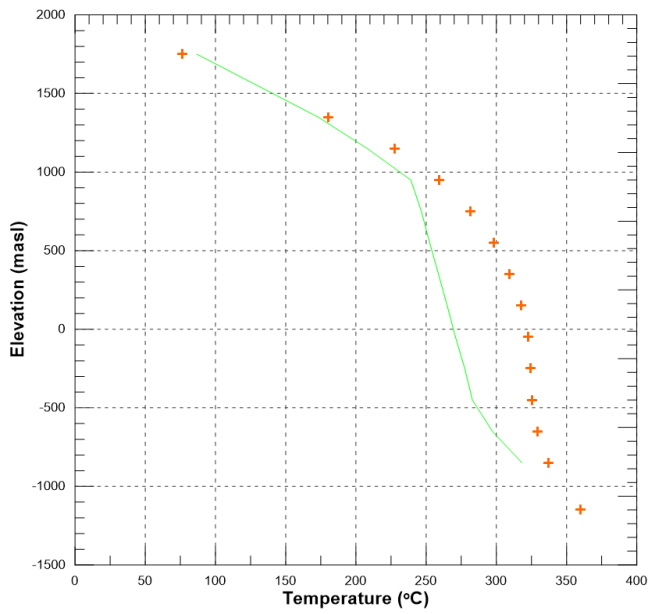
— Observed Temperature
+ + + Calculated Temperature

Well OW-907B



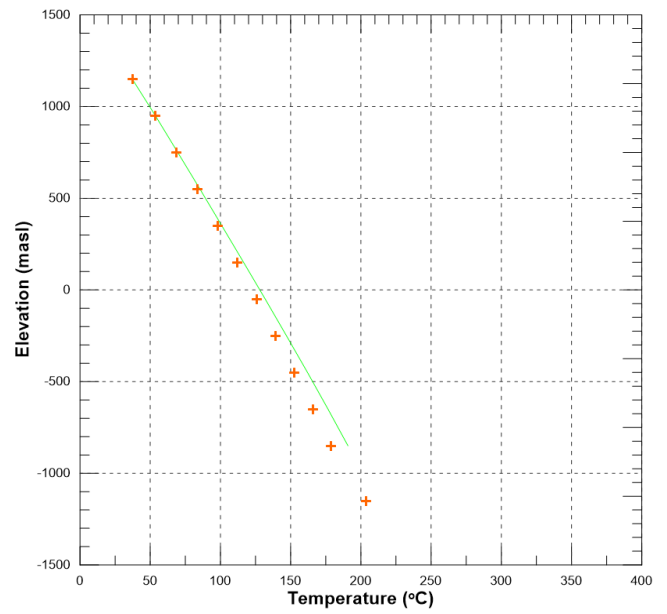
— Observed Pressure
+ + + Calculated Pressure

Well OW-908



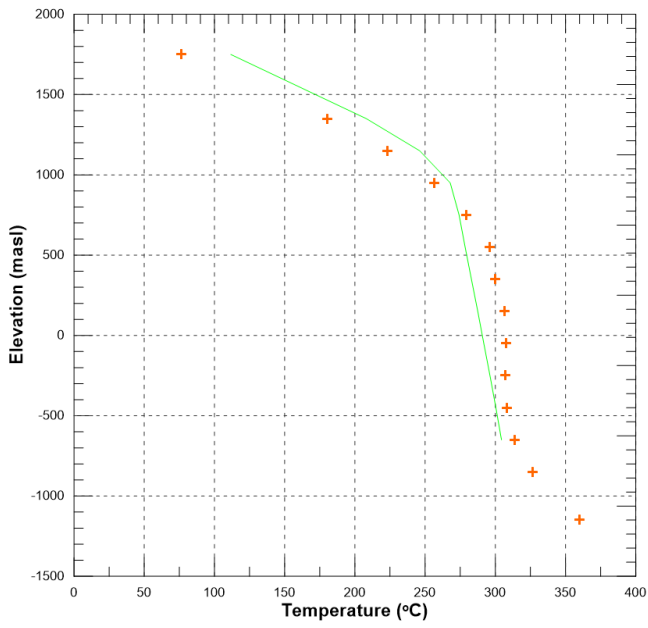
— Observed Temperature
+ + + Calculated Temperature

Well OW-908

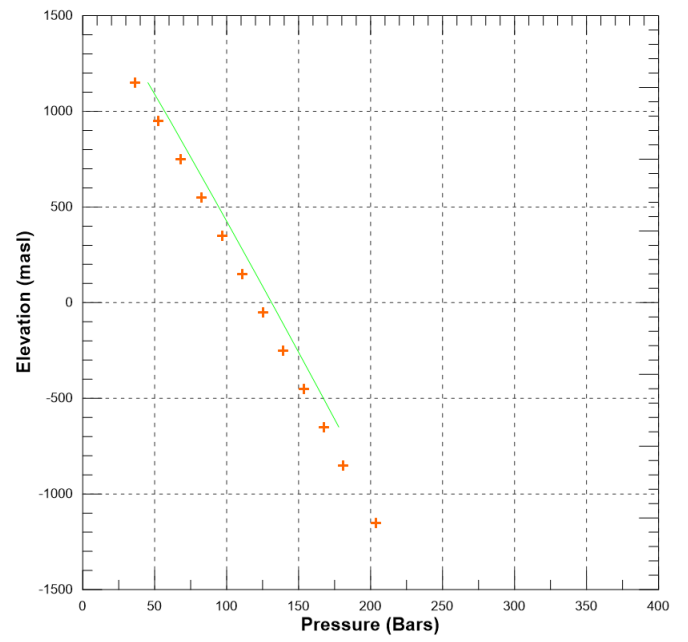


— Observed Temperature
+ + + Calculated Temperature

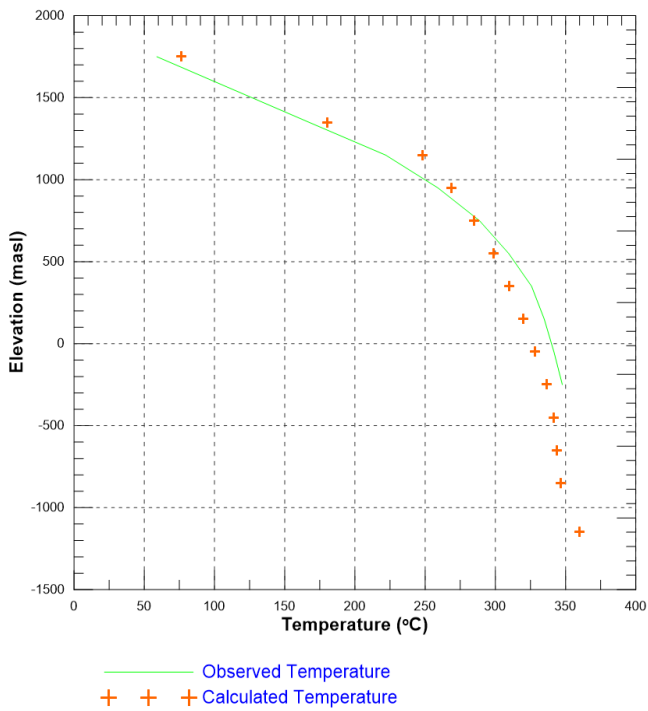
Well OW-908A



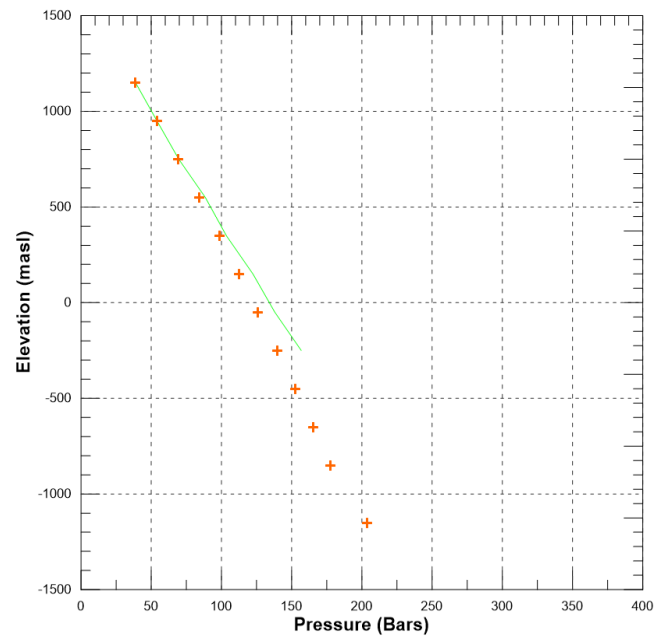
Well OW-908A



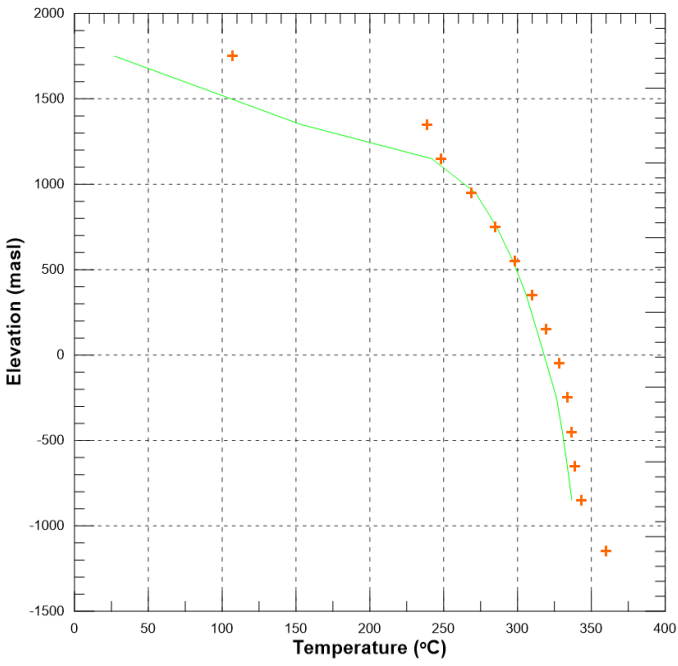
Well OW-908B



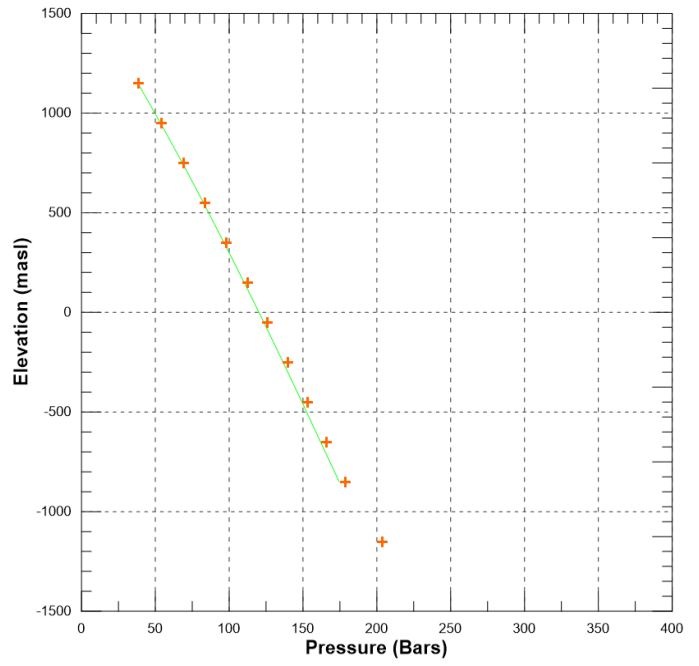
Well OW-908B



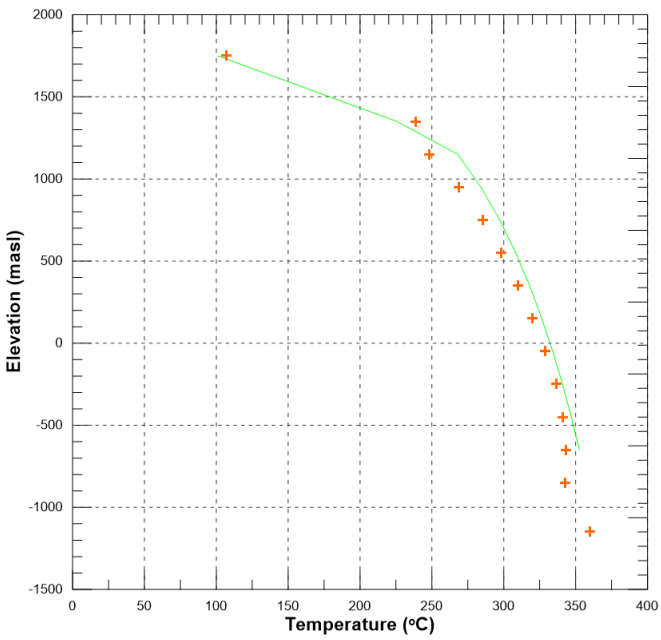
Well OW-909



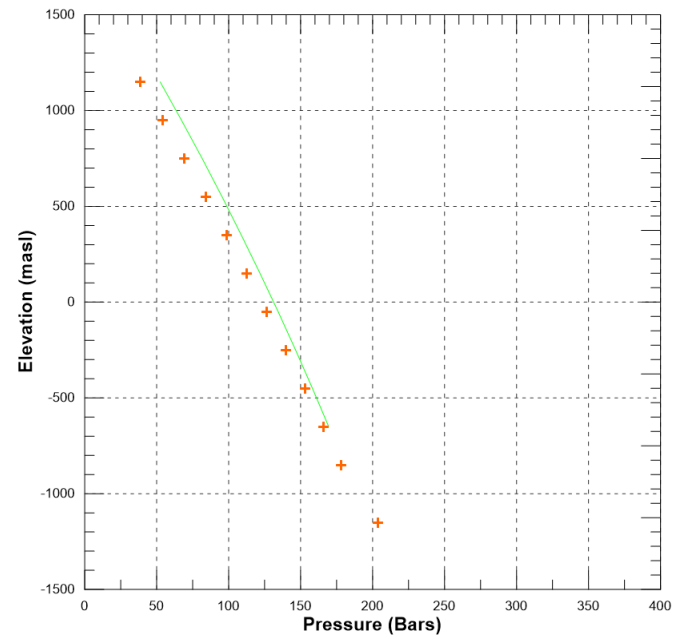
Well OW-909



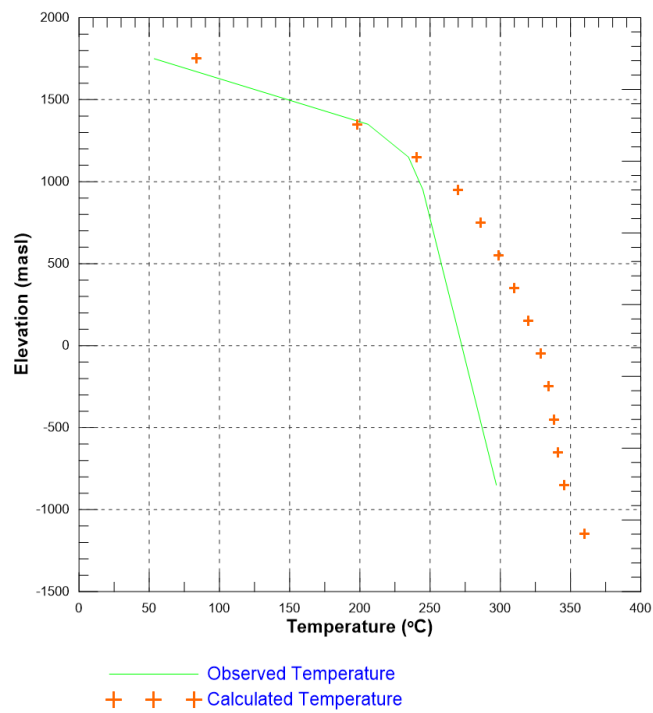
Well OW-909A



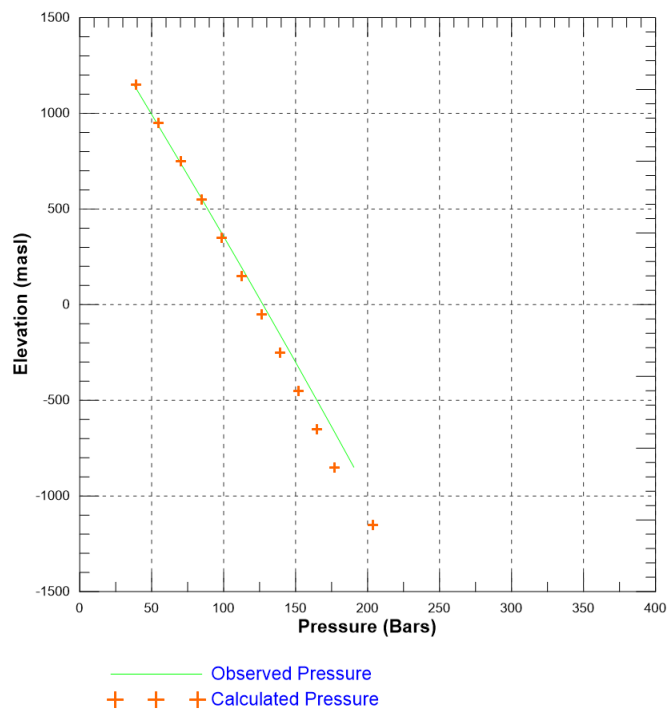
Well OW-909A



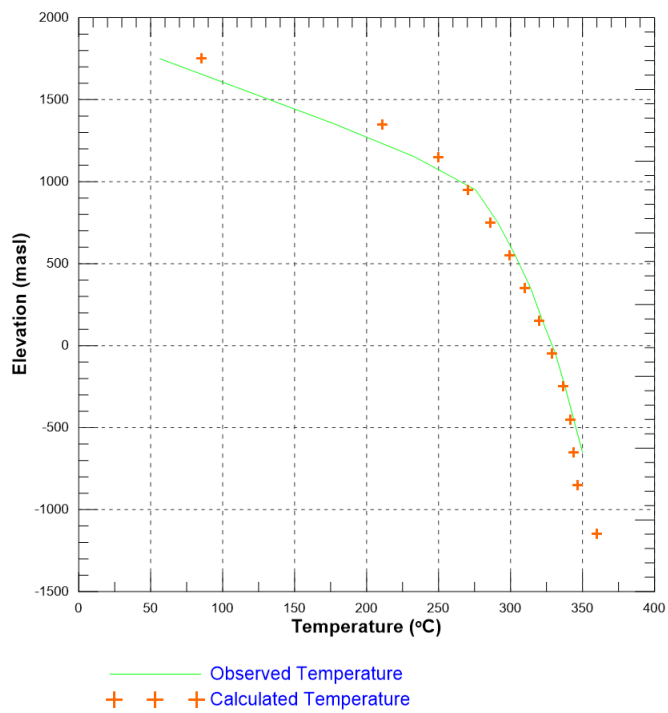
Well OW-910



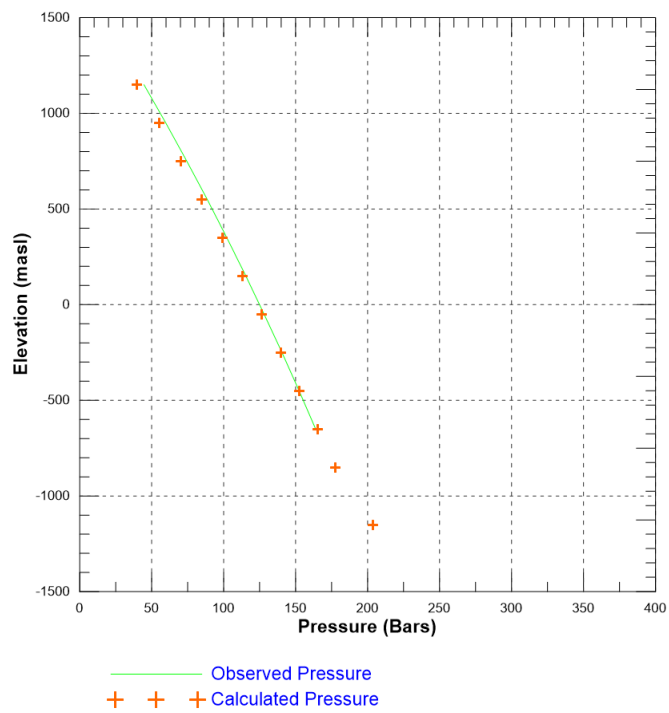
Well OW-910



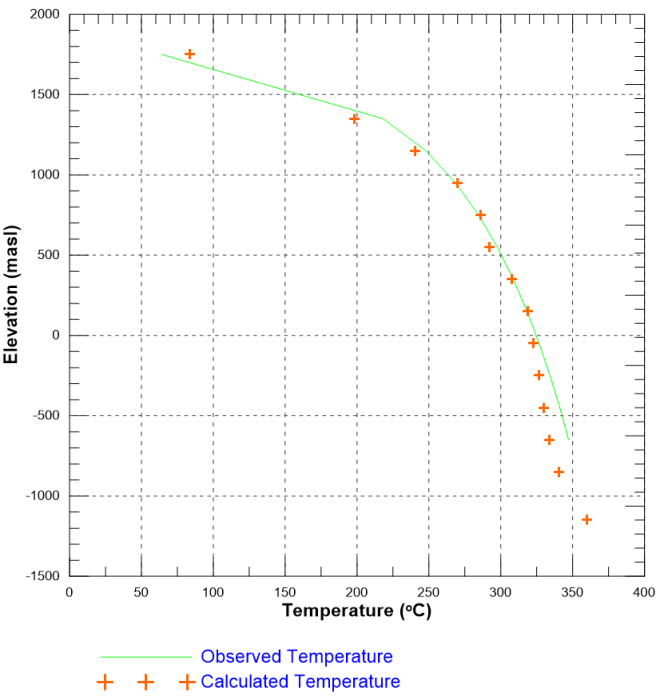
Well OW-910A



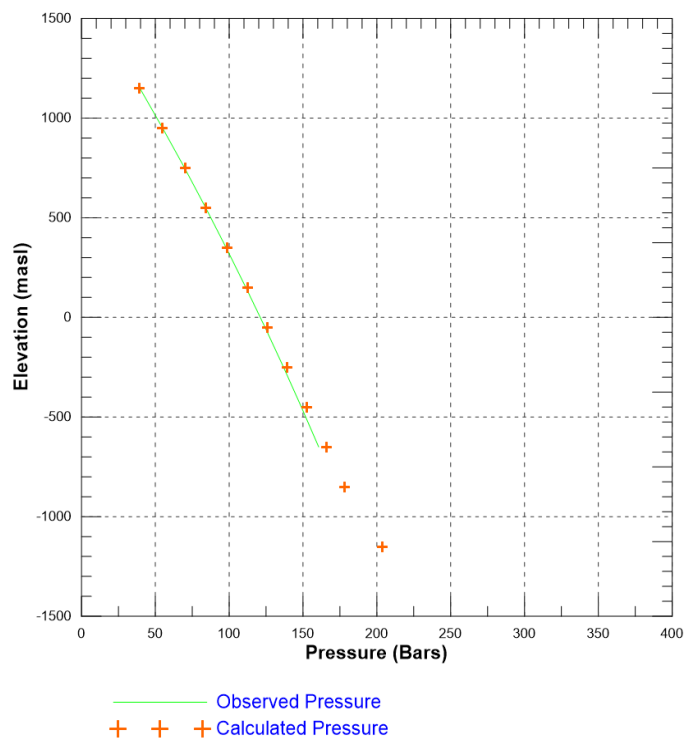
Well OW-910A



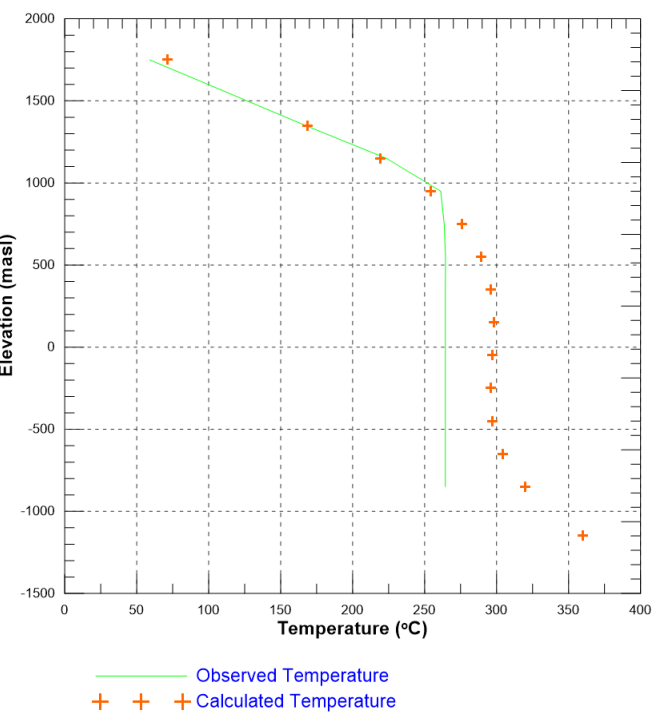
Well OW-910B



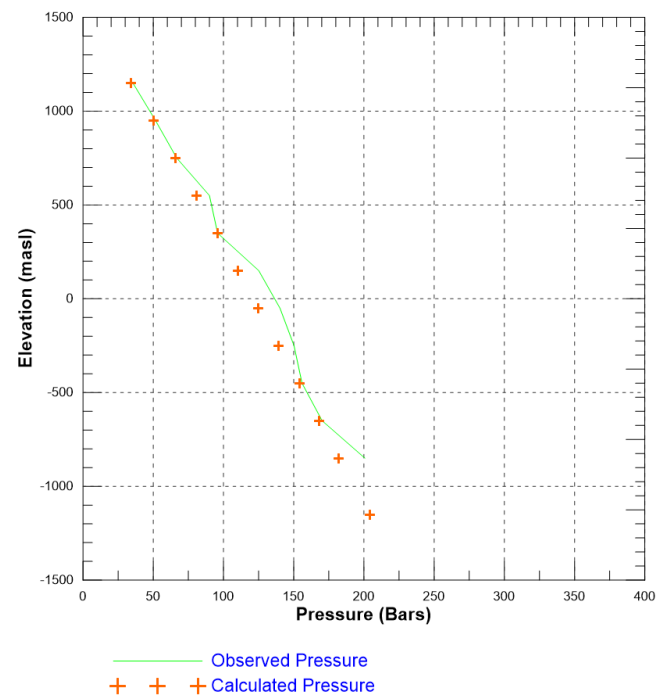
Well OW-910B



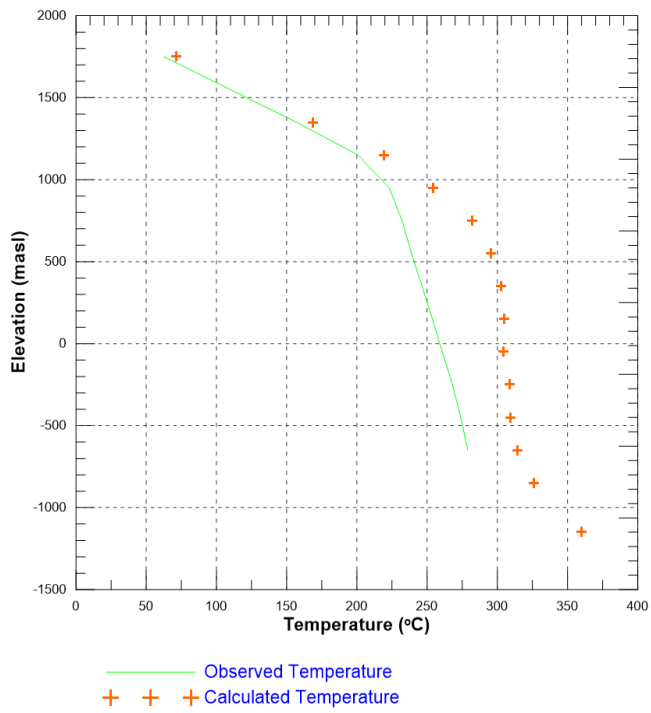
Well OW-911



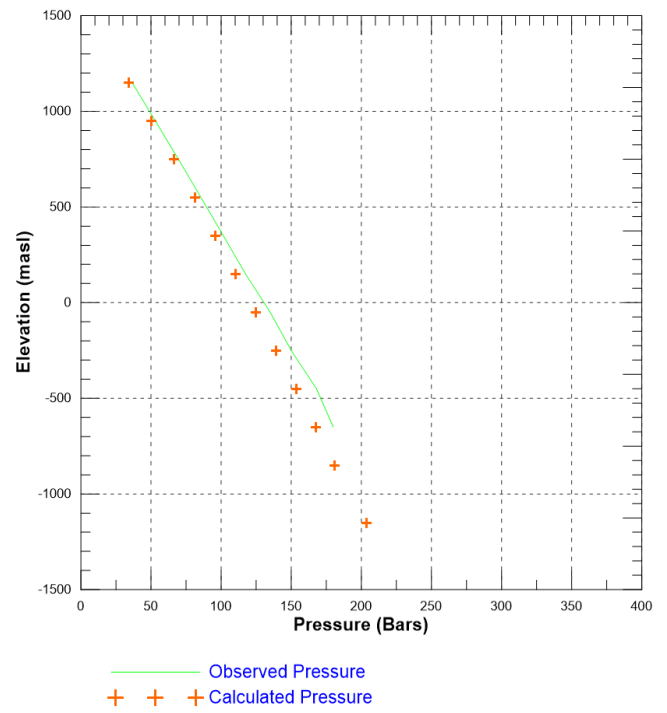
Well OW-911



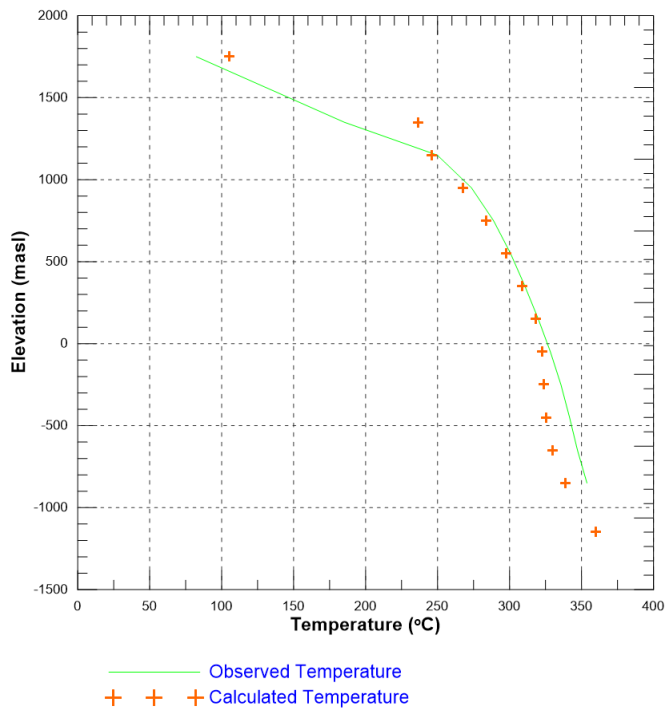
Well OW-911A



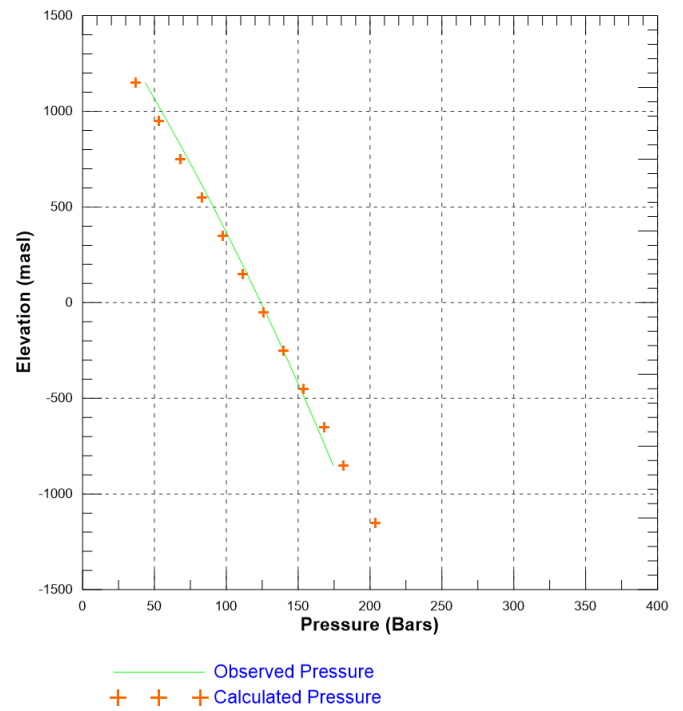
Well OW-911A



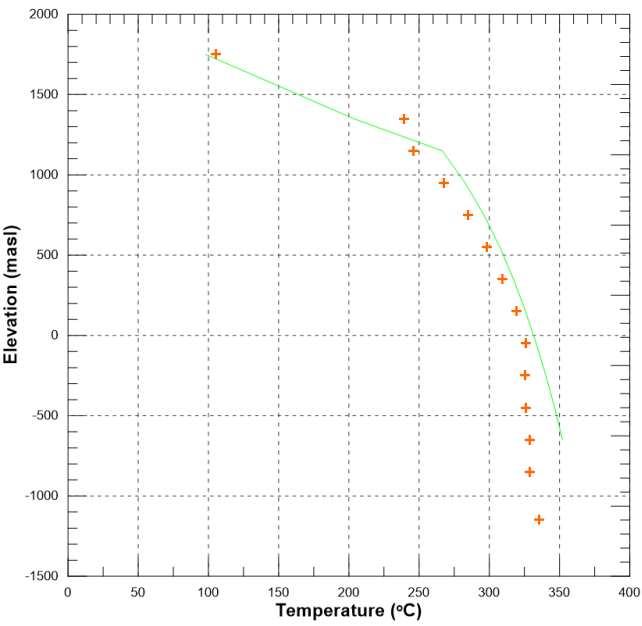
Well OW-912



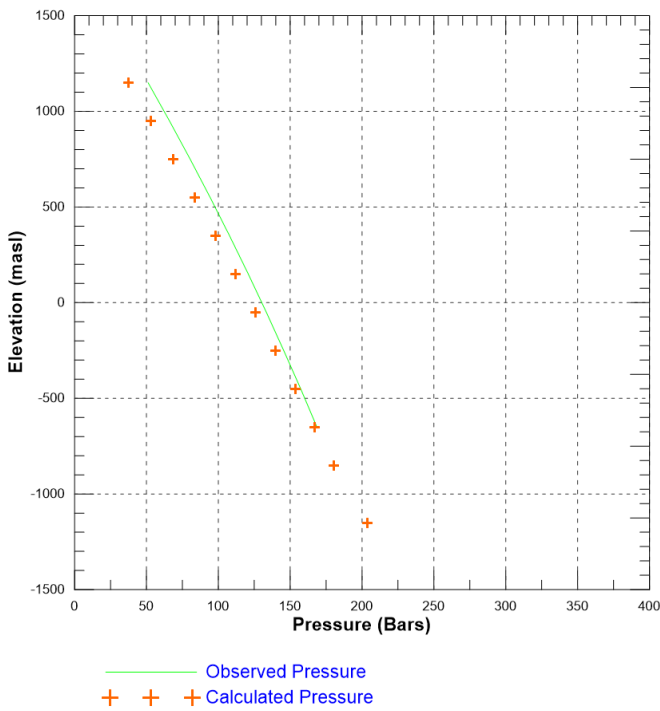
Well OW-912



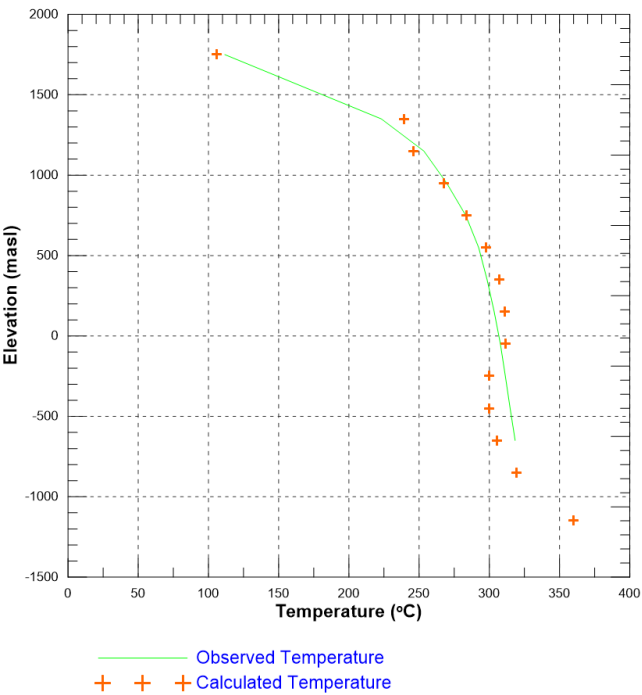
Well OW-912A



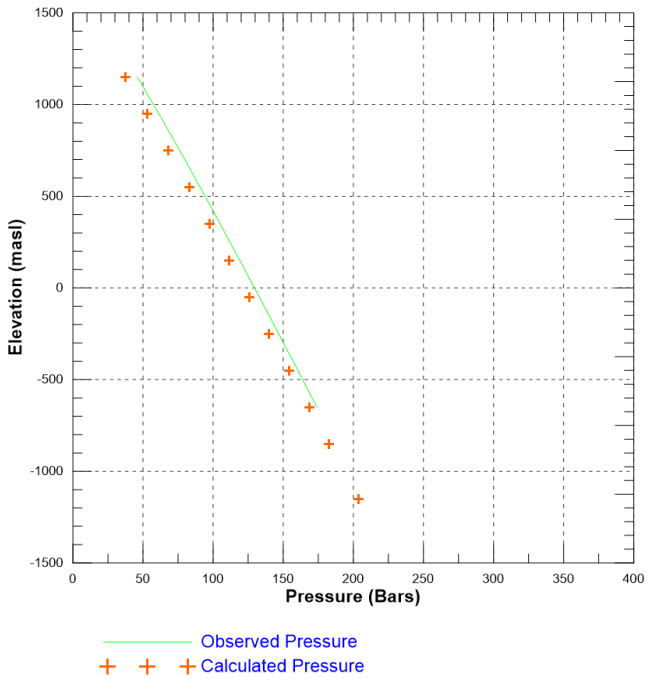
Well OW-912A



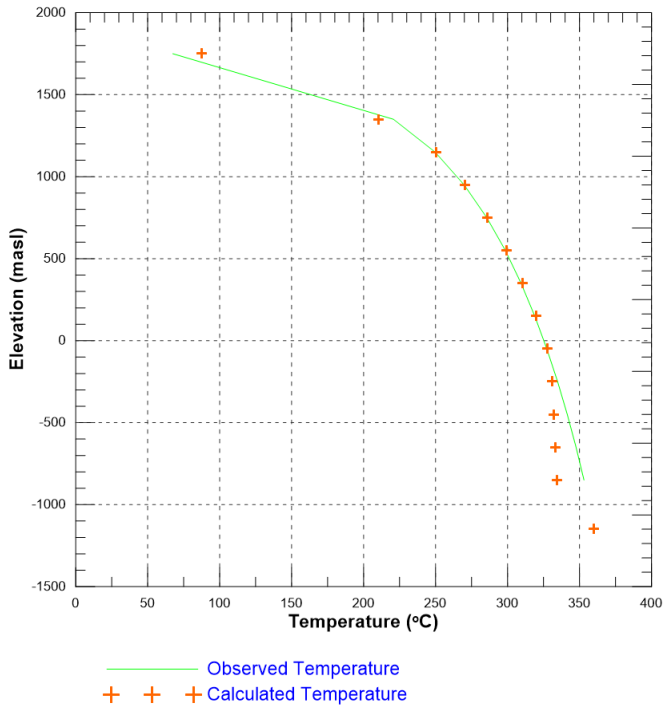
Well OW-912B



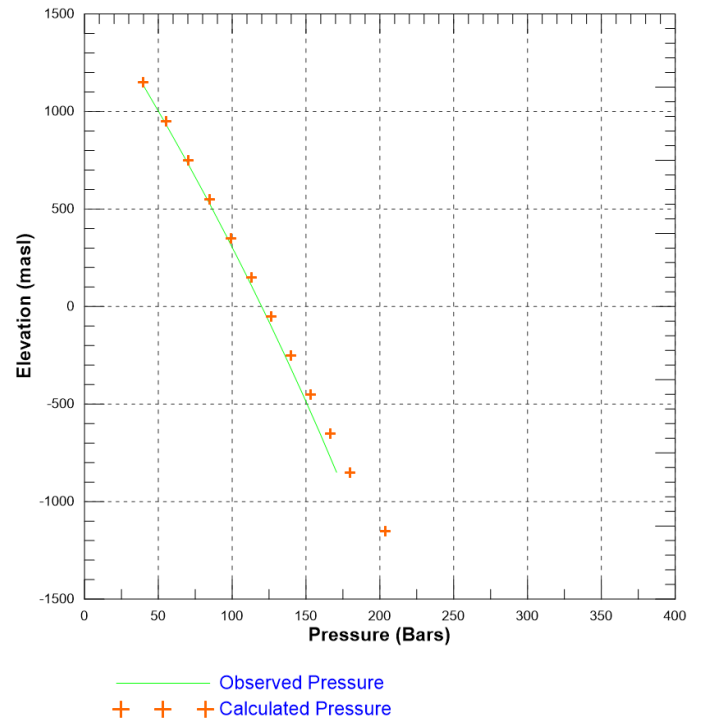
Well OW-912B



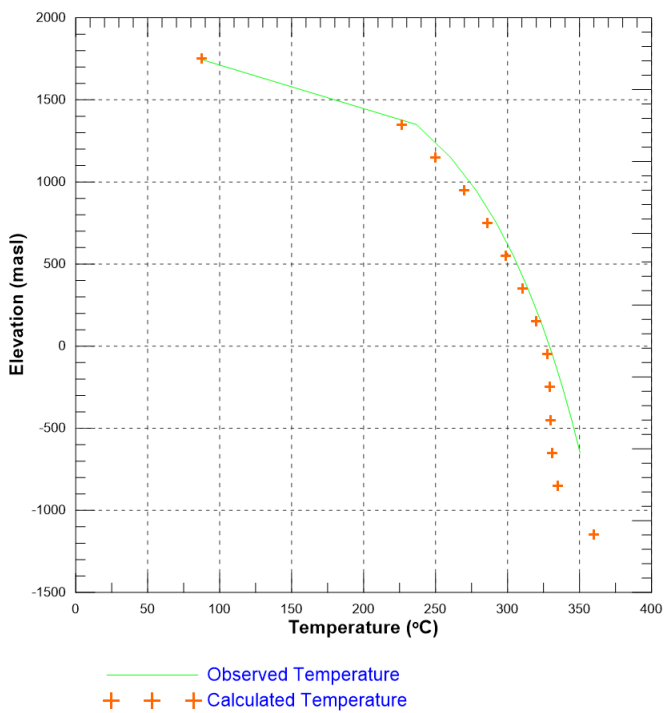
Well OW-914



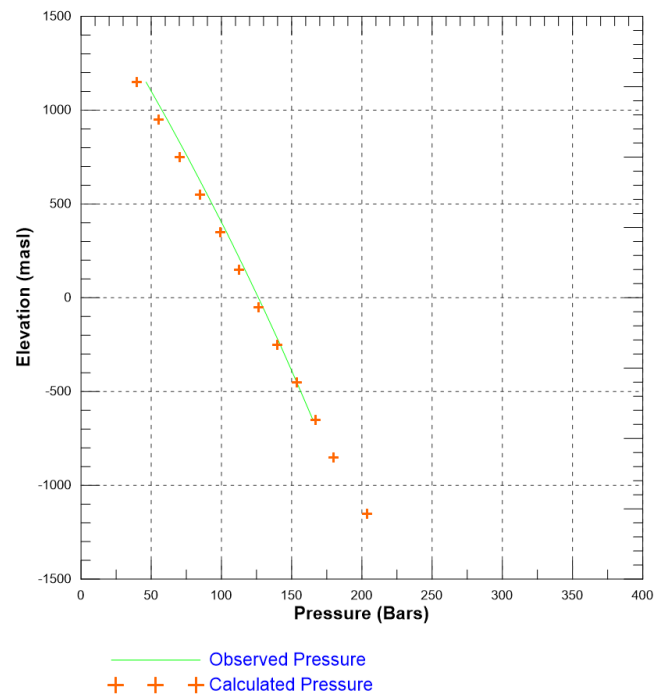
Well OW-914



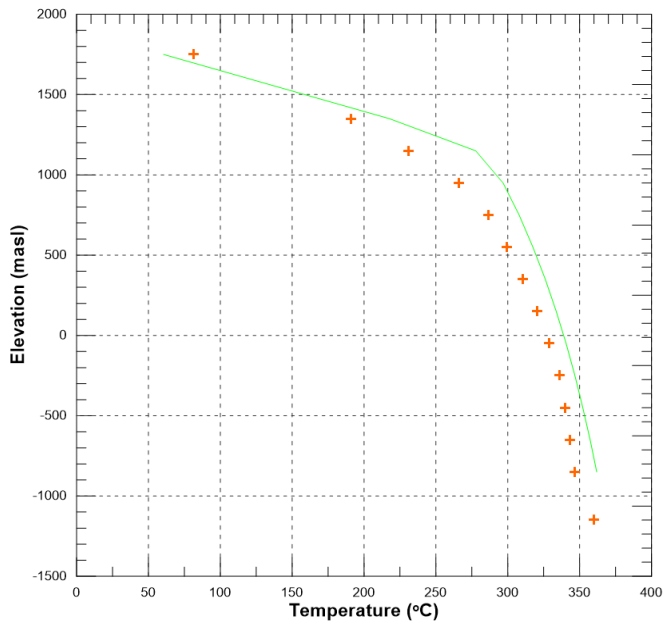
Well OW-914B



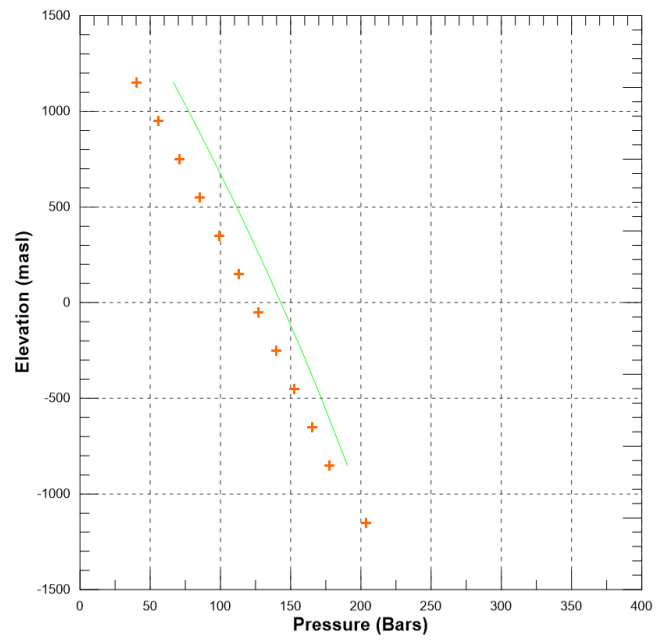
Well OW-914B



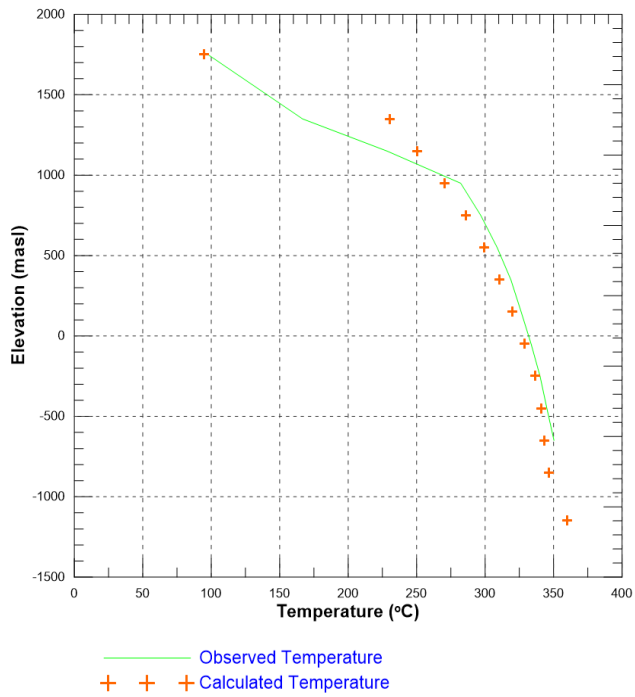
Well OW-915



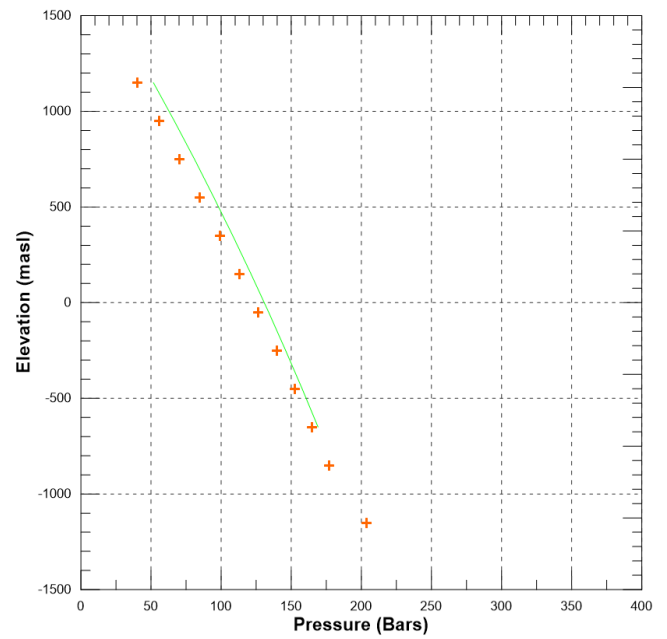
Well OW-915



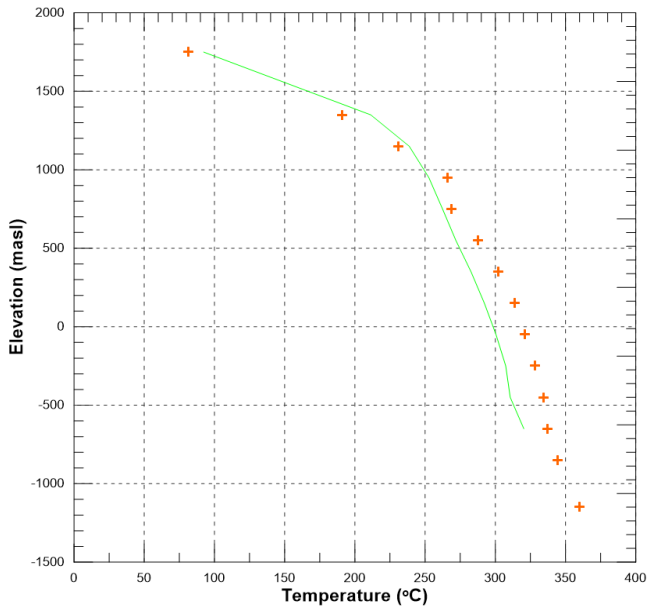
Well OW-915A



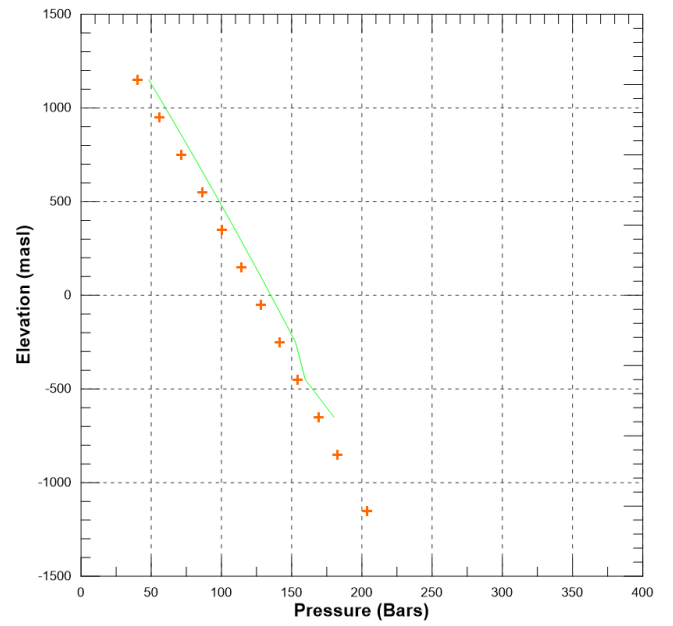
Well OW-915A



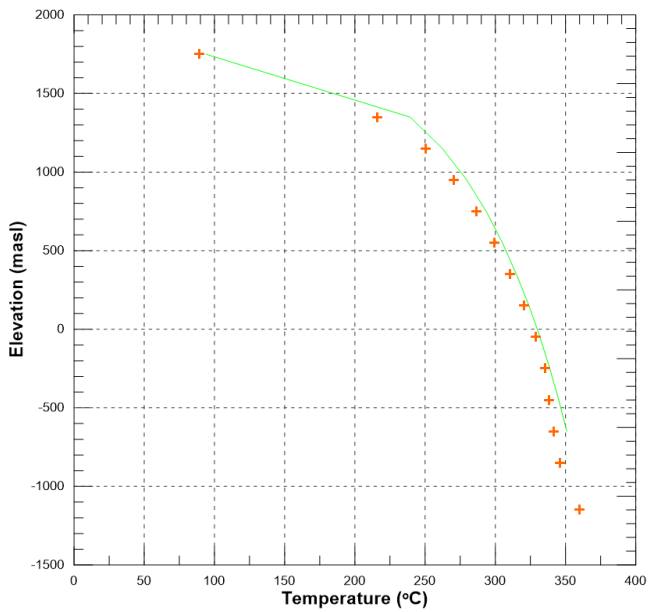
Well OW-915B



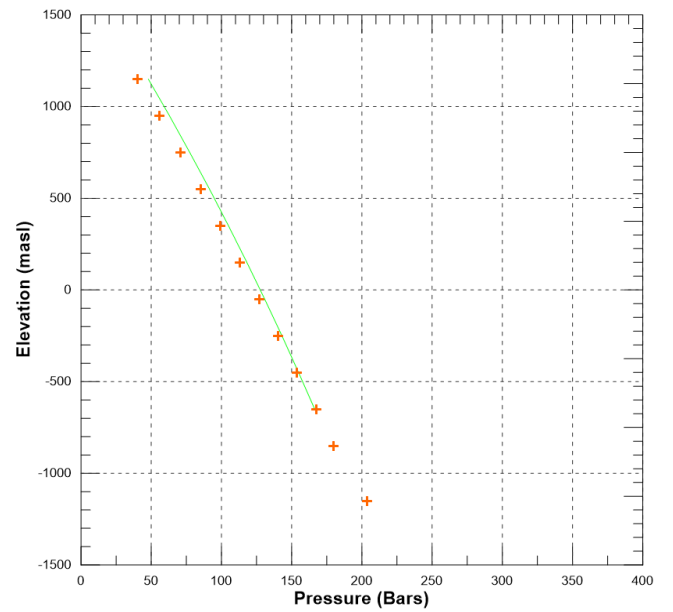
Well OW-915B



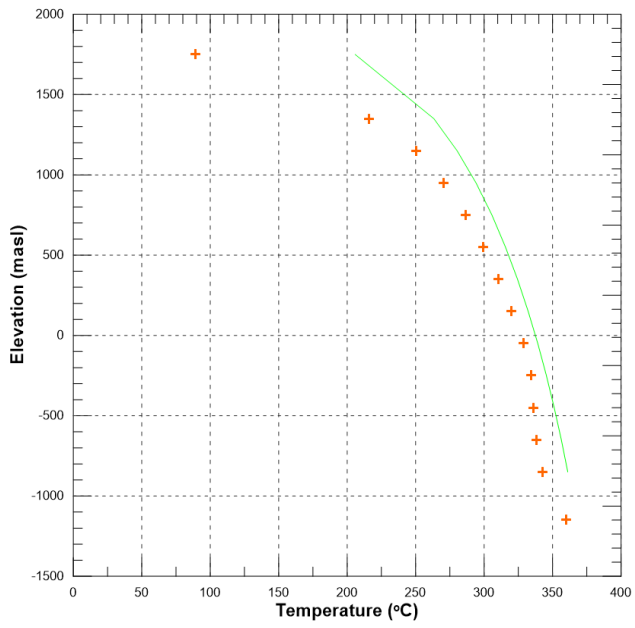
Well OW-915C



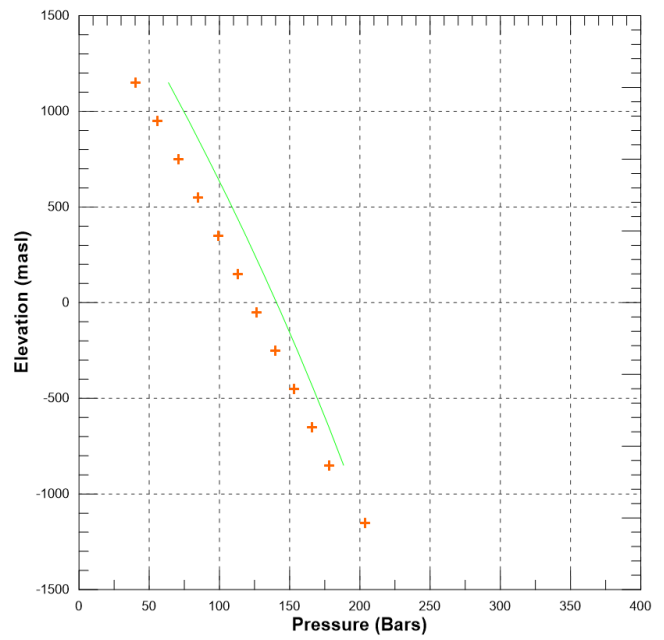
Well OW-915C



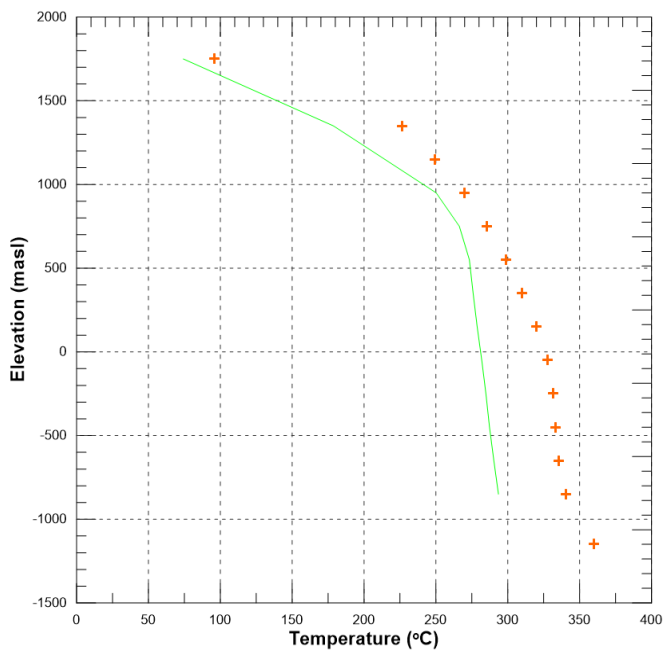
Well OW-915D



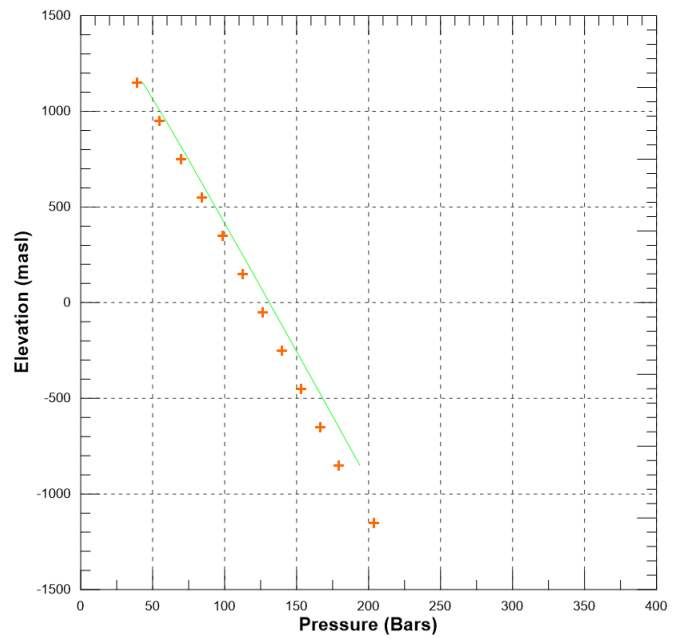
Well OW-915D



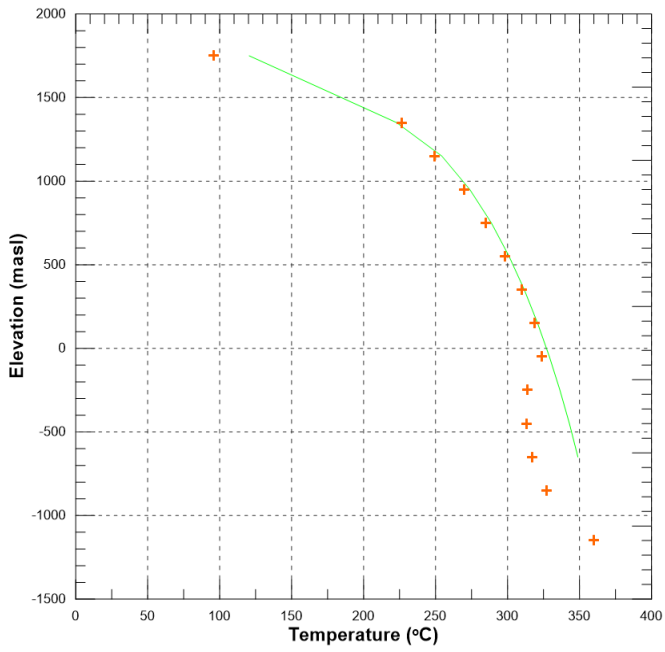
Well OW-916



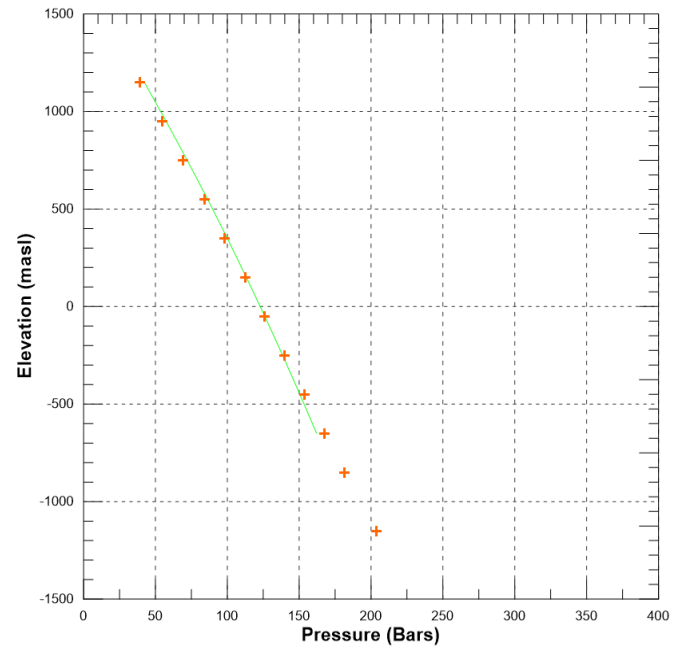
Well OW-916



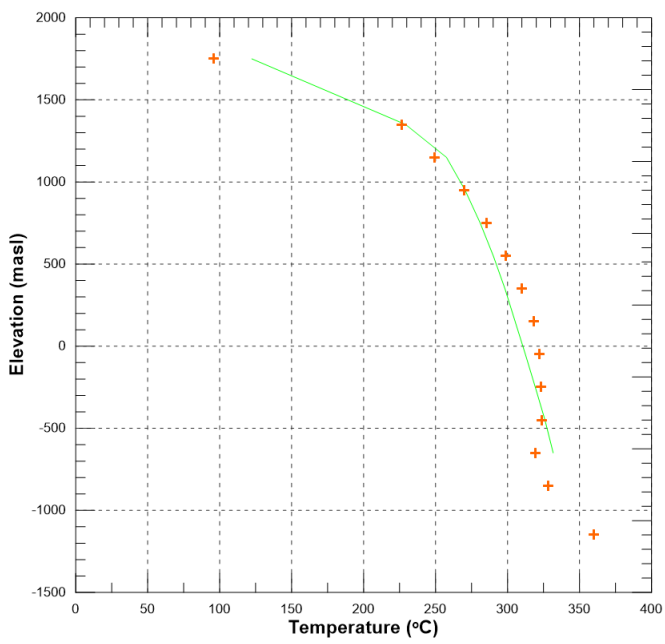
Well OW-916A



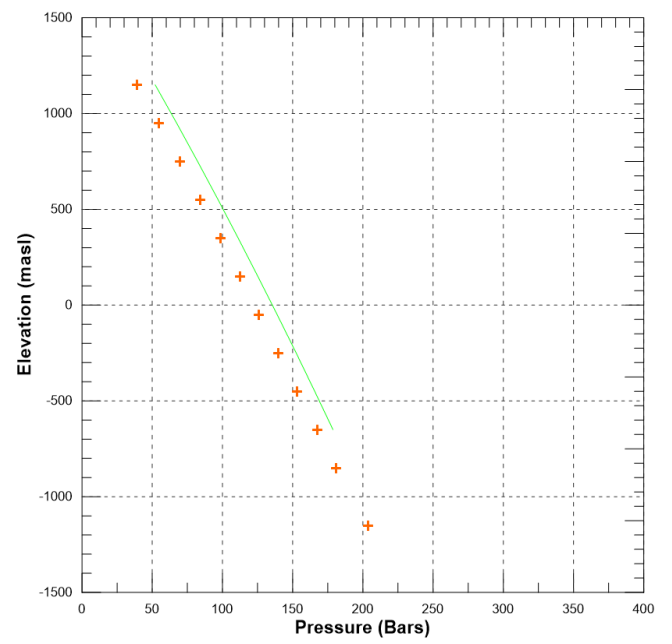
Well OW-916A



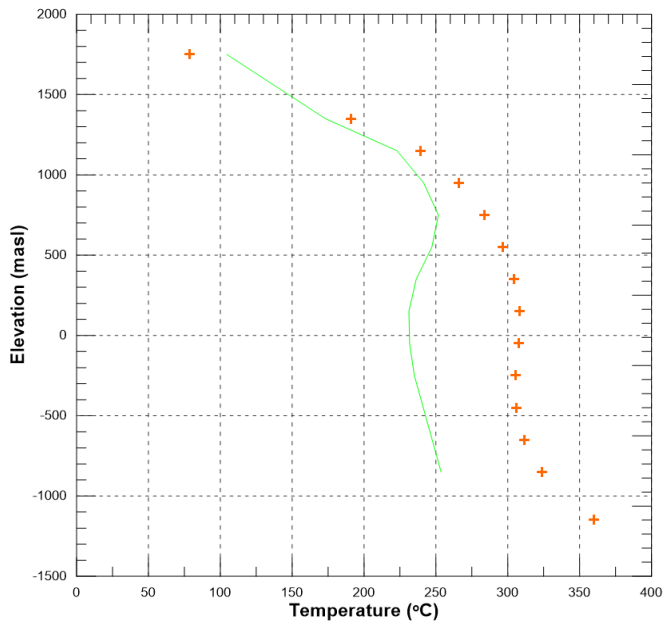
Well OW-916B



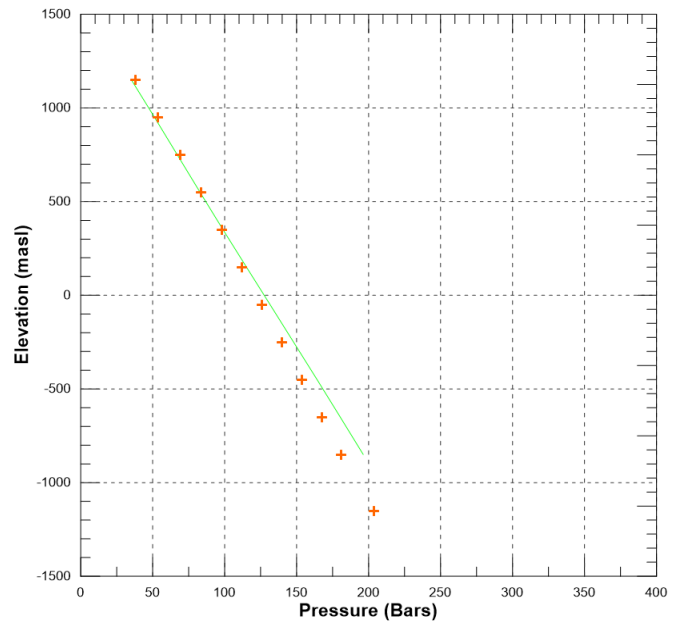
Well OW-916B



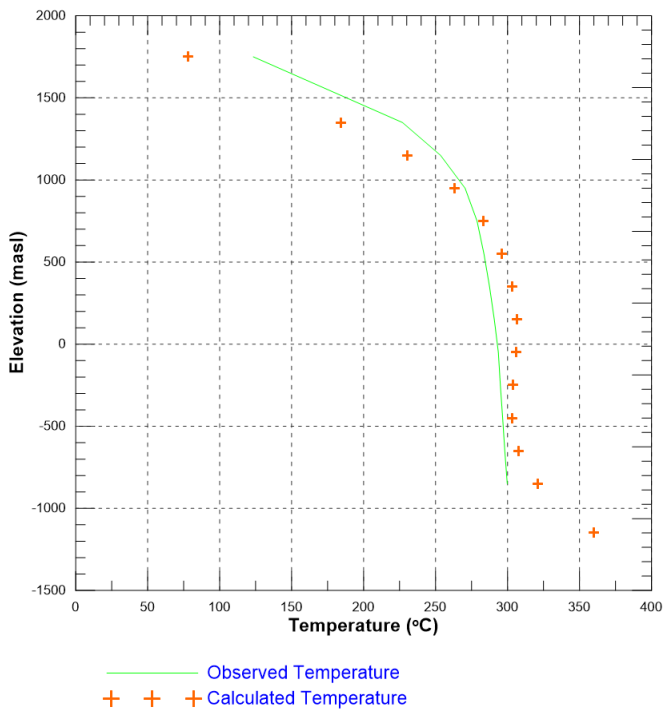
Well OW-917



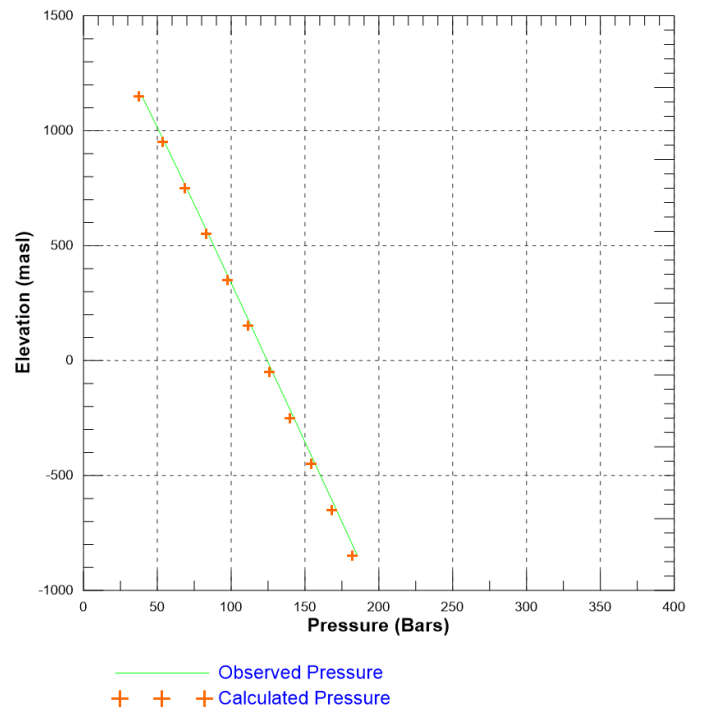
Well OW-917



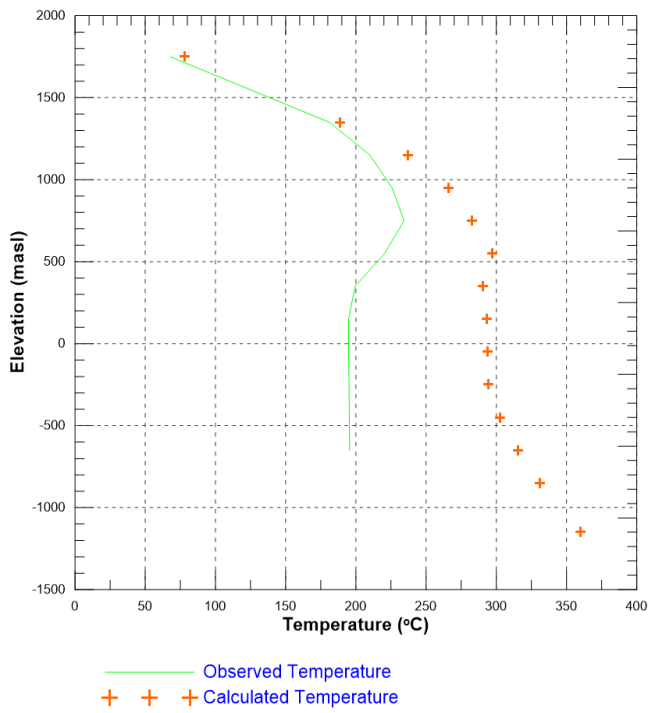
Well OW-918



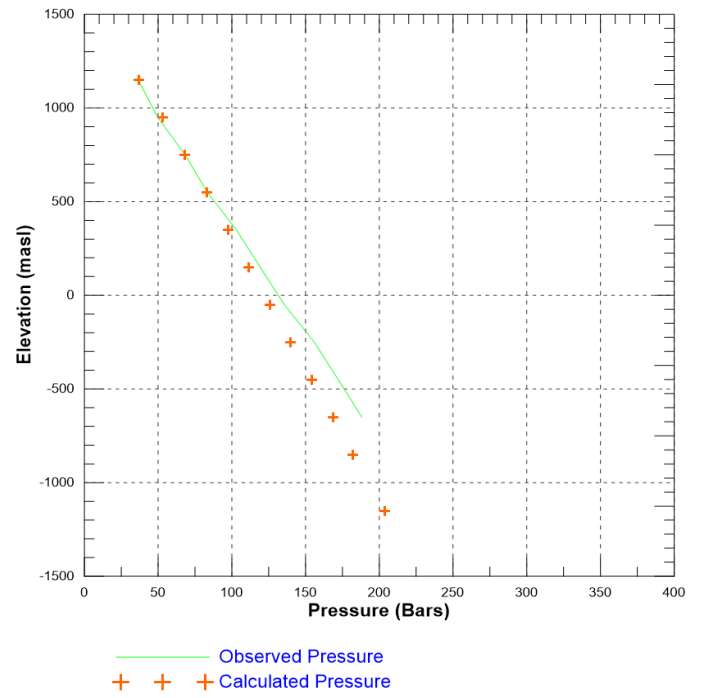
Well OW-918



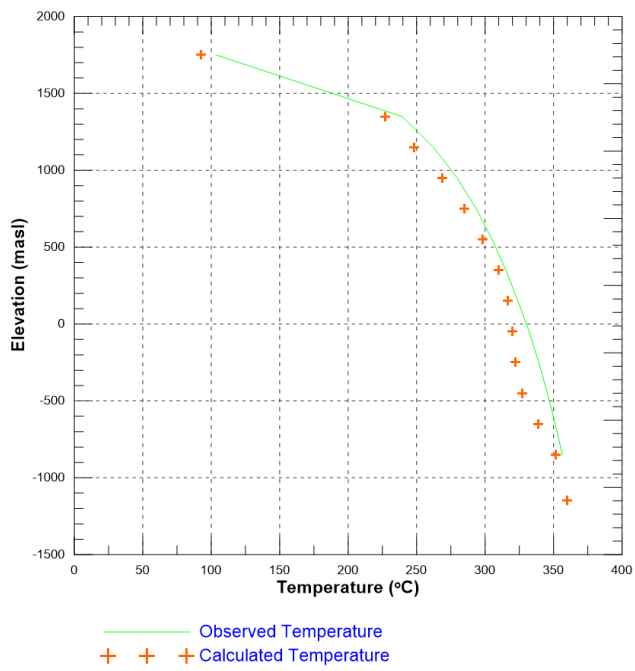
Well OW-918A



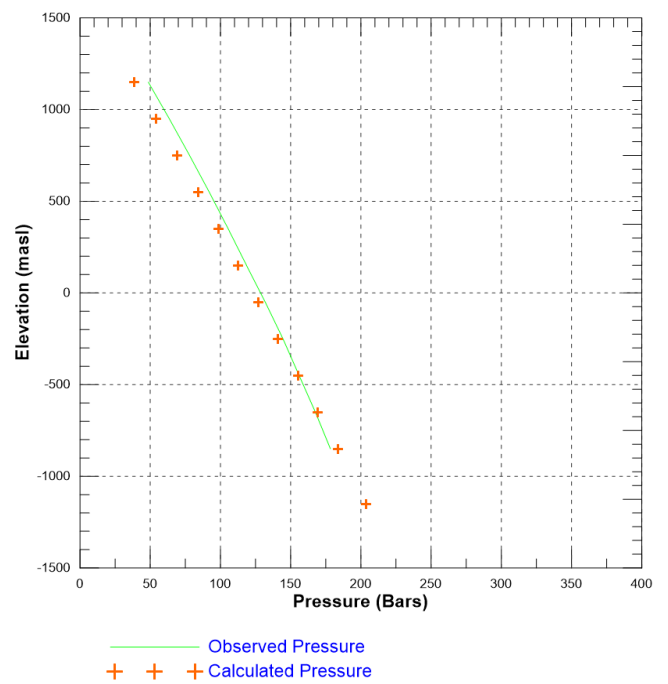
Well OW-918A



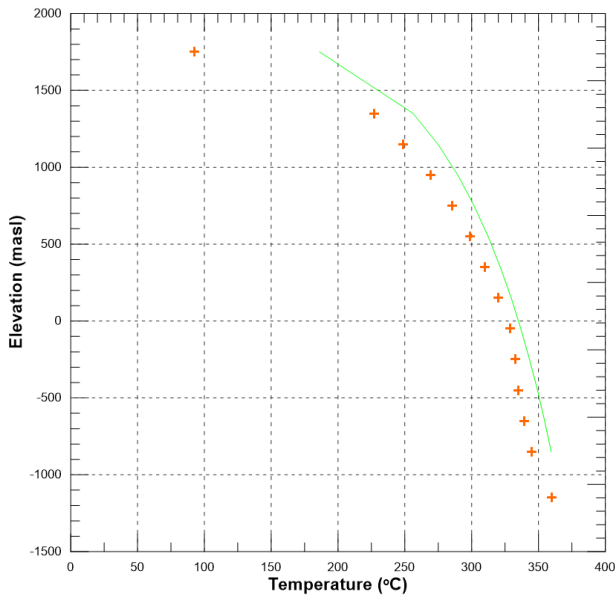
Well OW-919



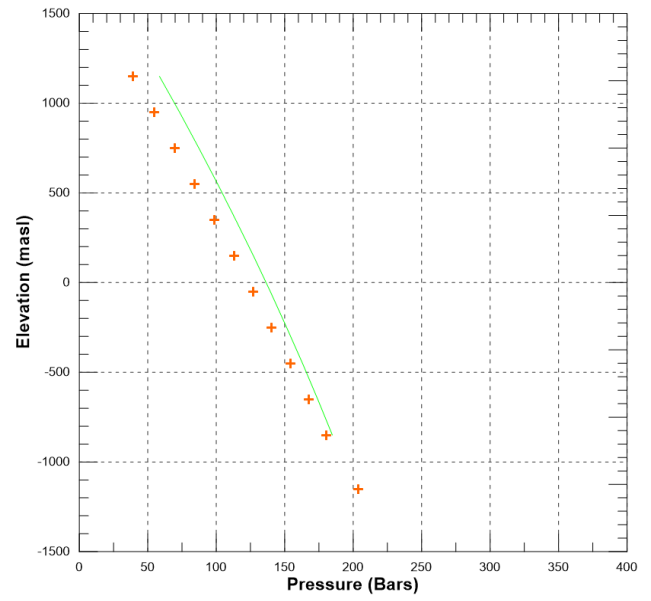
Well OW-919



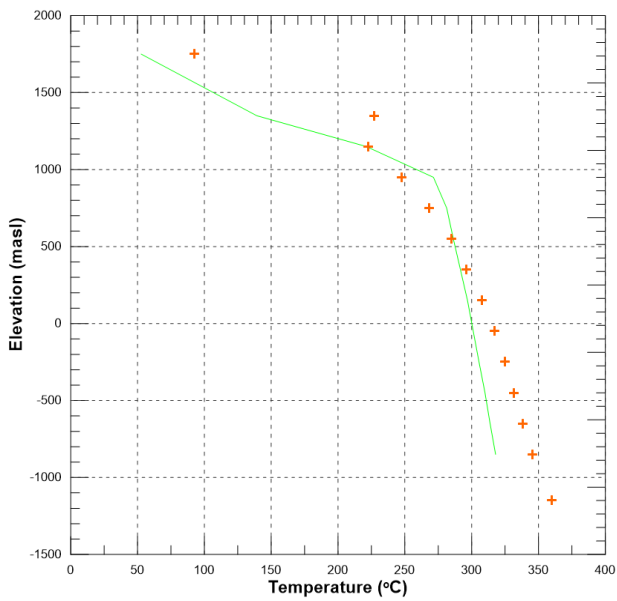
Well OW-919A



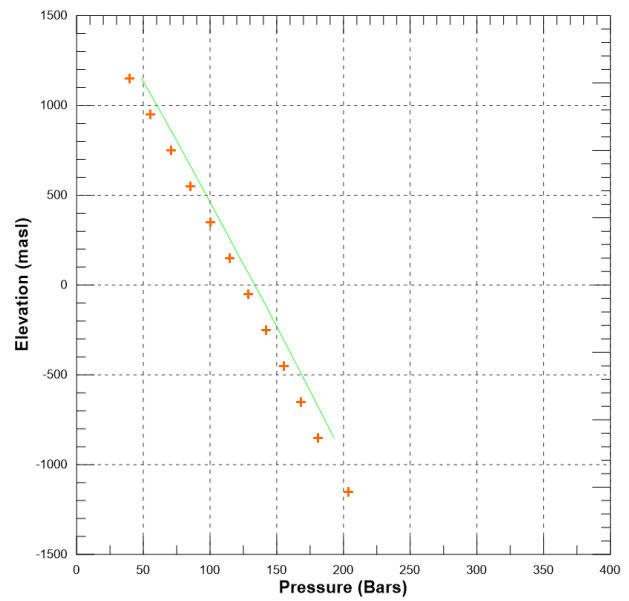
Well OW-919A



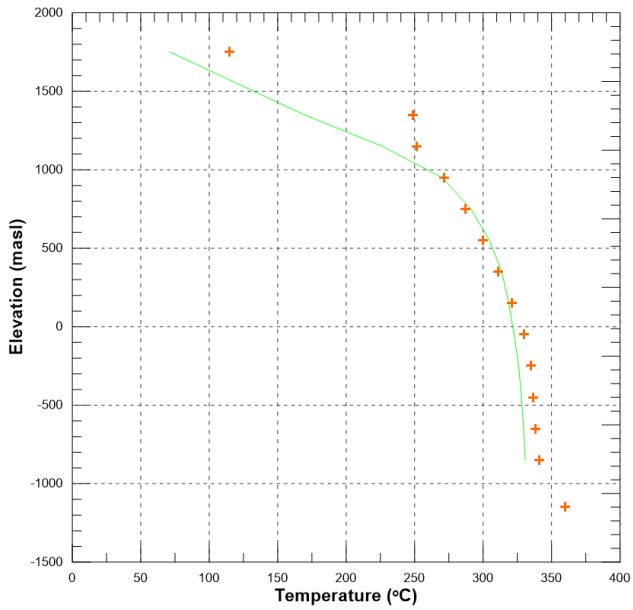
Well OW-919B



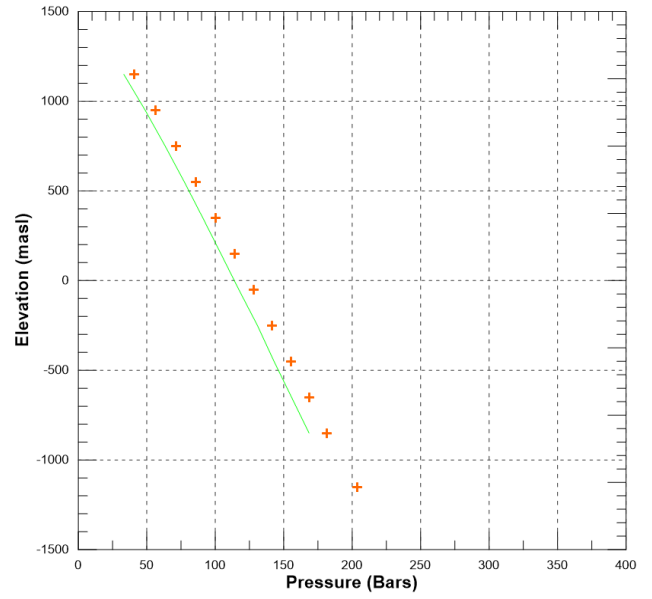
Well OW-919B



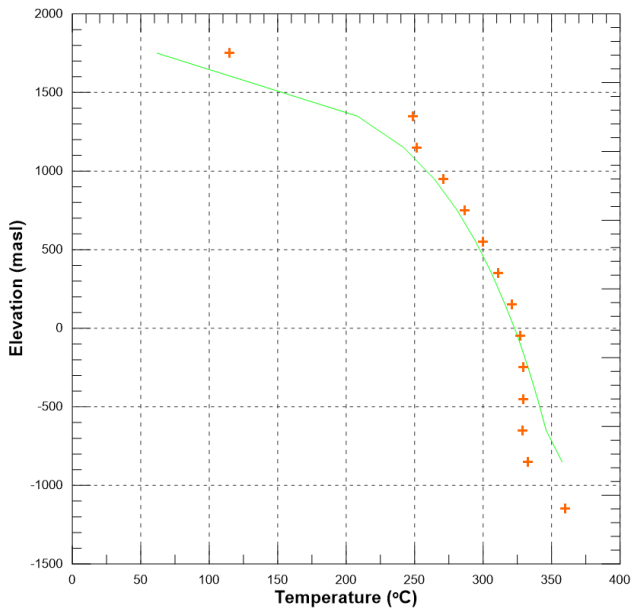
Well OW-921



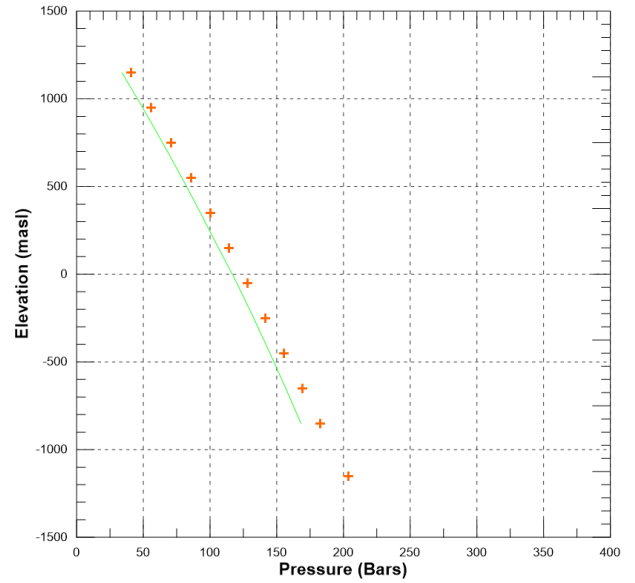
Well OW-921



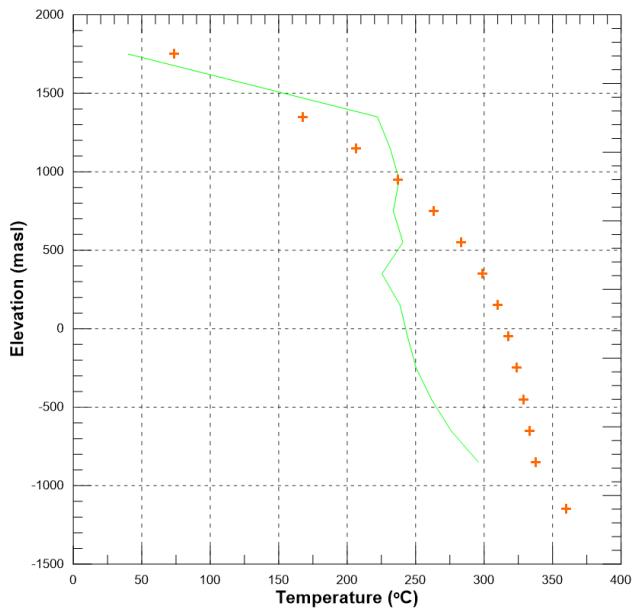
Well OW-921A



Well OW-921A

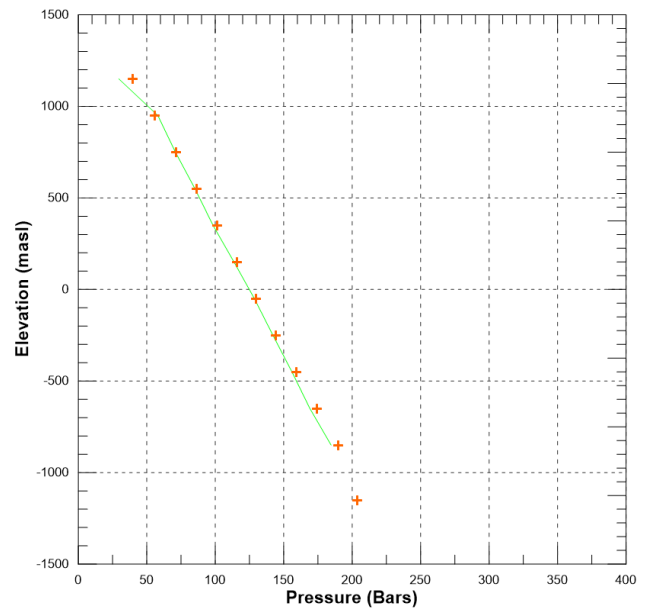


Well OW-926



— Observed Temperature
+ + + Calculated Temperature

Well OW-926



— Observed Pressure
+ + + Calculated Pressure